Biochemical Journal (2017) **474** 1669–1687
DOI: 10.1042/BCJ20160942

Research Article

Tumor protein D52 expression is post-transcriptionally regulated by T-cell intercellular antigen (TIA) 1 and TIA-related protein via mRNA stability

Hiromi Motohashi[1,*], Yoshiki Mukudai[1]*, Chihiro Ito[1], Kosuke Kato[1], Toshikazu Shimane[1], Seiji Kondo[1,2] and Tatsuo Shirota[1]

[1]Department of Oral and Maxillofacial Surgery, School of Dentistry, Showa University, 2-1-1 Kitasenzoku, Ota-ku, Tokyo 145-8515, Japan and [2]Department of Oral and Maxillofacial Surgery, Faculty of Medicine, Fukuoka University, 7-45-1 Nanakuma, Jonan-ku, Fukuoka 814-0180, Japan

Correspondence: Yoshiki Mukudai (mukudai@dent.showa-u.ac.jp)

Although tumor protein D52 (TPD52) family proteins were first identified nearly 20 years ago, their molecular regulatory mechanisms remain unclear. Therefore, we investigated the post-transcriptional regulation of TPD52 family genes. An RNA immunoprecipitation (RIP) assay showed the potential binding ability of TPD52 family mRNAs to several RNA-binding proteins, and an RNA degradation assay revealed that TPD52 is subject to more prominent post-transcriptional regulation than are TPD53 and TPD54. We subsequently focused on the 3′-untranslated region (3′-UTR) of TPD52 as a *cis*-acting element in post-transcriptional gene regulation. Several deletion mutants of the 3′-UTR of TPD52 mRNA were constructed and ligated to the 3′-end of a reporter green fluorescence protein gene. An RNA degradation assay revealed that a minimal *cis*-acting region, located in the 78-280 region of the 5′-proximal region of the 3′-UTR, stabilized the reporter mRNA. Biotin pull-down and RIP assays revealed specific binding of the region to T-cell intracellular antigen 1 (TIA-1) and TIA-1-related protein (TIAR). Knockdown of TIA-1/TIAR decreased not only the expression, but also the stability of TPD52 mRNA; it also decreased the expression and stability of the reporter gene ligated to the 3′-end of the 78-280 fragment. Stimulation of transforming growth factor-β and epidermal growth factor decreased the binding ability of these factors, resulting in decreased mRNA stability. These results indicate that the 78-280 fragment and TIA-1/TIAR concordantly contribute to mRNA stability as a *cis*-acting element and *trans*-acting factor(s), respectively. Thus, we here report the specific interactions between these elements in the post-transcriptional regulation of the TPD52 gene.

Introduction

Tumor protein D (TPD) 52 family proteins were first identified nearly 20 years ago [1], and four members (i.e. TPD52, 53, 54 and 55) have since been identified (reviewed in refs [2,3]). The mammalian TPD52 and related proteins all contain a coiled-coil motif and harbor proline, glutamic-acid, serine and threonine (PEST) sequences at the N- and C-terminals [4,5]. The first recognized member of this protein family was TPD52, which was identified as an overexpressed gene in various cancer cells [1]. Since then, much information has been accumulated on this protein family. For instance, TPD52 interacts with MAL2 [6], annexin V1 [7], syntaxin 1 and VAMP2 [8]. Recent investigations have suggested that TPD52 may be a novel vaccine target (reviewed in ref. [9]). In addition, other members of the protein family, such as TPD53, 54 and 55, have been reported to be highly expressed in colon [10,11], ovary [12–14], testis [15] and prostate cancers [16,17], and lymphomas [18], leukemia cells [18,19] and brain tumors

*These authors contributed equally to this work.

Received: 18 October 2016
Revised: 9 March 2017
Accepted: 15 March 2017

Accepted Manuscript online: 15 March 2017
Version of Record published: 4 May 2017

Biochemical Journal (2017) 474 1669–1687
DOI: 10.1042/BCJ20160942

[20]. Furthermore, we recently reported that TPD52 and 54 are highly expressed in oral squamous carcinoma cells (OSCCs) and affect cell attachment to the extracellular matrix, cell migration and Akt/protein kinase B activation [21,22], suggesting an important role of TPD52 family genes on growth and metastasis in OSCCs as well as in other cancer cells. Although these studies revealed a variety of physiological and pathological functions for the TPD52 family of proteins in the metabolism of not only cancer cells, but also of normal cells, and strongly suggested that the expression of these genes is highly regulated in various steps, the molecular regulatory mechanisms underlying these functions remain poorly understood.

Post-transcriptional gene regulation, such as RNA processing, RNA export and RNA degradation, plays an important role in gene expression as well as in transcription, translation and post-translation, and many studies concerning molecular post-transcriptional mechanisms have been reported (reviewed in refs [23,24]). RNA-binding proteins (RBPs) and/or non-coding RNAs, such as microRNAs, bind to *cis*-acting elements within mRNAs, and this interaction determines the fate of mRNA stability (reviewed in ref. [25]). Although it was recently reported that guanosine- and uridine-rich or uridine-rich element sequence motifs were found in many coding and non-coding RNAs [26], in mammalian cells, adenosine- and uridine-rich elements (AREs) are the most well-known *cis*-acting elements of mRNA that act as a target for rapid RNA degradation (reviewed in ref. [27]). AREs range in size from 50 to 150 nucleotides. Generally, they contain multiple copies of the penta-nucleotide AUUUA motif, and have a high content of uridine (U) residues and sometimes of adenosine (A) residues (reviewed in refs [28,29]). AREs are capable of binding to RBPs, such as Hu-antigen R (HuR) (reviewed in ref. [30]), ARE-binding factor-1 (AUF-1) (reviewed in ref. [31]), tristetraprolin (TTP) (reviewed in refs [32,33]), nuclear factor 90 (NF-90) (reviewed in ref. [34]) and T-cell intracellular antigen 1 (TIA-1)/TIA-1-related protein (TIAR) (reviewed in ref. [35]). Such interactions can induce the stabilization or destabilization of RNA mediated by mechanisms that depend on the RBPs. Indeed, mRNA stability is an important factor in the control of gene expression. Many studies have shown that the mRNA 3′-untranslated region (3′-UTR) plays an important role in the regulation of gene expression at the post-transcriptional level, and it is well known to stabilize or destabilize other mRNAs encoding a wide range of cytokines, growth factors and proto-oncogenes (reviewed in refs [32,36–38]).

In general, the 3′-UTRs of human TPD52 family mRNAs are longer than the coding regions; in particular, that of TPD52 mRNA is quite long at ∼3300 nucleotides, and it harbors 15 AUUUA pentamer motifs. This evidence led us to hypothesize that the 3′-UTRs of TPD52 family mRNAs are involved in the post-transcriptional regulation of their own gene expression as a *cis*-acting element, and we thus focused on the role of this structure in RNA stability. As a result, we uncovered in the present study that the 3′-UTRs of TPD52, 53 and 54 mRNAs regulate the expression of their respective genes in a post-transcriptional manner by altering mRNA stability, and that TIA-1/TIAR binds to one of the minimal *cis*-acting elements (∼200 nucleotides in length) of the 3′-UTR of TPD52 mRNA as a *trans*-acting factor, playing a critical role in stabilizing TPD52 mRNA, which undergoes a negative feedback loop downstream from transforming growth factor-β (TGF-β) and epidermal growth factor (EGF) signaling.

Materials and methods

Cell cultures

Normal human periodontal ligament fibroblasts (Lonza, Basel, Switzerland), SAS cells [39] and HeLa cells (kind gifts from Dr Niitsu, Sapporo Medical University) were grown in high-glucose Dulbecco's modified Eagle's medium supplemented with 10% fetal bovine serum. All cells were maintained at 37°C in an atmosphere containing 5% CO_2 and 100% humidity.

Reagents

Recombinant human TGF-β1 and EGF were purchased from R&D (Minneapolis, MN, U.S.A.). Actinomycin D, endoribonuclease-prepared small interfering RNAs (esiRNAs) for human TIA-1 and TIAR, and control esiRNA (for firefly luciferase) were purchased from Sigma–Aldrich (St Louis, MO, U.S.A.). Anti-HuR, anti-TIA-1/TIAR, anti-AUF-1, anti-TTP and anti-NF-90 antibodies as well as preimmune rabbit IgG were purchased from Santa Cruz (Dallas, TX, U.S.A.). Anti-TIA-1 and anti-TIAR antibodies were purchased from Medical & Biological Laboratories (Aichi, Japan). Anti-lamin B1 and anti-α-tubulin antibodies were purchased from Cell Signaling Technology (Danvers, MA, U.S.A.). Anti-TPD52 antibody was purchased from Abcam

Biochemical Journal (2017) **474** 1669–1687
DOI: 10.1042/BCJ20160942

(Branford, CT, U.S.A.), and anti-TPD53 and 54 antibodies were purchased from Proteintech (Rosemont, IL, U.S.A.). Unless otherwise specified, the other reagents were purchased from a standard supplier.

Protein preparation and Western blot analysis

Total cellular proteins were prepared as described previously [40]. Proteins from the nuclear and cytosolic fractions were extracted using the CelLytic NuCLEAR Extraction Kit (Sigma–Aldrich). For Western blot analysis, 20 μg of protein was subjected to sodium dodecyl sulfate–polyacrylamide gel electrophoresis (SDS–PAGE) on a 4–20% gradient gel (Bio-Rad, Hercules, CA, U.S.A.). The blot was then transferred onto a polyvinylidene difluoride membrane with iBlot 2 (Thermo Fisher, Waltham, MA, U.S.A.). The subsequent blocking, primary antibody reaction, secondary horseradish peroxidase-conjugated antibody (GE Healthcare, Buckinghamshire, U.K.) reaction and washing steps were performed as described previously [40]. The bands were visualized using Amersham ECL Western Blotting Detection Reagents (GE Healthcare) and a ChimiDoc XRS Plus ImageLab System (Bio-Rad).

RNA immunoprecipitation assay

The RNA immunoprecipitation (RIP) assay was carried out using the RiboCluster Profiler RIP assay kit (Medical & Biological Laboratories) and protein G sepharose beads (Sigma–Aldrich) according to the manufacturers' protocols. Cellular RNA was pulled down with anti-HuR, anti-TIA-1/TIAR (or anti-TIA-1 and anti-TIAR), anti-AUF-1, anti-TTP and anti-NF-90 antibodies, and preimmune rabbit IgG. The co-precipitated RNA was purified and sequentially subjected to RT-PCR for TPD52, 53 and 54, and glyceraldehyde 3-phosphate dehydrogenase (GAPDH) (Figure 1) or green fluorescent protein (GFP) (Figures 6 and 9).

Purification of total RNA, cDNA synthesis, RT-PCR and RT-qPCR

Total cellular RNA was purified using TRIsol (Thermo Fisher, Waltham, MA, U.S.A.). Ten nanograms of total RNA were reverse-transcribed using the iScript cDNA Synthesis Kit (Bio-Rad), and an aliquot of the reverse-transcribed cDNA was diluted 1:20 to prepare the reaction mixture for PCR or qPCR. PCR and qPCR were carried out with Takara Ex Taq (Takara Bio, Shiga, Japan) and the KAPA SYBR FAST qPCR kit (Kapa Biosystems, Boston, MA, U.S.A.), respectively. For qPCR, statistical analysis was performed using the Bio-Rad iQ5 analysis software. The fold change in gene expression was calculated using the $2^{-\Delta\Delta C_t}$ method. The gene

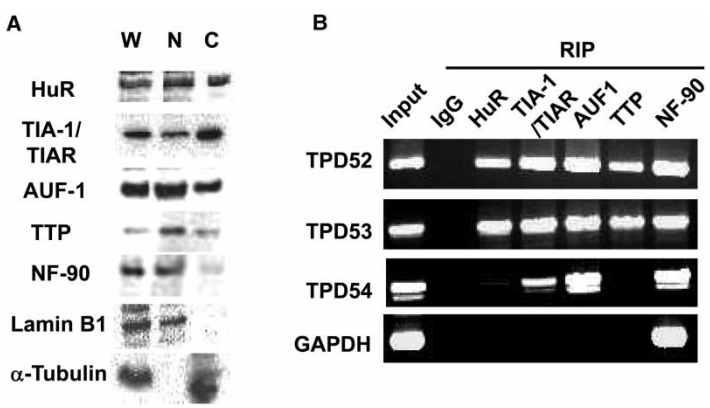

Figure 1. Binding profiles of ARBPs to human TPD52 family mRNAs.

(**A**) Intracellular distribution of ARBPs in SAS cells. Whole cellular (W), nuclear (N) and cytosolic (C) proteins were purified from SAS cells cultured in the absence of a growth factor, and 20 μg of each was subjected to Western blot analysis for HuR, TIA-1/TIAR, TTP, NF-90, Lamin B1 (an internal control for nuclear proteins) and α-tubulin (an internal control for cytosolic proteins). (**B**) Binding profiles of ARBPs to TPD52 family mRNAs. SAS cells were subjected to an RIP assay and subsequent RT-PCR (30 cycles for amplification) for TPD52, 53, 54 and GAPDH using preimmune rabbit IgG (a negative control) and anti-HuR, TIA-1/TIAR, TTP and NF-90 antibodies. On the left lane, 1 μg of total input RNA of SAS cells was subjected to RT-PCR (30 cycles) for TPD52, 53 and 54 as positive controls.

Biochemical Journal (2017) **474** 1669–1687
DOI: 10.1042/BCJ20160942

expression was first normalized to GAPDH for the nuclear run-on assay or 18S rRNA for the other assays within each sample group. All of the primer sequences are presented in Table 1 (qPCR primer pairs).

Nuclear run-on assay

The assay was carried out by supplying biotin-16-UTP (Roche Diagnostics, Mannheim, Germany) to nuclei, and labeled transcripts were bound to streptavidin–agarose beads (Sigma–Aldrich), as described previously [41]. The subsequently pulled down RNA was subjected to RT-qPCR. The transcriptional activity of each gene was normalized against GAPDH.

RNA degradation assay

The assay was carried out by adding actinomycin D (10 μg/ml) to cell cultures, as described previously [42]. Total cellular RNA was isolated at timed intervals and used for RT-qPCR, as described above.

Molecular constructs

The full-length 3′-UTR sequences of human TPD52, 53 and 54 cDNA were amplified from the cDNA of SAS cells using an RT-PCR technique with gene-specific primer pairs (Table 1) in which a terminal codon is located at the 5′-end of each sense primer. The amplified cDNAs were ligated into pcDNA3.1 NT-GFP-TOPO (Thermo Fisher) using a TOPO technique. The proper constructs, in which the sense strand 3′-UTR of TPD52,

Table 1 Primer pairs (sense and antisense strands) used for PCR, qPCR and mutagenesis PCR in the present study

TPD52 qPCR	Sense	GAGGAAGGAGAAGATGTTGC
	Antisense	GCCGAATTCAAGACTTCTCC
TPD53 qPCR	Sense	ACGAAGATGCAGTAGCC
	Antisense	GTCTCAACCCTCTCCTC
TPD54 qPCR	Sense	CATGGACTCCGCCGGCCAAG
	Antisense	CCCACTGTGGACAGGGCAGC
TIA1 qPCR	Sense	TCCCGCTCCAAAGAGTACATATGAG
	Antisense	AAACAATTGCATGTGCTGCACTTTC
TIAR qPCR	Sense	CAACTGGAAAATCCAAAGGCTATGG
	Antisense	GACGCAATTCCTCCACAGTACACAG
18S RNA qPCR	Sense	TCCTGCCAGTAGCATATGCTG
	Antisense	AGAGGAGCGAGCGACCAAAGG
GAPDH qPCR	Sense	GCTCTCCAGAACATCATCCCTGCC
	Antisense	CGTTGTCATACCAGGAAATGAGCTT
GFP qPCR	Sense	GCTACATACGGAAAGCTTACCC
	Antisense	CGAAAGGGCAGATTGTGTC
TPD52 3′-UTR Full	Sense	TGAGATTCCTACCTTTGTTC
	Antisense	GTTGCCAAATAGCATTTATT
TPD53 3′-UTR Full	Sense	TAAGTCCAGCCAGCGTGCAG
	Antisense	GTCATTAAAATCAATTCTTT
TPD54 3′-UTR Full	Sense	TAAGCCTGTGGTTGCTTCAC
	Antisense	AAAGGAATGCTTTATTGACA
TPD52 3′-UTR 1-2073	Sense	Same as TPD52 3′-UTR Full Sense
	Antisense	TCTAGAAAAGTGATTCTCCATT
TPD52 3′-UTR 1-870	Sense	Same as TPD52 3′-UTR Full Sense
	Antisense	GGTAGATGTCTAGATCTAAACTTTCA
TPD52 3′-UTR 871-3523	Sense	TGAAGCTGGTAAAAATGACAATATC
	Antisense	Same as TPD52 3′-UTR Full Antisense
TPD52 3′-UTR 2073-3523	Sense	TGACATCTACCTATACTTAATCTAA
	Antisense	Same as TPD52 3′-UTR Full Antisense
TPD52 3′-UTR 78-280	Sense	CCTTTGATGCCATGAATTTCTACCA
	Antisense	TCATGGCATCAAAGGGCAATTCCACC

Biochemical Journal (2017) **474** 1669–1687
DOI: 10.1042/BCJ20160942

53 or 54 cDNA was ligated to the end of the GFP gene (Figure 3A), were amplified, and these chimeric gene constructs were designated as 'GFP-TPD52 Full', 'GFP-TPD53 Full' or 'GFP-TPD54 Full', respectively. For the construction of deletion mutants (Figures 4A and 5A) of the 3′-UTR of human TPD52 cDNA, several techniques were employed. For the construction of GFP-TPD52 3′-UTR 1-2073, 1-870, 871-3523 and 2073-3523, the deletion mutants were amplified by PCR from GFP-TPD52 Full as a template using primer pairs (TPD52 3′-UTR 1-2073, 1-870, 871-3523 and 2073-3523 in Table 1) and ligated into the pcDNA3.1 NT-GFP-TOPO vector. For the construction of GFP-TPD52 3′-UTR Δ871-2072, GFP-TPD52 Full was digested by *Xba*I and was self-ligated by T4 ligase (Takara Bio). For the construction of GFP-TPD52 3′-UTR 1-280 and 1-77, GFP-TPD52 Full was double-digested by *Dde*I and *Eco*RV, and *Eco*T22I and *Eco*RV, respectively. After enzymatic digestion, the vectors were blunted by T4 DNA polymerase and self-ligated by T4 ligase (Takara Bio). For the construction of GFP-TPD52 3′-UTR 78-280, a mutagenesis PCR was carried out using the PrimeSTAR Mutagenesis Basal Kit (Takara Bio) and mutagenesis primers (TPD52 3′-UTR 78-280 in Table 1). The constructs of all wild-type and deletion-mutant genes were confirmed by nucleotide sequencing.

Flow cytometry analysis

In the present study, we employed a GFP protein located downstream from the cytomegalovirus (CMV) promoter (pcDNA3.1 NT-GFP; Thermo Fisher) as a reporter gene, as described previously [43]. The cells were seeded in a six-well culture plate in the presence or absence of TGF-β1 or EGF (10 ng/ml each). Control GFP (pcDNA3.1 NT-GFP control vector) and chimeric GFP vectors with or without esiRNA were (co-)transfected into the cells using Lipofectamine 2000 (Thermo Fisher). The next day, the expression of GFP protein was measured by flow cytometry (FACSVerse, BD Bioscience, San Jose, CA, U.S.A.). To ensure equal transient transfection of the reporter gene [44,45], each experiment was repeated more than five times, and results that were reproducible more than three times were used.

RNA biotin pull-down assay

The assay was carried out as described recently [46] with a slight modification. The sequences of several deletion mutants of human TPD52 3′-UTR were ligated into pGEM3Zf(−) (Promega, Madison, WI, U.S.A.), and the ligated and unligated pGEM3Zf(−) were linearized by digestion with *Xba*I. In addition, the sequence of full-length 3′-UTR of TPD52 mRNA was ligated into pGEM T-Easy (Promega) by a TA-cloning technique, and the clone, in which the sense strand was positioned from the T7 promoter, was selected and linearized by digestion with *Sal*I. Subsequently, the linearized plasmids were used as templates for the synthesis of biotinylated RNA probes. Biotinylated RNA was transcribed by T7 RNA polymerase (Roche Diagnostics) in the presence of 0.35 mM biotin-16-UTP. After 4 h of incubation at 37°C, 1 μl of RQ1 DNase (Promega) was added to the reaction mixture and was incubated for another 15 min. Non-incorporated nucleotides were removed using a G-25 microspin column (GE Healthcare) and subsequent ethanol precipitation. For RNA–protein binding, 5 μg of biotinylated RNA probe and 100 μg of cytosolic protein from SAS cells were incubated at 4°C for 16 h in 500 μl of 1× IP buffer (Sigma–Aldrich) supplemented with 5 μl of protein inhibitor cocktail (Sigma–Aldrich) and 5 μl of RNase inhibitor (Takara Bio). The RNA–protein complexes were precipitated using 20 μl of streptavidin–agarose beads (Sigma–Aldrich) in 500 μl of 1× IP buffer at room temperature for 4 h. The beads were washed five times with 1× IP buffer and once with 0.1× IP buffer (500 μl each time), and precipitated using a centrifuge. The beads were then directly denatured with 1× SDS–PAGE sample buffer (Bio-Rad) containing 5% of 2-mercaptoethanol (Wako, Osaka, Japan), and the extracts were directly subjected to Western blot analysis.

Statistical analysis

Unless otherwise specified, all experiments were repeated at least three times, and similar results were obtained in the repeated experiments. Statistical analysis of the repeatability of the assay results was carried out using a paired Student's *t*-test. Data are expressed as the means ± standard deviation of triplicate data.

Results

TPD52 family mRNAs bind to RBPs

As shown in Supplementary Figure S1, the 3′-UTR of the human TPD52 cDNA is much longer than the coding region, and it harbors 15 AUUUA pentamers and several AUUUA pentamer-like sequences, suggesting

Biochemical Journal (2017) **474** 1669–1687
DOI: 10.1042/BCJ20160942

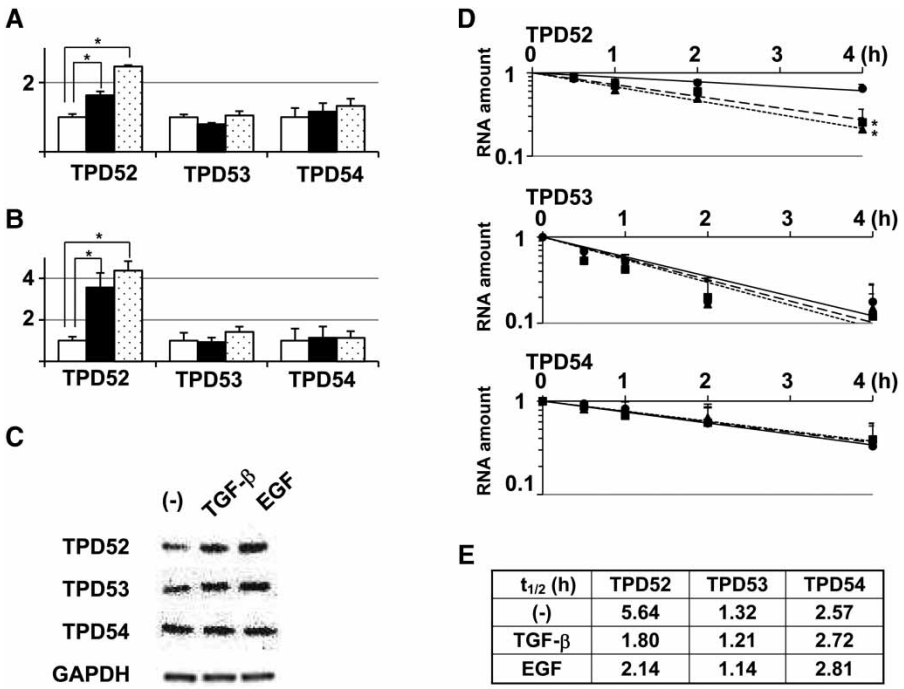

$t_{1/2}$ (h)	TPD52	TPD53	TPD54
(-)	5.64	1.32	2.57
TGF-β	1.80	1.21	2.72
EGF	2.14	1.14	2.81

Figure 2. TPD52 family genes undergo post-transcriptional regulation.

SAS cells were cultured in the absence (open boxes and solid lines) or presence of 10 ng/ml of TGF-β1 (closed boxes and hatched lines) or EGF (shaded boxes and dotted lines) for 24 h, and then the cells were subjected to RT-qPCR for steady-state mRNA (**A**), a nuclear run-on assay (**B**), Western blotting analysis using 20 μg of total cellular protein (**C**) and an RNA degradation assay (**D** and **E**) for TPD52, 53 and 54. For RT-qPCR for the steady-state mRNA and the nuclear run-on assay, the values of control cells (**A** and **B**) were designated as '1', and relative values are shown. For the RNA degradation assay, the steady-state amount of RNA at time 0 was designated as '1', and relative values with the SD are plotted on a semi-logarithmic graph. At the bottom of (**D**), the calculated half-life ($t_{1/2}$) of each mRNA is shown in hours (**E**). *$P < 0.05$ versus each control.

its ability to bind to RBPs. Although TPD53 and 54 cDNAs also have these features, the length of their cDNAs is shorter than that of TPD52. Therefore, we first investigated whether TPD52 family mRNAs are capable of binding to several representative RBPs, including HuR, TIA-1/TIAR, AUF-1, TTP and NF-90 (Figure 1). Western blotting analysis (Figure 1A) revealed the presence of RBPs in the cytosolic and nuclear fractions of SAS cells. However, the subcellular distribution differed for each RBP. For instance, TIA1/TIAR located predominantly in the cytosol, whereas NF-90 located predominantly in the nucleus. AUF-1 and TTP located predominantly in the nucleus, whereas HuR uniformly existed in both the nucleus and the cytosol. Next, cells were subjected to the RIP assay (Figure 1B). TPD52 and 53 mRNAs bound to all of the RBPs, whereas TPD54 mRNA bound to only TIA-1/TIAR, AUF-1 and NF-90. The results that the preimmune rabbit IgG did not bind to TPD52, 53 and 53 mRNAs, and that NF-90 bound only to GAPDH mRNA were in agreement with the results of a previous study [47], and demonstrated the stringency of the RIP assay.

The stability of TPD52 mRNA is altered in cell-specific and stimulation-specific manners

Since the results from the previous subsection indicated the possibility that TPD52 family mRNAs might be post-transcriptionally regulated, we investigated the relationships between the steady-state amount, transcriptional activity and stability of TPD52, 53 and 54 mRNAs in SAS cells (Figure 2). TPD52 family proteins, with the exception of TPD55, were reported to be robustly expressed in several types of cancer cells [10–22], and many studies have reported that these cells generally secrete various growth factors, including TGF-β1 and EGF, in an autocrine manner, resulting in the up-regulation of various oncogenes and the enhancement of cell proliferation; thus, it was suggested that these growth factors might modulate the expression of TPD52 family genes, although the molecular relationship between these growth factors and TPD52 family genes has scarcely been reported.

Biochemical Journal (2017) **474** 1669–1687
DOI: 10.1042/BCJ20160942

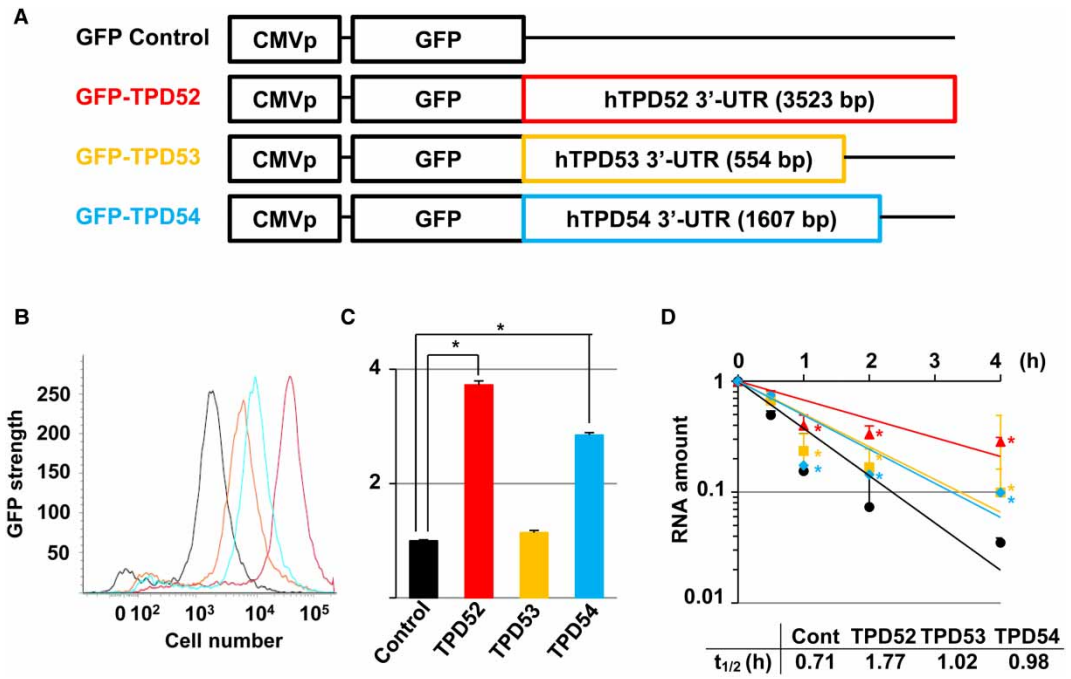

Figure 3. Effects of the 3′-UTRs of TPD52 family mRNA on post-transcriptional regulation using the GFP reporter gene system.

(**A**) A schematic representation of the chimeric GFP reporter genes. Full-length cDNAs of human TPD52, 53 or 54 mRNA 3′-UTR were ligated to the 3′-end of the GPF gene downstream from a CMV promoter. (**B**–**D**) Control (black) and chimeric GFP (GFP-TPD52 (red), 53 (orange) and 54 (blue)) genes were transfected into SAS cells, and the cells were cultured for 2 days in the absence of a growth factor. Then, the cells were subjected to flow cytometry (**B**), RT-qPCR (**C**) for steady-state mRNA and an RNA degradation assay (**D**) for the GFP reporter gene. For measuring steady-state mRNA, the value of the control GFP mRNA was designated as '1', and relative values are shown. For the RNA degradation assay, the amount of mRNA at time 0 was designated as '1', and relative values with the SD are plotted on a semi-logarithmic graph. At the bottom of the RNA degradation assay, the calculated half-life ($t_{1/2}$) of each control and chimeric gene is shown in hours. *$P < 0.05$ versus each control.

RT-qPCR for steady-state mRNAs (Figure 2A) revealed that the steady-state mRNA level of TPD52 was increased by stimulation with TGF-β1 and EGF. However, those of TPD53 and 54 barely changed ($P > 0.05$). Western blotting analysis (Figure 2C) results for the protein expressions of TPD52, 53 and 54 were in agreement with the total amount of each mRNA. Nuclear run-on (Figure 2B) and RNA degradation (Figure 2D,E) assays showed that the transcriptional activities of the TPD53 and 54 genes reflected the amount of steady-state mRNA, and that mRNA stability was barely changed by stimulation with TGF-β1 and EGF. However, for the TPD52 gene, the transcriptional activity did not always correspond with the amount of steady-state mRNA: namely, the transcriptional activity was strong for the amount of steady-state mRNA detected. Importantly, the RNA degradation assay demonstrated that the stability of TPD52 mRNA decreased faster after stimulation with TGF-β1 and EGF (Figure 2D). These results indicated that the mRNA stability of TPD52 plays a more important role in the post-transcriptional regulation of gene expression when compared with TPD53 and 54.

The 3′-UTR of TPD52 family mRNAs is mainly involved in post-transcriptional regulation

To investigate the role of the 3′-UTRs of TPD52 family mRNAs in post-transcriptional regulation, we carried out a reporter assay employing GFP as a reporter [43–45]. As shown in Figure 3A, the 3′-UTRs of TPD52, 53 and 54 mRNAs were ligated to the 3′-end of a GFP gene downstream from a CMV promoter. Then, the control GFP vector (Control GFP) and three chimeric vectors (GFP-TPD52, 53 and 54) were transfected into SAS cells, and flow cytometry was carried out to measure the intensity of GFP fluorescence (Figure 3B). Contrary to our expectation, the 3′-UTRs of TPD52, 53 and 54 showed enhancing effects on the expression of the reporter gene: namely, the 3′-UTR of TPD52 mRNA strongly enhanced the expression of the reporter,

Biochemical Journal (2017) **474** 1669–1687
DOI: 10.1042/BCJ20160942

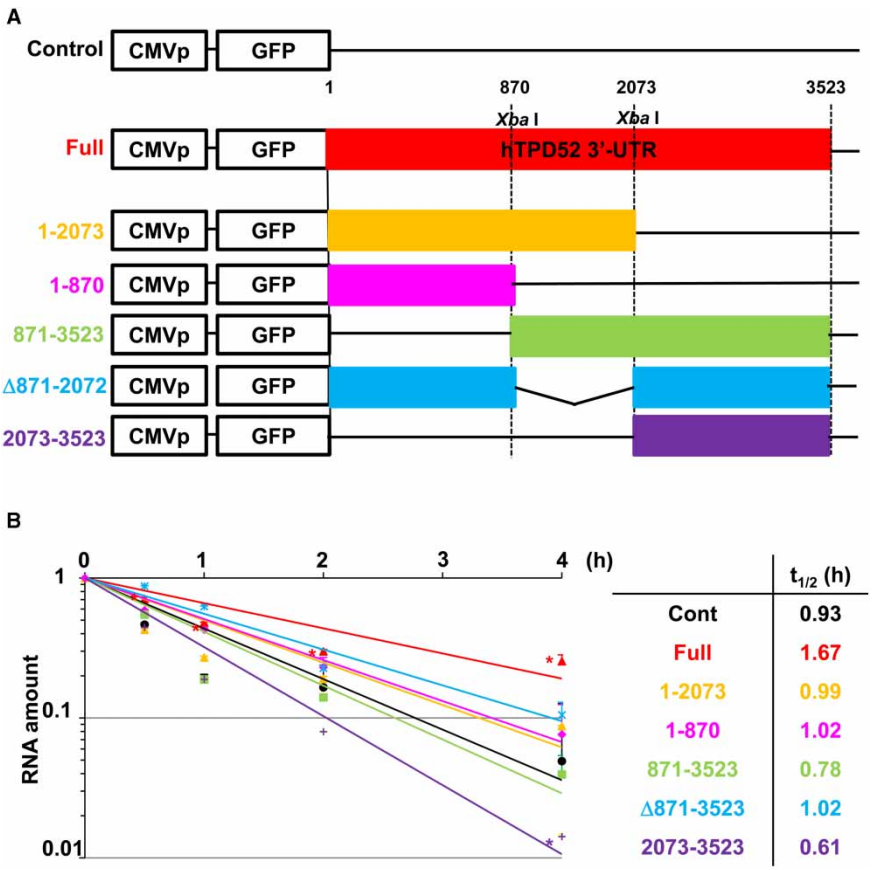

Figure 4. Identification of a minimum functional *cis*-acting element in the human TPD52 mRNA 3′-UTR for reporter GFP gene expression (1).

(**A**) A schematic representation of the deletion cDNAs. Full-length (Full) or deletion-mutant (1-2073 to 2073-3523) cDNAs of the human TPD52 mRNA 3′-UTR were ligated to the 3′-end of the GPF gene downstream from a CMV promoter. At the top, the restriction enzymes used for the construction of the deletion mutants are shown (see 'Materials and methods'). (**B**) RNA degradation assay. Control GFP and chimeric GFP-TPD52 deletion-mutant genes (shown in **A**) were transfected into SAS cells, and the cells were cultured for 2 days in the absence of a growth factor. Then, the cells were subjected to an RNA degradation assay for GFP reporter gene stability. On the right side, the calculated half-life ($t_{1/2}$) of each control and chimeric gene is shown in hours. *$P < 0.05$ versus the control.

whereas that of TPD53 and 54 mRNAs showed weaker effects. Next, we investigated the effects of the 3′-UTRs of TPD52, 53 and 54 mRNAs on the stability of reporter mRNA. The amount of steady-state mRNA correlated to the expression level of the reporter (Figure 3C). Importantly, the enhanced amount of steady-state reporter mRNA was dependent on mRNA stability (Figure 3D). These results indicated that the 3′-UTRs of TPD52, 53 and 54 mRNAs harbor RNA stabilizers, and that the TPD52 mRNA has a stronger RNA-stabilizing effect than TPD53 and 54 mRNAs. Therefore, we subsequently focused on the 3′-UTR of TPD52 mRNA and further investigated its detailed functions in the following experiments.

A minimal *cis*-acting element of TPD52 mRNA is located at the 5′-proximal region of the 3′-UTR

We attempted to seek out the element involved in the strong enhancement of the mRNA stability of the reporter gene. First, we constructed five deletion mutants of the 3′-UTR of the TPD52 mRNA (1-2073 to 2073-3523 in Figure 4A). The full-length 3′-UTR showed the strongest enhancing effect for the stability of the reporter gene mRNA, while the deletion mutants of the 1-2073 and 1-870 fragments showed the second and third strongest stabilizing effect, respectively (Figure 4B). Interestingly, the deletion mutants lacking the 871-3523 and 2073-3523 fragments destabilized the reporter genes, indicating that these fragments contain one

Biochemical Journal (2017) **474** 1669–1687
DOI: 10.1042/BCJ20160942

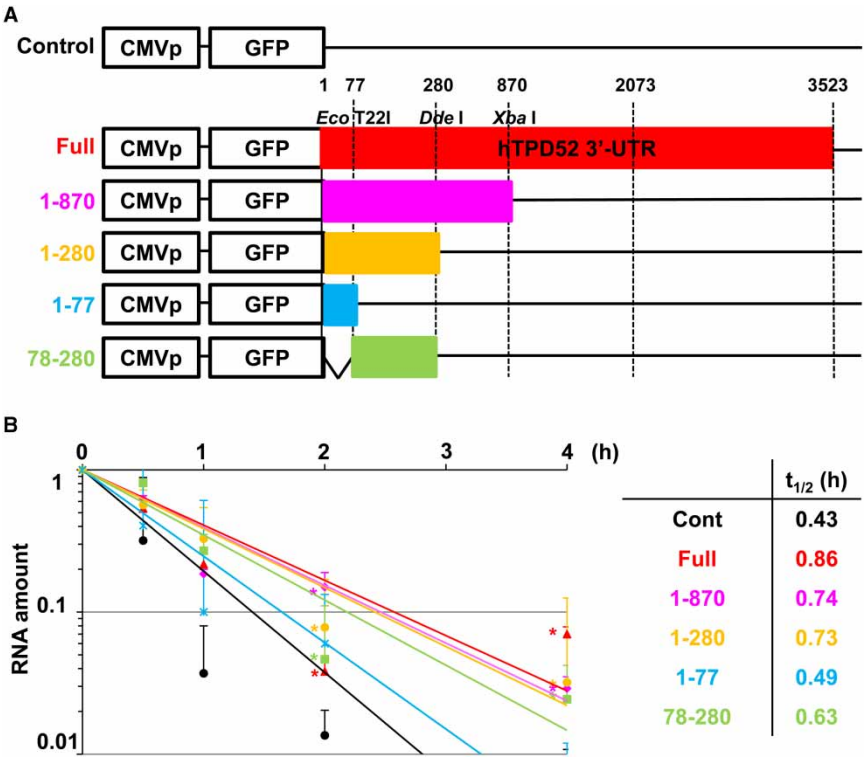

Figure 5. Identification of a minimum functional *cis*-acting element in the human TPD52 mRNA 3′-UTR for reporter GFP gene expression (2).

(**A**) A schematic representation of the deletion cDNAs. Full-length (Full) or deletion-mutant (1-870 to 28-280) cDNAs of the human TPD52 mRNA 3′-UTR were ligated to the 3′-end of the GPF gene downstream from a CMV promoter. At the top, the restriction enzymes used for the construction of the deletion mutants are shown (see 'Materials and methods'). (**B**) RNA degradation assay. Control GFP and chimeric GFP-TPD52 deletion-mutant genes (shown in **A**) were transfected into SAS cells, and the cells were cultured for 2 days in the absence of a growth factor. Then, the cells were subjected to an RNA degradation assay for GFP reporter gene stability. On the right side, the calculated half-life ($t_{1/2}$) of each control and chimeric gene is shown in hours. *$P < 0.05$ versus the control.

or more destabilizing *cis*-elements, even though the stabilizing elements are present elsewhere. Therefore, we concluded that the 1-870 fragment harbors the strongest *cis*-element that enhances mRNA stability. Next, deletion mutants with shorter sequences from the 1-870 region were constructed (1-280, 1-77 and 78-280 in Figure 5A). The results of the RNA degradation assay (Figure 5B) showed that the full-length 3′-UTR enhanced the stability of the reporter mRNA the most, followed by the 1-870 and 1-280 fragments. The 1-77 fragment showed a very weak effect, suggesting little involvement of the 1-77 fragment within the 1-280 region. Importantly, the 78-280 fragment still showed stabilizing effects, although the effect was weaker than that of the full-length 3′-UTR. These results indicate that a minimal *cis*-acting element for enhancing RNA stability exists in the 78-280 region.

The 78-280 region binds to TIA-1/TIAR

Next, we searched for a *trans*-acting factor capable of binding to the 78-280 region. The biotin pull-down (Figure 6A) and RIP (Figure 6B) assays showed that the 1-280 and 78-280 fragments bound only to TIA-1/TIAR, and not to HuR, AUF-1, TTP or NF-90, even though the full-length 3′-UTR bound to all of the AU-rich element binding proteins (ARBPs). These results indicated that TIA-1/TIAR, at the least, is a *trans*-acting factor that binds to the *cis*-acting 78-280 fragment, and this binding might regulate the stability of TPD52 mRNA.

Biochemical Journal (2017) **474** 1669–1687
DOI: 10.1042/BCJ20160942

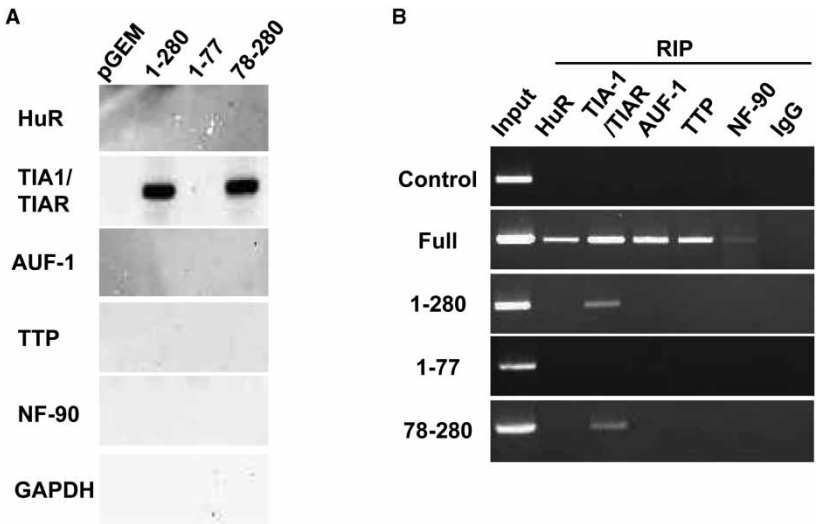

Figure 6. Binding profiles of the cytosolic proteins of SAS cells to the human TPD52 mRNA 3′-UTR fragment.
(**A**) Biotin pull-down assay. Four biotin-labeled RNA fragments (pGEM, 1-280, 1-77 and 78-280) corresponding to the ones shown in Figure 5A were incubated with cytosolic protein from SAS cells cultured in the absence of a growth factor. The biotin-labeled RNA–protein complex was pulled down using streptavidin–sepharose beads. Then, the co-precipitated proteins were eluted and were subjected to Western blot analysis for HuR, TIA-1/TIAR, AUF-1, TTP, NF-90 and GAPDH. (**B**) RIP assay. Control GFP and three chimeric GFP-TPD52 deletion-mutant genes (1-280, 1-77 and 78-280) were transfected into SAS cells, and the cells were cultured for 2 days in the absence of a growth factor. Then, the cells were subjected to an RIP assay for the GFP gene using anti-HuR, TIA-1/TIAR, TTP and NF-90 antibodies and preimmune IgG (as a negative control). On the left lane, 1 μg of total input RNA was also subjected to RT-PCR for the GFP gene. The amplification cycle of subsequent RT-PCR was 25.

Knockdown of TIA-1/TIAR decreases the stability of TPD52 mRNA

The roles of TIA-1 and TIAR on the stability of TPD52 mRNA were investigated by employing esiRNAs against TIA-1 and TIAR in SAS cells. Western blotting analysis (Figure 7A) revealed successful knockdown of TIA-1 and TIAR by each esiRNA. The nuclear run-on assay (Figure 7B) showed no decrease in TPD52 transcriptional activity ($P > 0.05$ for each cell type). However, RT-qPCR for steady-state RNA (Figure 7C) showed a significant decrease in TPD52 mRNA, indicating that the effects were caused not at the transcriptional level, but at the post-transcriptional level. Furthermore, the RNA degradation assay (Figure 7D) revealed that knockdown of TIA-1 and TIAR triggered a decrease in the stability of TPD52 mRNA, demonstrating that the TPD52 mRNA-stabilizing ability of TIA-1 and TIAR is due to their role as a *trans*-acting factor. The same experiments were carried out in HeLa cells and fibroblasts (Supplementary Figure S2); similar results were observed in these cells as in SAS cells, suggesting that the important role of TIA-1 and TIAR as a *trans*-acting factor in stabilizing TPD52 mRNA is not dependent on cell type.

Specific interaction between the 78-280 fragment and TIA-1/TIAR

Then, we investigated the 78-280 fragment-specific effects on expression and RNA stability of the reporter via knockdown of TIA-1 and TIAR in SAS cells (Figure 8). As expected, the expression and mRNA stability of the control fragments were not affected by knockdown of TIA-1 or TIAR (Figure 8A,D). However, the expression and mRNA stability of the GFP full-length 3′-UTR were slightly attenuated by knockdown of TIA-1 and TIAR (Figure 8B,E). The expression of the GFP 78-280 fragment was also decreased by TIA-1 and TIAR knockdown (Figure 8C), and notably, the stability of these mRNAs was more significantly decreased when compared with full-length RNAs (Figure 8F), indicating the 78-280 region as a crucial *cis*-acting element for the stability of TPD52 mRNA. These results indicated that the 78-280 fragment and TIA-1/TIAR function in maintaining mRNA stability as a *cis*-acting element and *trans*-acting factor(s), respectively, and that the specific interaction between them might play a critical role, at least in part, in the post-transcriptional regulation of the TPD52 gene.

Biochemical Journal (2017) **474** 1669–1687
DOI: 10.1042/BCJ20160942

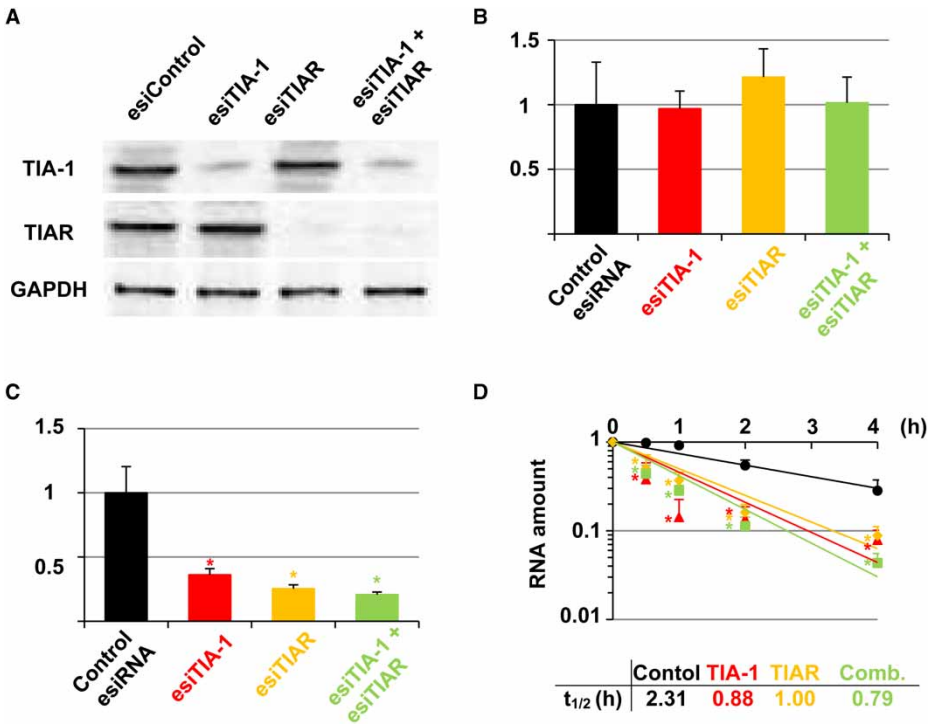

Figure 7. Effects of the knockdown of TIA-1 and TIAR on the transcriptional activity and steady-state expression of the TPD52 gene.

(**A**) Western blotting analysis. Control esiRNA, esiRNA for TIA-1 and TIAR or a combination were transfected into SAS cells. After 24 h, the medium was replaced with fresh medium, and the cells were cultured in the absence of a growth factor for another 24 h. Then, total cellular proteins were collected, and 20 μg of each was subjected to Western blotting analysis for TIA-1, TIAR and GAPDH (an internal control). (**BD**) Control esiRNA (black), esiRNA for TIA-1 (red) and TIAR (orange) or a combination (green) were transfected into SAS cells. After 24 h, the medium was replaced with fresh medium, and the cells were cultured in the absence of a growth factor for another 24 h. Then, the cells were subjected to a nuclear run-on assay (**B**), RT-qPCR for total cellular RNA (**C**) and an RNA degradation assay (**D**) for TPD52. The gene expression was first normalized to GAPDH (for the nuclear run-on assay) or 18S rRNA (for RT-qPCR) within each sample group; the value of the control esiRNA was designated as '1', and relative values are shown. For the RNA degradation assay, the steady-state amount of RNA at time 0 was designated as '1', and relative values with the SD are plotted on a semi-logarithmic graph. At the bottom, the calculated half-life ($t_{1/2}$) of each control and chimeric gene is shown in hours. *$P < 0.05$ versus the control esiRNA.

Stimulation of TGF-β and EGF decreased not only the binding of TIA-1/TIAR to the 78-280 region, but also the stability of reporter mRNA

As described in Figure 2, stimulation of TGF-β and EGF decreased the stability of TPD52 mRNA, resulting in a negative feedback loop in the subsequent gene expression. Therefore, we investigated the effects of these growth factors on the binding profile of the 3′-UTR of TPD52 mRNA and on expression and mRNA stability of chimeric reporter genes (Figure 9). Western blotting analysis (Figure 9A) showed that stimulation of TGF-β and EGF scarcely altered the total cellular protein expression or subcellular distribution of TIA-1 and TIAR. Biotin pull-down (Figure 9B) and RIP (Figure 9C) assays showed little effect of these growth factors on the binding of TIA-1 and TIAR to full-length 3′-UTR of TPD52 mRNA, while those proteins did not bind to control RNAs. Interestingly, however, the binding ability of TIA-1 and TIAR to the 78-280 region, a minimal *cis*-acting element for mRNA stability, was significantly decreased, although the binding affinity was weaker than that of full-length 3′-UTR. Furthermore, the expression of the reporter GFP protein, measured by flow cytometry (Figure 9D), was decreased by the stimulation of the growth factors, and the RNA degradation assay (Figure 9E) showed that these effects were caused by the decrease in mRNA stability. Of note, the decreasing ability of TGF-β and EGF on the stability of the reporter gene was more effective for the 78-280 region than

Biochemical Journal (2017) **474** 1669–1687
DOI: 10.1042/BCJ20160942

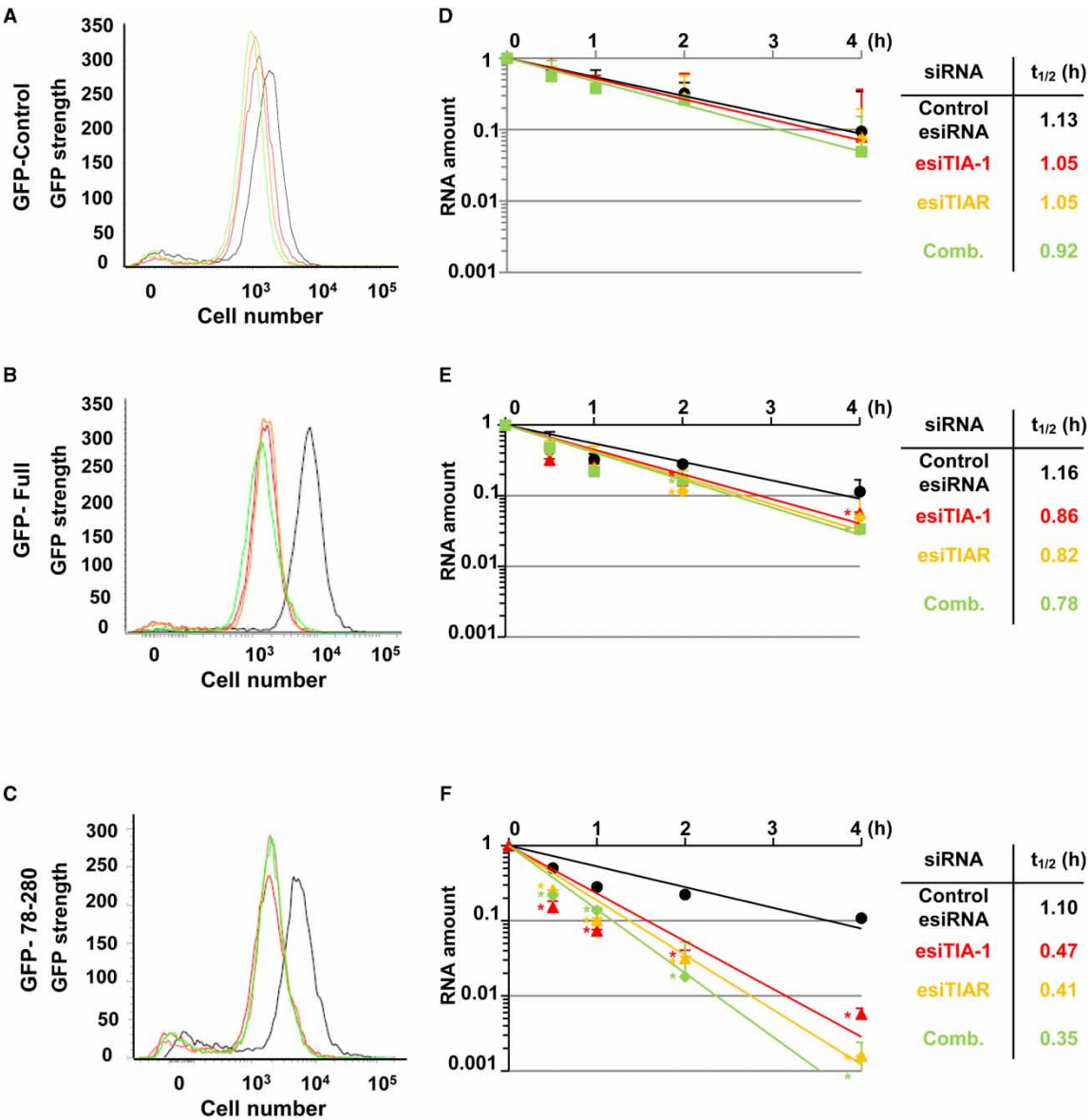

Figure 8. Effects of knockdown of TIA-1 and TIAR on expression and mRNA stability of the GFP chimeric reporter gene.
Control GFP and chimeric GFP-TPD52 full (GFP-Full) and deletion-mutant (GFP-78-280), as shown in Figure 5A, in the presence of control esiRNA (black), esiRNA for TIA-1 (red) and TIAR (orange), or a combination of esiRNAs (green), were co-transfected into SAS cells, and the cells were cultured for 2 days. Then, the cells were subjected to flow cytometry (**AC**) for GFP reporter gene expression and an RNA degradation assay (**D–F**) for GFP reporter gene stability. On the right side, the calculated half-life ($t_{1/2}$) of each control and chimeric gene is shown in hours. *$P < 0.05$ versus the esiRNA control.

for full-length, suggesting that this region may be a crucial *cis*-acting element on mRNA stability in the negative feedback loop, which is triggered by the stimulation of TGF-β and EGF.

Stimulation of TGF-β and EGF has additive effects on decreased protein expression and mRNA stabilization of the reporter gene in TIA-1/TIAR-knocked-down cells.

Finally, we examined the additive or synergistic effects of TGF-β and EGF along with knockdown of TIA-1 and TIAR on reporter genes. The GFP reporter gene assay (Supplementary Figure S3) showed that the expressions

Biochemical Journal (2017) **474** 1669–1687
DOI: 10.1042/BCJ20160942

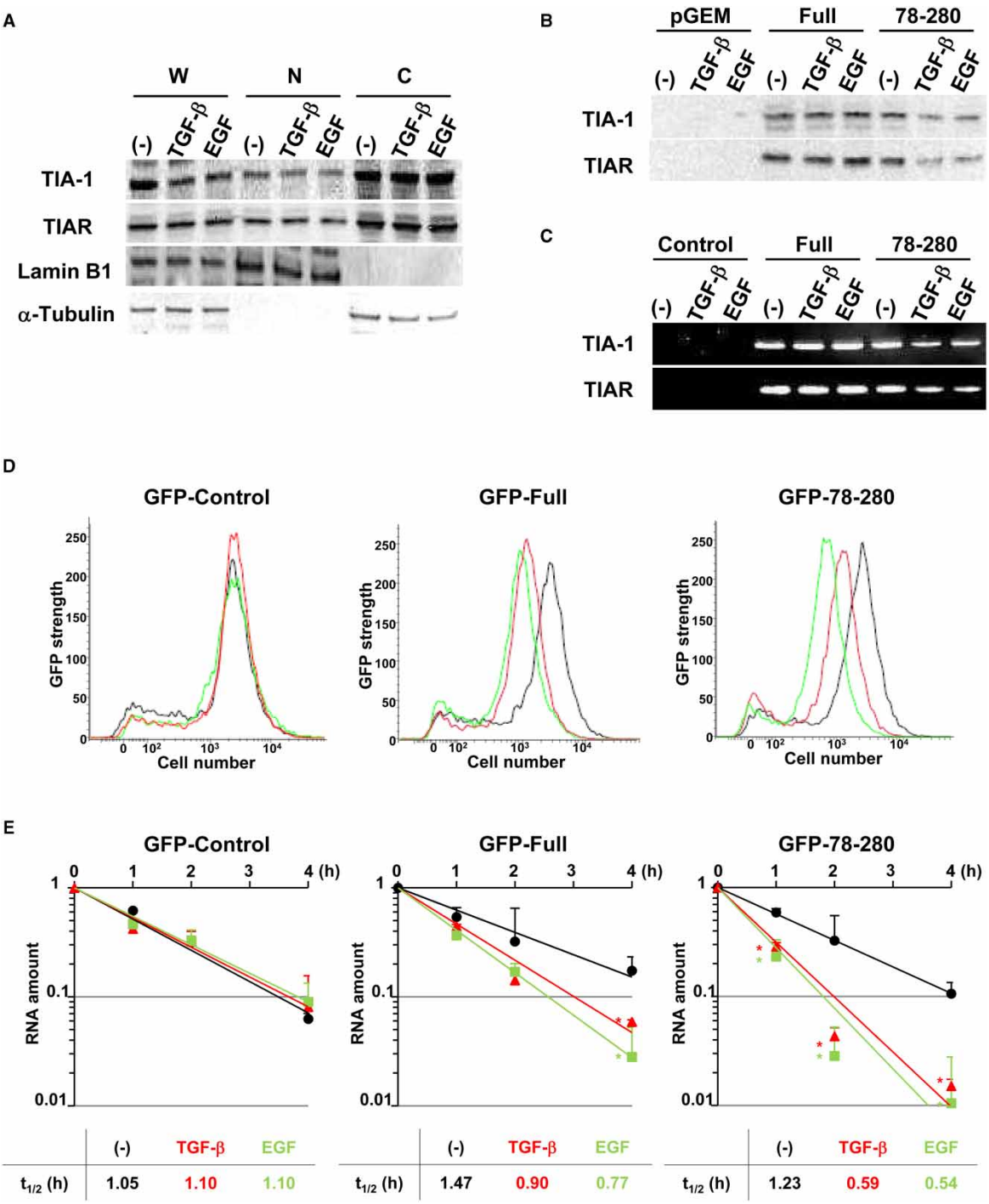

Figure 9. Effects of TGF-β and EGF on the binding profile of TIA-1 and TIAR to 3′-UTR of TPD52 mRNA and on expression and mRNA stability of the GFP chimeric reporter gene. Part 1 of 2

(**A**) Western blotting analysis. SAS cells were cultured in the absence (–) or presence of 10 ng/ml of TGF-β1 or EGF for 24 h. Then, whole cellular (W), nuclear (N) and cytosolic (C) proteins were purified, and 20 μg of each was subjected to Western blot analysis for TIA-1, TIAR, Lamin B1 and α-tubulin. (**B**) Biotin pull-down assay. SAS cells were cultured in the absence (–) or presence of 10 ng/ml TGF-β1 or EGF for 24 h, and then cytosolic proteins were purified. Three biotin-labeled RNA fragments (pGEM, Full and 78-280) corresponding to the ones shown in Figure 5A were incubated with the cytosolic proteins from SAS cells. The biotin-labeled RNA–protein complex was pulled down using streptavidin–sepharose beads. Then, the co-precipitated proteins were eluted and subjected to Western blot analysis for TIA-1 and TIAR. (**C**) RIP assay. Control GFP (Control), chimeric

Biochemical Journal (2017) **474** 1669–1687
DOI: 10.1042/BCJ20160942

Figure 9. Effects of TGF-β and EGF on the binding profile of TIA-1 and TIAR to 3′-UTR of TPD52 mRNA and on expression and mRNA stability of the GFP chimeric reporter gene. Part 2 of 2

GFP-TPD52 full (Full) and GFP-78-280 (78-280) genes were transfected into SAS cells. After 24 h, the medium was replaced with fresh medium, and the cells were cultured in the absence (–) or presence of 10 ng/ml TGF-β1 or EGF for another 24 h. Then, the cells were subjected to an RIP assay for the GFP gene using anti-TIA-1 and TIAR antibodies. The amplification cycle of subsequent RT-PCR was 25. (**D** and **E**) Flow cytometry and RNA degradation assay. Control GFP, chimeric GFP-TPD52 full and GFP-78-280 genes were transfected into SAS cells. After 24 h, the medium was replaced with fresh medium, and the cells were cultured in the absence (black) or presence of 10 ng/ml TGF-β1 (red) or EGF (green) for another 24 h. Then, the cells were subjected to flow cytometry (**D**) for GFP reporter gene expression and an RNA degradation assay (**E**) for GFP reporter gene stability. For the RNA degradation assay, the steady-state amount of RNA at time 0 was designated as '1', and relative values with the SD are plotted on a semi-logarithmic graph. At the bottom, the calculated half-life ($t_{1/2}$) of each control and chimeric gene is shown in hours. *$P < 0.05$ versus the control.

of the GFP-Full and -78-280 reporter genes were decreased by induction of esiRNAs for TIA-1 and TIAR, and were more effectively attenuated by stimulation of TGF-β and EGF, while these growth factors and esiRNAs had no effect on GFP-Control. RNA degradation assay (Figure 10) showed that the decreasing effects on reporter gene expression were caused by decreased mRNA stability. Knockdown of TIA-1 and TIAR decreased mRNA stability of GFP-Full and GFP-78-280, and the decreasing effects were more prominent in GFP-78-280 than in GFP-Full, in agreement with the results in Figure 8. Stimulation of TGF-β and EGF showed more decreased mRNA stability in these reporter genes, and these effects were likely to be additive, not synergistic. Of note, the stability of GFP-78-280 mRNA was most unstable by the combination of TGF-β/EGF stimulation and knockdown of TIA-1/TIAR ($t_{1/2} < 0.37$ h). These results reinforced the notion that the 78-280 region is a key *cis*-acting element of a negative feedback loop for mRNA stability, which is regulated by the binding of TIA-1/TIAR as a *trans*-acting factor and is located downstream from TGF-β and EGF stimulation.

Discussion

Since the first identification of TPD52, many physiological and pathological roles for TPD52 family genes have been demonstrated [2,3]. However, to the best of our knowledge, there have been no reports on the molecular mechanisms underlying their gene expression. Recently, we found that TPD52 and 54 concordantly regulate growth, invasion and metastasis in OSCCs (unpublished data), indicating crucial physiological and/or pathological roles of TPD52 and 54 in OSCCs, as were also observed in other cancer cells. In the present study, we were interested in and investigated the molecular regulatory mechanism of TPD52 family genes, particularly at the post-transcriptional level, in OSCCs, such as SAS cells. The RIP assay (Figure 1) revealed specific binding of TPD52, 53 and 54 mRNAs to RBPs, and the RNA degradation assay (Figure 2) indicated the involvement of the post-transcriptional regulation of the mRNAs in RNA stability. We thus hypothesized that the 3′-UTRs of TPD52, 53 and 54 mRNAs might play a more important role in RNA instability than in RNA stability. However, to our surprise, the reporter gene and RNA degradation (Figure 3) assays demonstrated the prominent positive involvement of TPD52 mRNA in RNA stability. The 3′-UTR of TPD52 mRNA is much longer than the coding region, and it harbors 15 AUUUA pentamer motifs (Supplementary Figure S1). The AUUUA pentamer motif is a well-known ARE that is found in many RNAs [48,49], and it plays a crucial role in the stabilization or destabilization of mRNAs [50,51]. Moreover, the number of AREs present in the 3′-UTR is important as there is an inverse relationship between the number of AREs and mRNA stability or instability [52]. Hence, the results of the present study suggested that the 3′-UTRs of TPD52, 53 and 54 potentially have enhancing effects on RNA stabilization, not on destabilization, and are subject to a negative feedback loop by cellular stimulation, such as by TGF-β and EGF. Moreover, the effect was observed more prominently in the 3′-UTR of TPD52 than in those of TPD53 and 54. Therefore, we subsequently focused on the 3′-UTR of TPD52 mRNA in mRNA stability.

In our experiments, we searched for a minimal *cis*-acting element that could stabilize reporter mRNA (Figures 4 and 5). We found that the 78-280 fragment stabilized reporter mRNA as strongly as the full-length 3′-UTR. These results demonstrated that the fragment acts as a strong minimal enhancing *cis*-element. The fact that the 3′-UTR of TPD52 mRNA is very long strongly suggests that other minimal enhancing *cis*-elements might also exist there and they might be capable of binding to a variety of RBPs, including TIA-1 and TIAR. More importantly, several deletion mutants (871-3523 and 2073-3523) showed a destabilizing effect, indicating

Biochemical Journal (2017) **474** 1669–1687
DOI: 10.1042/BCJ20160942

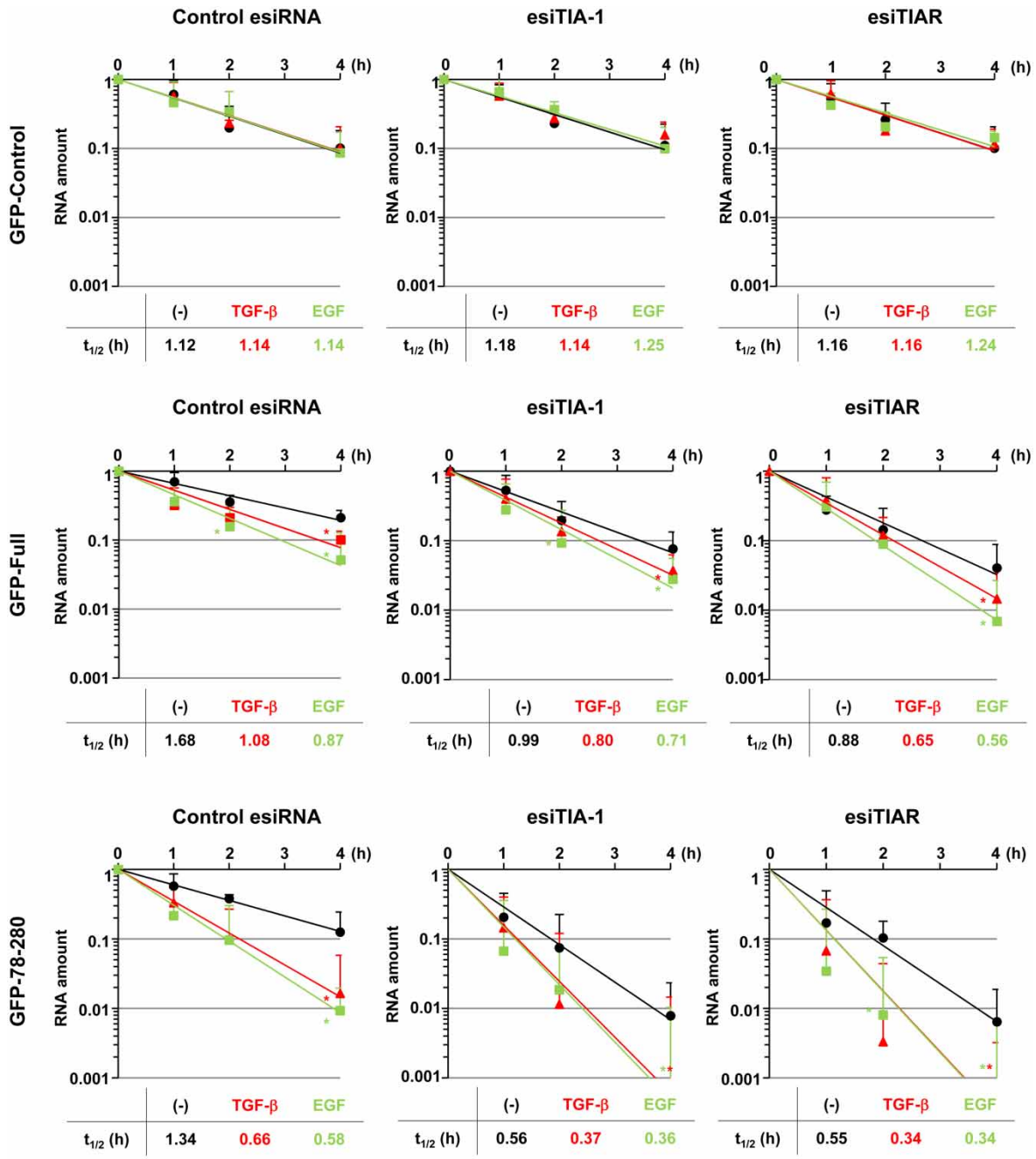

Figure 10. Effects of TGF-β and EGF on mRNA stability of the GFP chimeric reporter gene.

Control GFP and chimeric GFP-TPD52 full and GFP-78-280 genes, as shown in Figure 5A in the presence of control esiRNA, esiRNA for TIA-1 and TIAR, were co-transfected into SAS cells. After 24 h, the medium was replaced with fresh medium, and the cells were cultured in the absence (black) or presence of 10 ng/ml of TGF-β1 (red) or EGF (green) for another 24 h. Then, the cells were subjected to an RNA degradation assay for GFP reporter gene stability. The steady-state amount of RNA at time 0 was designated as '1', and relative values with the SD are plotted on a semi-logarithmic graph. At the bottom, the calculated half-life ($t_{1/2}$) of each control and chimeric gene is shown in hours. *$P < 0.05$ versus the control.

that these fragments contain one or more negative *cis*-elements affecting mRNA stability. These fragments may overcome the effects of stabilizing elements and may trigger rapid mRNA degradation. More detailed experiments will be required to determine the relationship between and involvement of these stabilizing and/or

Biochemical Journal (2017) **474** 1669–1687
DOI: 10.1042/BCJ20160942

destabilizing *cis*-elements. However, in the present study, we decided to focus on the 78-280 fragment, as a minimal mRNA-stabilizing *cis*-element, and we are planning to investigate the balance between stabilizing and/or destabilizing *cis*-elements in future studies.

The biotin pull-down and RIP assays (Figure 6) showed the specific binding of the 78-280 fragment to TIA-1/TIAR, and knockdown experiments (Figure 7 and Supplementary Figure S2) revealed that the proteins play a critical role in the stability of TPD52 mRNA in cancer and normal cells. Furthermore, the reporter and RNA degradation assays using deletion mutants (Figure 8) showed the specific interaction between the 78-280 fragment and TIA-1/TIAR rather than between full-length and TIA-1/TIAR, demonstrating the important role in the post-transcriptional regulation of the TPD52 gene, particularly in RNA stability. Thus, these results revealed that the 78-280 fragment may have a crucial role in the stability of TPD52 mRNA, although the precise functions of other regions remain unclear. Based on the results in Figure 1, other portions of the 3′-UTR of TPD52 mRNA might be capable of binding to TIA-1/TIAR and of positively and/or negatively regulating mRNA stability. This indicates the existence of a more precise and intricate mechanism for the post-transcriptional regulation of TPD52, and more detailed experiments on this will be required in the future. TIA-1/TIAR is not only a component of a stress granule, but also one of the most well-known RBPs; it constitutively binds to U-rich and AU-rich RNA sequences [53,54]. However, the detailed mechanisms behind its effects remain unclear. In addition, TIA-1/TIAR is reported to be involved in the translation [46,55,56] and alternative splicing [57–59] of many mRNAs. However, knockdown of TIA-1 and TIAR (Figure 7 and Supplementary Figure S2) resulted in no differences in the levels of steady-state mRNAs, suggesting that TIA-1/TIAR has little involvement in the translation of TPD52, although its involvement in alternative splicing requires further investigation.

Furthermore, we revealed that the interaction between 3′-UTR and TIA-1/TIAR is regulated by the stimulation of TGF-β and EGF, whereby mRNA stability undergoes a negative feedback loop (Figures 9 and 10 and Supplementary Figure S3); namely, the interaction between the 78-280 region, not full-length 3′-UTR, and TIA-/TIAR was negatively regulated by TGF-β and EGF stimulation, although the binding affinity between the 78-280 region and TIA-1/TIAR is weaker than that between full-length 3′UTR and TIA-1/TIAR. In addition, the mRNA stability of the reporter was decreased by stimulation of these growth factors, and this negative regulatory effect was always observed more prominently in GFP-78-280 than in GFP-full. As GFP-78-280 was a minimal *cis*-acting element, which was stripped from other positive or negative *cis*-acting elements, the reporter gene might be more susceptible to the negative feedback loop caused by the growth factors. These results may account for the discrepancy in mRNA stability between GFP-full and GFP-78-280 shown in Figure 8; i.e. other *cis*-acting elements could mask and/or overcome the rapid response of the 78-280 region to mRNA stability, although *cis*-acting functions of other regions in the 3′-UTR remain to be investigated. To the best of our knowledge, post-translational modifications (e.g. phosphorylation) of TIA-1/TIAR have not been reported, and it is unclear how the stimulation of these growth factors modulates the binding affinity and determines what protein intervenes between the *cis*-acting element and *trans*-acting factor. Previous studies have reported that a processing body and a stress granule, which play an important role in post-transcriptional regulation of mRNA, consist of many RBPs as mercenaries for transportation, stabilization and translation of mRNAs (reviewed in refs [60–62]). Therefore, in order to examine the detailed mechanism of feedback loops, more precise experiments are necessary in the future. However, taken together, we revealed here that the stability of TPD52 mRNA undergoes a negative feedback loop downstream from the stimulation of TGF-β and EGF, and that the 78-280 region plays a crucial role in the regulatory mechanism.

Based on the findings of the present study, we concluded that the expression of TPD52 is subject to post-transcriptional modifications that affect the stability of mRNA independently of translation. Furthermore, we identified TIA-1/TIAR as a *trans*-acting factor protein that binds to a *cis*-acting fragment located in the 78-280 proximal region of the 3′-UTR of TPD52 mRNA. The 3′-UTR might harbor other *cis*-acting regions, and other *trans*-acting RBPs might also bind there, resulting in the formation of a processing body and/or a stress granule [62]. However, to the best of our knowledge, we are the first to report the post-transcriptional regulatory mechanism of the TPD52 gene downstream from TGF-β and EGF signaling, and further studies to elucidate the detailed mechanisms underlying the expression of this gene are ongoing.

Abbreviations

3′-UTR, 3′-untranslated region; ARBPs, AU-rich element binding proteins; ARE, adenosine- and uridine-rich element; AUF-1, ARE-binding factor-1; CMV, cytomegalovirus; EGF, epidermal growth factor; esiRNA, endoribonuclease-prepared small interfering RNA; GAPDH, glyceraldehyde 3-phosphate dehydrogenase; GFP,

green fluorescent protein; HuR, Hu-antigen R; NF-90, nuclear factor 90; OSCC, oral squamous carcinoma cell; PEST, proline, glutamic-acid, serine and threonine; RBP, RNA-binding protein; RIP, RNA immunoprecipitation; SDS–PAGE, sodium dodecyl sulfate–polyacrylamide gel electrophoresis; TGF-β, transforming growth factor-β; TGF-β1, transforming growth factor-β1; TIA-1, T-cell intracellular antigen 1; TIAR, TIA-1-related protein; TPD, tumor protein D; TTP, tristetraprolin.

Author Contribution

H.M. together with Y.M. significantly contributed to and performed the present study, prepared the figures and wrote the manuscript. Y.M. also conceived the idea and applied for the grant supporting the study. C.I. and K.K. helped to perform the experiments. T.S., S.K. and T.S. applied for the grant supporting the study and helped to draft the figures and the manuscript. All authors read and approved the final manuscript.

Funding

The present study was supported by Grants-in-Aid for Scientific Research (KAKENHI) from the Japan Society for the Promotion of Science (JSPS) (KAKENHI C to Y.M. [15K11301], S.K. [24593060] and T.S. [15K11269]).

Acknowledgements

The authors thank Prof. Niitsu (Sapporo Medical University) for providing SAS and HeLa cells. In addition, the authors thank all staff members of the Department of Oral and Maxillofacial Surgery, School of Dentistry, Showa University, for their helpful suggestions, and Ms Miho Yoshihara for secretarial assistance.

Competing Interests

The Authors declare that there are no competing interests associated with the manuscript.

References

1 Byrne, J.A., Tomasetto, C., Garnier, J.M., Rouyer, N., Mattei, M.G., Bellocq, J.P. et al. (1995) A screening method to identify genes commonly overexpressed in carcinomas and the identification of a novel complementary DNA sequence. *Cancer Res.* **55**, 2896–2903 PMID:7796418
2 Byrne, J.A., Frost, S., Chen, Y. and Bright, R.K. (2014) Tumor protein D52 (TPD52) and cancer-oncogene understudy or understudied oncogene? *Tumour Biol.* **35**, 7369–7382 doi:10.1007/s13277-014-2006-x
3 Boutros, R., Fanayan, S., Shehata, M. and Byrne, J.A. (2004) The tumor protein D52 family: many pieces, many puzzles. *Biochem. Biophys. Res. Commun.* **325**, 1115–1121 doi:10.1016/j.bbrc.2004.10.112
4 Byrne, J.A., Mattei, M.-G. and Basset, P. (1996) Definition of the tumor protein D52 (TPD52) gene family through cloning of D52 homologues in human (hD53) and mouse (mD52). *Genomics* **35**, 523–532 doi:10.1006/geno.1996.0393
5 Nourse, C.R., Mattei, M.-G., Gunning, P. and Byrne, J.A. (1998) Cloning of a third member of the D52 gene family indicates alternative coding sequence usage in D52-like transcripts. *Biochim. Biophys. Acta, Gene Struct. Expr.* **1443**, 155–168 doi:10.1016/S0167-4781(98)00211-5
6 Wilson, S.H.D., Bailey, A.M., Nourse, C.R., Mattei, M.-G. and Byrne, J.A. (2001) Identification of MAL2, a novel member of the mal proteolipid family, though interactions with TPD52-like proteins in the yeast two-hybrid system. *Genomics* **76**, 81–88 doi:10.1006/geno.2001.6610
7 Thomas, D.D.H., Kaspar, K.M., Taft, W.B., Weng, N., Rodenkirch, L.A. and Groblewski, G.E. (2002) Identification of annexin VI as a Ca^{2+}-sensitive CRHSP-28-binding protein in pancreatic acinar cells. *J. Biol. Chem.* **277**, 35496–35502 doi:10.1074/jbc.M110917200
8 Proux-Gillardeaux, V., Galli, T., Callebaut, I., Mikhailik, A., Calothy, G. and Marx, M. (2003) D53 is a novel endosomal SNARE-binding protein that enhances interaction of syntaxin 1 with the synaptobrevin 2 complex in vitro. *Biochem. J.* **370**, 213–221 doi:10.1042/bj20021309
9 Bright, R.K., Bright, J.D. and Byrne, J.A. (2014) Overexpressed oncogenic tumor-self antigens. *Hum. Vaccin. Immunother.* **10**, 3297–3305 doi:10.4161/hv.29475
10 Malek, R.L., Irby, R.B., Guo, Q.M., Lee, K., Wong, S., He, M. et al. (2002) Identification of Src transformation fingerprint in human colon cancer. *Oncogene* **21**, 7256–7265 doi:10.1038/sj.onc.1205900
11 Petrova, D.T., Asif, A.R., Armstrong, V.W., Dimova, I., Toshev, S., Yaramov, N. et al. (2008) Expression of chloride intracellular channel protein 1 (CLIC1) and tumor protein D52 (TPD52) as potential biomarkers for colorectal cancer. *Clin. Biochem.* **41**, 1224–1236 doi:10.1016/j.clinbiochem.2008.07.012
12 Fejzo, M.S., Dering, J., Ginther, C., Anderson, L., Ramos, L., Walsh, C. et al. (2008) Comprehensive analysis of 20q13 genes in ovarian cancer identifies *ADRM1* as amplification target. *Genes Chromosomes Cancer* **47**, 873–883 doi:10.1002/gcc.20592
13 Byrne, J.A., Balleine, R.L., Fejzo, M.S., Mercieca, J., Chiew, Y.-E., Livnat, Y. et al. (2005) Tumor protein D52 (TPD52) is overexpressed and a gene amplification target in ovarian cancer. *Int. J. Cancer* **117**, 1049–1054 doi:10.1002/ijc.21250
14 Byrne, J.A., Maleki, S., Hardy, J.R., Gloss, B.S., Murali, R., Scurry, J.P. et al. (2010) MAL2 and tumor protein D52 (TPD52) are frequently overexpressed in ovarian carcinoma, but differentially associated with histological subtype and patient outcome. *BMC Cancer* **10**, 497 doi:10.1186/1471-2407-10-497
15 Cao, Q., Chen, J., Zhu, L., Liu, Y., Zhou, Z., Sha, J. et al. (2006) A testis-specific and testis developmentally regulated tumor protein D52 (TPD52)-like protein TPD52L3/hD55 interacts with TPD52 family proteins. *Biochem. Biophys. Res. Commun.* **344**, 798–806 doi:10.1016/j.bbrc.2006.03.208
16 Wang, R., Xu, J., Saramäki, O., Visakorpi, T., Sutherland, W.M., Zhou, J. et al. (2004) *PrLZ*, a novel prostate-specific and androgen-responsive gene of the TPD52 family, amplified in chromosome 8q21.1 and overexpressed in human prostate cancer. *Cancer Res.* **64**, 1589–1594 doi:10.1158/0008-5472.CAN-03-3331

Biochemical Journal (2017) **474** 1669–1687
DOI: 10.1042/BCJ20160942

17 Rubin, M.A., Varambally, S., Beroukhim, R., Tomlins, S.A., Rhodes, D.R., Paris, P.L. et al. (2004) Overexpression, amplification, and androgen regulation of TPD52 in prostate cancer. *Cancer Res.* **64**, 3814–3822 doi:10.1158/0008-5472.CAN-03-3881
18 Barbaric, D., Byth, K., Dalla-Pozza, L. and Byrne, J.A. (2006) Expression of tumor protein D52-like genes in childhood leukemia at diagnosis: clinical and sample considerations. *Leuk. Res.* **30**, 1355–1363 doi:10.1016/j.leukres.2006.03.009
19 Kang, H., Wilson, C.S., Harvey, R.C., Chen, I.-M., Murphy, M.H., Atlas, S.R. et al. (2012) Gene expression profiles predictive of outcome and age in infant acute lymphoblastic leukemia: a Children's Oncology Group study. *Blood* **119**, 1872–1881 doi:10.1182/blood-2011-10-382861
20 Cheung, H.C., Baggerly, K.A., Tsavachidis, S., Bachinski, L.L., Neubauer, V.L., Nixon, T.J. et al. (2008) Global analysis of aberrant pre-mRNA splicing in glioblastoma using exon expression arrays. *BMC Genomics* **9**, 216 doi:10.1186/1471-2164-9-216
21 Mukudai, Y., Kondo, S., Fujita, A., Yoshihama, Y., Shirota, T. and Shintani, S. (2013) Tumor protein D54 is a negative regulator of extracellular matrix-dependent migration and attachment in oral squamous cell carcinoma-derived cell lines. *Cell. Oncol.* **36**, 233–245 doi:10.1007/s13402-013-0131-y
22 Fujita, A. and Kondo, S. (2015) Identification of TPD54 as a candidate marker of oral epithelial carcinogenesis. *J. Oral Maxillofac. Surg. Med. Pathol.* **27**, 770–774 doi:10.1016/j.ajoms.2015.03.011
23 Wu, X. and Brewer, G. (2012) The regulation of mRNA stability in mammalian cells: 2.0. *Gene* **500**, 10–21 doi:10.1016/j.gene.2012.03.021
24 Iadevaia, V. and Gerber, A.P. (2015) Combinatorial control of mRNA fates by RNA-binding proteins and non-coding RNAs. *Biomolecules* **5**, 2207–2222 doi:10.3390/biom5042207
25 Mitchell, S.F. and Parker, R. (2014) Principles and properties of eukaryotic mRNPs. *Mol. Cell* **54**, 547–558 doi:10.1016/j.molcel.2014.04.033
26 Vlasova, I.A., Tahoe, N.M., Fan, D., Larsson, O., Rattenbacher, B., Sternjohn, J.R. et al. (2008) Conserved GU-rich elements mediate mRNA decay by binding to CUG-binding protein 1. *Mol. Cell* **29**, 263–270 doi:10.1016/j.molcel.2007.11.024
27 Barreau, C., Paillard, L. and Osborne, H.B. (2005) AU-rich elements and associated factors: are there unifying principles? *Nucleic Acids Res.* **33**, 7138–7150 doi:10.1093/nar/gki1012
28 Wilson, G.M. and Brewer, G. (1999) The search for trans-acting factors controlling messenger RNA decay. *Prog. Nucleic Acid Res. Mol. Biol.* **62**, 257–291 doi:10.1016/S0079-6603(08)60510-3
29 Chen, C.-Y. and Shyu, A.-B. (1995) AU-rich elements: characterization and importance in mRNA degradation. *Trends Biochem. Sci.* **20**, 465–470 doi:10.1016/S0968-0004(00)89102-1
30 Simone, L.E. and Keene, J.D. (2013) Mechanisms coordinating ELAV/Hu mRNA regulons. *Curr. Opin. Genet. Dev.* **23**, 35–43 doi:10.1016/j.gde.2012.12.006
31 White, E.J.F., Brewer, G. and Wilson, G.M. (2013) Post-transcriptional control of gene expression by AUF1: mechanisms, physiological targets, and regulation. *Biochim. Biophys. Acta* **1829**, 680–688 doi:10.1016/j.bbagrm.2012.12.002
32 Brooks, S.A. and Blackshear, P.J. (2013) Tristetraprolin (TTP): interactions with mRNA and proteins, and current thoughts on mechanisms of action. *Biochim. Biophys. Acta, Gene Regul. Mech.* **1829**, 666–679 doi:10.1016/j.bbagrm.2013.02.003
33 Sanduja, S., Blanco, F.F. and Dixon, D.A. (2011) The roles of TTP and BRF proteins in regulated mRNA decay. *Wiley Interdiscip. Rev. RNA* **2**, 42–57 doi:10.1002/wrna.28
34 Masuda, K., Kuwano, Y., Nishida, K., Rokutan, K. and Imoto, I. (2013) NF90 in posttranscriptional gene regulation and microRNA biogenesis. *Int. J. Mol. Sci.* **14**, 17111–17121 doi:10.3390/ijms140817111
35 Waris, S., James Wilce, M.C. and Wilce, J.A. (2014) RNA recognition and stress granule formation by TIA proteins. *Int. J. Mol. Sci.* **15**, 23377–23388 doi:10.3390/ijms151223377
36 Ross, C.R., Brennan-Laun, S.E. and Wilson, G.M. (2012) Tristetraprolin: roles in cancer and senescence. *Ageing Res. Rev.* **11**, 473–484 doi:10.1016/j.arr.2012.02.005
37 Taylor, G.A., Carballo, E., Lee, D.M., Lai, W.S., Thompson, M.J., Patel, D.D. et al. (1996) A pathogenetic role for TNFα in the syndrome of cachexia, arthritis, and autoimmunity resulting from tristetraprolin (TTP) deficiency. *Immunity* **4**, 445–454 doi:10.1016/S1074-7613(00)80411-2
38 Carballo, E., Lai, W.S. and Blackshear, P.J. (1998) Feedback inhibition of macrophage tumor necrosis factor-α production by tristetraprolin. *Science* **281**, 1001–1005 doi:10.1126/science.281.5379.1001
39 Okumura, K., Konishi, A., Tanaka, M., Kanazawa, M., Kogawa, K. and Niitsu, Y. (1996) Establishment of high- and low-invasion clones derived for a human tongue squamous-cell carcinoma cell line SAS. *J. Cancer Res. Clin. Oncol.* **122**, 243–248 doi:10.1007/BF01209653
40 Yasuda, A., Kondo, S., Nagumo, T., Tsukamoto, H., Mukudai, Y., Umezawa, K. et al. (2011) Anti-tumor activity of dehydroxymethylepoxyquinomicin against human oral squamous cell carcinoma cell lines in vitro and in vivo. *Oral Oncol.* **47**, 334–339 doi:10.1016/j.oraloncology.2011.03.001
41 Lee, Y.-L., Chiao, C.-H. and Hsu, M.-T. (2011) Transcription of muscle actin genes by a nuclear form of mitochondrial RNA polymerase. *PLoS ONE* **6**, e22583 doi:10.1371/journal.pone.0022583
42 Mukudai, Y., Kubota, S., Eguchi, T., Kondo, S., Nakao, K. and Takigawa, M. (2005) Regulation of chicken *ccn2* gene by interaction between RNA *cis*-element and putative *trans*-factor during differentiation of chondrocytes. *J. Biol. Chem.* **280**, 3166–3177 doi:10.1074/jbc.M411632200
43 Benjamin, D., Colombi, M. and Moroni, C. (2004) A GFP-based assay for rapid screening of compounds affecting ARE-dependent mRNA turnover. *Nucleic Acids Res.* **32**, e89 doi:10.1093/nar/gnh086
44 Hitti, E., Al-Yahya, S., Al-Saif, M., Mohideen, P., Mahmoud, L., Polyak, S.J. et al. (2010) A versatile ribosomal protein promoter-based reporter system for selective assessment of RNA stability and post-transcriptional control. *RNA* **16**, 1245–1255 doi:10.1261/rna.2026310
45 Al-Zoghaibi, F., Ashour, T., Al-Ahmadi, W., Abulleef, H., Demirkaya, O. and Khabar, K.S.A. (2007) Bioinformatics and experimental derivation of an efficient hybrid 3′ untranslated region and use in expression active linear DNA with minimum poly(A) region. *Gene* **391**, 130–139 doi:10.1016/j.gene.2006.12.013
46 Wigington, C.P., Jung, J., Rye, E.A., Belauret, S.L., Philpot, A.M., Feng, Y. et al. (2015) Post-transcriptional regulation of programmed cell death 4 (*PDCD4*) mRNA by the RNA-binding proteins human antigen R (HuR) and T-cell intracellular antigen 1 (TIA1). *J. Biol. Chem.* **290**, 3468–3487 doi:10.1074/jbc.M114.631937
47 Pullmann, Jr, R., Kim, H.H., Abdelmohsen, K., Lal, A., Martindale, J.L., Yang, X. et al. (2007) Analysis of turnover and translation regulatory RNA-binding protein expression through binding to cognate mRNAs. *Mol. Cell. Biol.* **27**, 6265–6278 doi:10.1128/MCB.00500-07

48 Bakheet, T., Frevel, M., Williams, B.R.G., Greer, W. and Khabar, K.S.A. (2001) ARED: human AU-rich element-containing mRNA database reveals an unexpectedly diverse functional repertoire of encoded proteins. *Nucleic Acids Res.* **29**, 246–254 doi:10.1093/nar/29.1.246
49 Halees, A.S., El-Badrawi, R. and Khabar, K.S.A. (2008) ARED organism: expansion of ARED reveals AU-rich element cluster variations between human and mouse. *Nucleic Acids Res.* **36**, D137–D140 doi:10.1093/nar/gkm959
50 Bevilacqua, A., Ceriani, M.C., Capaccioli, S. and Nicolin, A. (2003) Post-transcriptional regulation of gene expression by degradation of messenger RNAs. *J. Cell. Physiol.* **195**, 356–372 doi:10.1002/jcp.10272
51 Wilusz, C.J., Wormington, M. and Peltz, S.W. (2001) The cap-to-tail guide to mRNA turnover. *Nat. Rev. Mol. Cell Biol.* **2**, 237–246 doi:10.1038/35067025
52 Hao, S. and Baltimore, D. (2009) The stability of mRNA influences the temporal order of the induction of genes encoding inflammatory molecules. *Nat. Immunol.* **10**, 281–288 doi:10.1038/ni.1699
53 Kim, H.S., Wilce, M.C.J., Yoga, Y.M.K., Pendini, N.R., Gunzburg, M.J., Cowieson, N.P. et al. (2011) Different modes of interaction by TIAR and HuR with target RNA and DNA. *Nucleic Acids Res.* **39**, 1117–1130 doi:10.1093/nar/gkq837
54 Kim, H.S., Kuwano, Y., Zhan, M., Pullmann, Jr, R., Mazan-Mamczarz, K., Li, H. et al. (2007) Elucidation of a C-rich signature motif in target mRNAs of RNA-binding protein TIAR. *Mol. Cell. Biol.* **27**, 6806–6817 doi:10.1128/MCB.01036-07
55 Kawai, T., Lal, A., Yang, X., Galban, S., Mazan-Mamczarz, K. and Gorospe, M. (2006) Translational control of cytochrome c by RNA-binding proteins TIA-1 and HuR. *Mol. Cell. Biol.* **26**, 3295–3307 doi:10.1128/MCB.26.8.3295-3307.2006
56 Piecyk, M., Wax, S., Beck, A.R.P., Kedersha, N., Gupta, M., Maritim, B. et al. (2000) TIA-1 is a translational silencer that selectively regulates the expression of TNF-α. *EMBO J.* **19**, 4154–4163 doi:10.1093/emboj/19.15.4154
57 Wang, I., Hennig, J., Jagtap, P.K.A., Sonntag, M., Valcarcel, J. and Sattler, M. (2014) Structure, dynamics and RNA binding of the multi-domain splicing factor TIA-1. *Nucleic Acids Res.* **42**, 5949–5966 doi:10.1093/nar/gku193
58 Förch, P., Puig, O., Kedersha, N., Martínez, C., Granneman, S., Séraphin, B. et al. (2000) The apoptosis-promoting factor TIA-1 is a regulator of alternative pre-mRNA splicing. *Mol. Cell* **6**, 1089–1098 doi:10.1016/S1097-2765(00)00107-6
59 McAlinden, A., Liang, L., Mukudai, Y., Imamura, T. and Sandell, L.J. (2007) Nuclear protein TIA-1 regulates *COL2A1* alternative splicing and interacts with precursor mRNA and genomic DNA. *J. Biol. Chem.* **282**, 24444–24454 doi:10.1074/jbc.M702717200
60 Parker, R. and Sheth, U. (2007) P bodies and the control of mRNA translation and degradation. *Mol. Cell* **25**, 635–646 doi:10.1016/j.molcel.2007.02.011
61 Pérez-Ortín, J.E., Alepuz, P., Chávez, S. and Choder, M. (2013) Eukaryotic mRNA decay: methodologies, pathways, and links to other stages of gene expression. *J. Mol. Biol.* **425**, 3750–3775 doi:10.1016/j.jmb.2013.02.029
62 Anderson, P., Kedersha, N. and Ivanov, P. (2015) Stress granules, P-bodies and cancer. *Biochim. Biophys. Acta, Gene Regul. Mech.* **1849**, 861–870 doi:10.1016/j.bbagrm.2014.11.009

Hindawi Publishing Corporation
Evidence-Based Complementary and Alternative Medicine
Volume 2016, Article ID 6087213, 11 pages
http://dx.doi.org/10.1155/2016/6087213

Research Article

Methanol and Butanol Extracts of *Paeonia lutea* Leaves Repress Metastasis of Squamous Cell Carcinoma

Yoshiki Mukudai,[1] Meilin Zhang,[2] Sunao Shiogama,[1] Seiji Kondo,[1] Chihiro Ito,[1] Hiromi Motohashi,[1] Kosuke Kato,[1] Miharu Fujii,[1] Satoru Shintani,[1] Hideyuki Shigemori,[3] Kazunaga Yazawa,[4] and Tatsuo Shirota[1]

[1]*Department of Oral and Maxillofacial Surgery, School of Dentistry, Showa University, 2-1-1 Kitasenzoku, Ota-ku, Tokyo 145-8515, Japan*
[2]*Graduate School of Life and Environmental Sciences, University of Tsukuba, Tsukuba, Ibaraki 305-8572, Japan*
[3]*Faculty of Life and Environmental Sciences, University of Tsukuba, Tsukuba, Ibaraki 305-8572, Japan*
[4]*Division of Health Food Science, Institute for Nanoscience and Nanotechnology, Waseda University, 2-2 Wakamatsu-cho, Shinjuku-ku, Tokyo 162-0041, Japan*

Correspondence should be addressed to Yoshiki Mukudai; mukudai@dent.showa-u.ac.jp

Received 15 December 2015; Accepted 28 April 2016

Academic Editor: Yew-Min Tzeng

Squamous cell carcinoma (SCC) is one of the most common cancers of the head and neck region worldwide and is generally treated surgically in combination with radiotherapy and/or chemotherapy. However, anticancer agents have numerous serious side effects, and alternative, less toxic agents that are effective as chemotherapeutics for SCC are required. The Paeoniaceae family is widely used in traditional Chinese medicine. We examined methanol and butanol extracts of *Paeonia lutea* (*P. lutea*) leaves for their potential as an anticancer agent. Both extracts decreased the proliferation of SCC cells, induced apoptotic cell death, and modulated migration, adhesion, chemotaxis, and haptotaxis in an extracellular matrix- (ECM-) dependent manner due to altered expression of several integrin subunits. Subsequently, SCC cells were subcutaneously transplanted into athymic nude mice; the extracts reduced the metastasis of SCC cells but had little effect on the volume of the primary tumor or survival or body weight of the mice. The results suggest that the extracts may hold promise for preventing cancer metastasis.

1. Introduction

Squamous cell carcinoma (SCC) is one of the most common cancers of the head and neck region worldwide, with more than sixty thousand patients diagnosed each year [1]. Commonly, SCC is treated surgically in combination with radiotherapy and/or chemotherapy. However, treatment outcome is unsatisfactory, with 20% to 50% of patients developing regional recurrence and/or distant metastasis [2]. In addition, anticancer agents often cause a variety of serious side effects; for example, *cis*-platinum (II) diammine dichloride (CDDP), which is often used for chemotherapy of SCC, causes nephrotoxicity [3], neurotoxicity [4], nausea, vomiting [5], ototoxicity [6], and xerostomia (dry mouth) [7, 8]. Hence, less toxic chemotherapeutics for SCC are required.

The Paeoniaceae family is widely used in traditional Chinese medicine. Previous studies reported that the root barks of Paeoniaceae are used as therapeutics for various diseases such as diabetes [9], Alzheimer's disease [10, 11], arthritis [12], inflammation [13], sepsis [14], brain-ischemia-reperfusion injury [15], and virus infections [16, 17]. Moreover, several studies have reported anticancer effects of Paeoniaceae family preparations [18–23].

Traditional Chinese medicine has been used to treat a variety of diseases for several thousands of years; therefore, we launched an interinstitutional collaborative project in 2010 to evaluate the therapeutic potential of herbal extracts for disorders of the head and neck region [23–26]. Here, we examined methanol and butanol extracts of *Paeonia lutea* (*P. lutea*) leaves for their potential as an anticancer agent. Our

results indicate that these extracts modulate the migration and adhesion of SCC cells to the extracellular matrix (ECM) by altering integrin subunit expression *in vitro* and reduce metastasis of the cells *in vivo*; however, transplanted tumor growth and survival of the recipient animals were essentially unaffected.

2. Materials and Methods

2.1. Plant Materials and Preparation of Plant Extracts. P. lutea leaves were collected from Tsukuba Peony Garden (Tsukuba, Ibaraki, Japan) in October 2012. A voucher specimen (UTHS1210) was deposited at the Laboratory of Natural Products Chemistry, Graduate School of Life and Environmental Sciences, University of Tsukuba. The leaves were air dried for 2 days at room temperature (dry weight, 350 g) and then extracted with methanol (4 L) for 1 week. The extraction was repeated once. The two methanol extracts were combined and concentrated *in vacuo* at 38°C to give the methanol extract (ME, 80.1 g). The extract was partitioned with ethyl acetate three times (800 mL each) and H_2O (800 mL). The ethyl acetate was evaporated to afford ethyl acetate soluble materials (EA, 28.5 g). The H_2O layer was partitioned with butanol three times (600 mL each) to give butanol-soluble (BU, 20.5 g), butanol-insoluble (BW, 2.1 g), and H_2O-soluble materials (W, 16.5 g). Finally, aliquots of each of these materials were dissolved in phosphate-buffered saline (PBS) at a concentration of 1 mg/mL and sterilized by passage through a Millex syringe filter (Merck Millipore, Billerica, MA).

2.2. Cell Culture and Anchorage-Independent Growth Assay. SAS cells, a human oral SCC cell line [27], were cultured in high-glucose Dulbecco's Modified Eagle Medium (DMEM; Wako, Osaka, Japan) supplemented with 10% fetal bovine serum (FBS) and penicillin-streptomycin solution (Sigma-Aldrich, St. Louis, MO) at 37°C, 5% CO_2, and 100% humidity. Anchorage-independent growth assay was carried out using a commercial kit (Cytoselect 96-Well *In Vitro* Tumor Sensitivity Assay kit, Cell Biolabs, San Diego, CA) as described previously [28].

2.3. Cell Growth and Apoptosis Assays. One thousand cells were seeded into each well of a 96-well tissue culture plate. After 48 h, the cells were assayed using the tetrazolium salt 3-[4,5-dimethylthiazol-2-yl]-2,5-diphenyltetrazolium bromide (MTT) assay, as described previously [29]. The activities of caspases 3/7, 8, and 9 were measured using a Caspase-Glo (Promega, Madison, WI) and GloMax-Multi+ Detection System (Promega) according to the manufacturer's protocol. Genomic DNA fragmentation was investigated using a commercial kit (Apopladder EX; Takara, Shiga, Japan) according to the manufacturer's protocol.

2.4. Protein Preparation and Western Blotting Analysis. Total cellular protein was prepared as described previously [30]. Protein concentration was measured using Quick Start Bradford Reagent (Bio-Rad, Hercules, CA) using bovine serum albumin (BSA) as a standard. Protein aliquots were stored at −80°C until use. For Western blot analysis, 20 μg of total cellular protein was subjected to sodium dodecyl sulfate polyacrylamide electrophoresis (SDS-PAGE) on a 4% to 20% gradient gel (Bio-Rad); then the blot was transferred onto a polyvinylidene difluoride membrane (Life Technologies, Carlsbad, CA). Blocking, 1st and horseradish-peroxidase-conjugated 2nd antibody reactions and washing were conducted as previously described [28]. The chemiluminescence signals were visualized using Amersham ECL Western Blotting Detection Reagents (GE Healthcare UK Ltd., Buckinghamshire, UK) and ChimiDoc XRS Plus ImageLab System (Bio-Rad). The 1st and 2nd antibodies were purchased from common suppliers.

2.5. Adhesion, Wound Healing, and Migration Assays. The cells were grown in a monolayer culture in the presence or absence of the various *P. lutea* leaf extracts. After 3 d, the cells were assayed. Adhesion and wound healing assays were carried out using commercial kits (CytoSelect 48-Well Cell Adhesion Assay, CytoSelect 24-Well Wound Healing Assay, Cell Biolabs) according to the manufacturer's protocol. To assay migration, a chemotaxis chamber containing a membrane with 8 mm pores (Chemotaxicell, Kurabo, Osaka Japan) was coated with 50 μg/mL bovine type I collagen (Koken, Tokyo, Japan) or 50 μg/mL bovine fibronectin (Sigma-Aldrich) according to the manufacturer's protocol and was set into each well of a 24-well culture plate. After drying the Chemotaxicell membrane, 500 μL of DMEM with or without 10% FBS was added to the bottom of the well as a chemoattractant, 200 μL of DMEM containing 2×10^4 cells was added to the chamber, then the plate was incubated for 24 h at 37°C, 5% CO_2, and 100% humidity. The membranes were then washed, removed from the chamber, fixed with 4% formaldehyde (Wako, Osaka, Japan), and stained with crystal violet (Wako). The membranes were examined under an optical microscope and photographs (×400) were taken.

2.6. Animals. The care and treatment of the experimental animals complied with the Showa University Guidelines for Animal Experiments, and the experimental protocol was approved by the Animal Experimentation Committee of Showa University. The dorsal flank of four-week-old female athymic Balb/c *nu/nu* mice (CLEA Japan, Tokyo) was subcutaneously injected with a PBS-suspension of 1×10^6 SAS cells, as described previously [30]. After 1 week, tumor formation was measured (approximately 10 mm^3), and the mice were divided into 6 groups (control, ME, EA, BU, BW, and W). Therefore, the 7th day after SAS cell injection was designated "day 1," thereafter. Each herbal extract was suspended in PBS at the concentration of 2 mg/mL and 100 mg/kg body weight was orally administrated using a sterilized feeding needle once every three days for 40 or 70 days. In the control group, only PBS (0.1 mL) was administrated. The body weight and diameters (large and small) of each mouse were measured and

the tumor volume was determined by direct measurement and calculated using the formula [30] $\pi/6 \times (\text{large diameter}) \times (\text{small diameter})^2$. On day 40 or 70, the mice were sacrificed, and the tumors together with the surrounding soft tissue, liver, and lungs were harvested for histochemical analysis.

2.7. Histochemistry and Immunohistochemistry. The tissue was fixed, embedded, sliced, and subjected to hematoxylin-eosin (HE) staining as described previously [31]. Immunohistochemistry was conducted as described previously [31]. After 24 h incubation with a 1/50 dilution of primary antibody for human cytokeratin 10/13 (Santa Cruz Biotechnology, Santa Cruz, CA), the slide was incubated with Simple Stain MAX-PO (Nichirei, Tokyo, Japan) and visualized using Envision HRP/Kit (Dako, Kyoto, Japan); the manufacturer's suggested protocol for each commercial kit was used.

2.8. Statistical Analysis. Unless otherwise specified, all experiments were repeated at least *twice*, and similar results were obtained in the repeat experiments. Statistical analysis for mouse survival was determined by the log rank test. Other statistical analyses were carried out using two-tailed, unpaired Student's t-test. Data are expressed as means ± standard deviation of at least three data items. A p value < 0.05 was considered significant.

3. Results

3.1. Extracts of P. lutea Leaves Decreased Proliferation of SCC Cells in an Anchorage-Independent Manner, but No Effect Was Observed on Monolayer Cultures. We first investigated the effects of the *P. lutea* leaf extracts on the proliferation of SCC cells (Figure 1). Only 100 μg/mL EA had a significant effect on monolayer cultures ((a) and (b)). In contrast, all extracts showed a significant growth-inhibitory effect on soft agar cultures using the MTT assay (c). Importantly, phase-microscopy images (d) indicated that all the extracts decreased both the number and size of SCC cells compared to the control culture. These results suggest that extracts of *P. lutea* leaves are likely to reduce both the proliferation and malignancy of SCC cells.

3.2. Extracts of P. lutea Leaves Induce Apoptotic Cell Death of SCC Cells in Soft Agar Culture. We tested the hypothesis that the reduced MTT activity was due to apoptotic cell death by investigating the apoptotic effects of the extracts (Figure 2). Caspase activity assays (a) revealed that 10–100 mg/mL of EA significantly increased caspase 3/7 and 9 activities in a monolayer culture, whereas all the extracts strongly increased caspase activities in a soft agar culture. On the other hand, a DNA ladder assay (b) showed almost no DNA fragmentation in monolayer cultures treated with any of the extracts, whereas significant DNA fragmentation was observed in all the test soft agar cultures, in disagreement with the caspase assays. Furthermore, we examined the effects of the extracts on modulating apoptosis-related protein expressions by Western blotting analysis (c). In both monolayer and soft agar cultures, EA and BU reduced the expression of Bcl-2, a mitochondrial antiapoptotic protein, but the expression of other proteins (p53, Bcl-X_L, Bax, Bad, Bid, Bak, and XIAP) was essentially unaltered. These results indicate that EA and BU might affect the mitochondrial apoptotic pathway, in an anchorage-independent manner.

3.3. Extracts of P. lutea Leaves Decreased the Adhesion of ECM. Next, we examined the effects of adhesion, migration, and invasion in an ECM-dependent manner (Figure 3). Cell adhesion assays (a) showed that EA and BU reduced the attachment of SCC cells to type I collagen (Col I) and fibronectin (FN); similar results regarding cell migration were obtained using a cell migration assay (b). Furthermore, a cell invasion assay (c) showed that EA and BA reduced SAS cell invasion of Col I and FN and that the effects were independent of a chemoattractant. Those results imply that EA and BU extracts decrease both chemotaxis and haptotaxis of SCC cells through the ECM, thereby potentially preventing the invasion and metastasis of SCC cells.

3.4. Extracts of P. lutea Leaves Decreased the Expression of Several Integrin Subunits. The adhesion, migration, and invasion of various cells, including cancer cells, rely on integrin proteins. We therefore investigated whether the extracts modulate the expression of major integrin subunits. Western blotting analysis indicated that BW and W had little effect on the expression of integrin subunits (Figure 4): the expression of α4, β3, β4, and β5 integrin subunits was attenuated by EA and BU, but expression of the other subunits was essentially unchanged. These results suggest that the altered response of SAS cells to the ECM is at least partly due to modulation of the expression of several integrin subunits.

3.5. Extracts of P. lutea Reduce Metastasis of SCC Cells. The results of the above *in vitro* experiments prompted us to investigate *in vivo* whether the extracts might be useful as a novel anticancer medicine. Each extract was orally administrated to SCC-transplanted nude mice (Figure 5). Contrary to our expectation, neither survival (a), body weight (b), nor tumor growth ((c) and (d)) was affected by the extracts compared to the control group. Furthermore, histochemical analysis (Figure 6) showed that all extracts had little effect on the primary tumor. Liver and lung tissues were examined to determine the effects of the extracts on metastasis. HE staining showed no obvious metastatic tumor cells. Immunohistochemistry for cytokeratin 10/13, a representative marker of SCC cells, showed positive cells in the control and ME, BW, and W extracts mice, indicating micrometastasis from the primary tumor. Interestingly, however, administration of EA and BU extracts significantly reduced the number of positive cells. These results indicate that EA and BU extracts of *P. lutea* exhibit pharmacological effects to decrease hepatic and pulmonary metastasis from epidermal SCC and suggest that the extracts may hold promise as anticancer therapeutics.

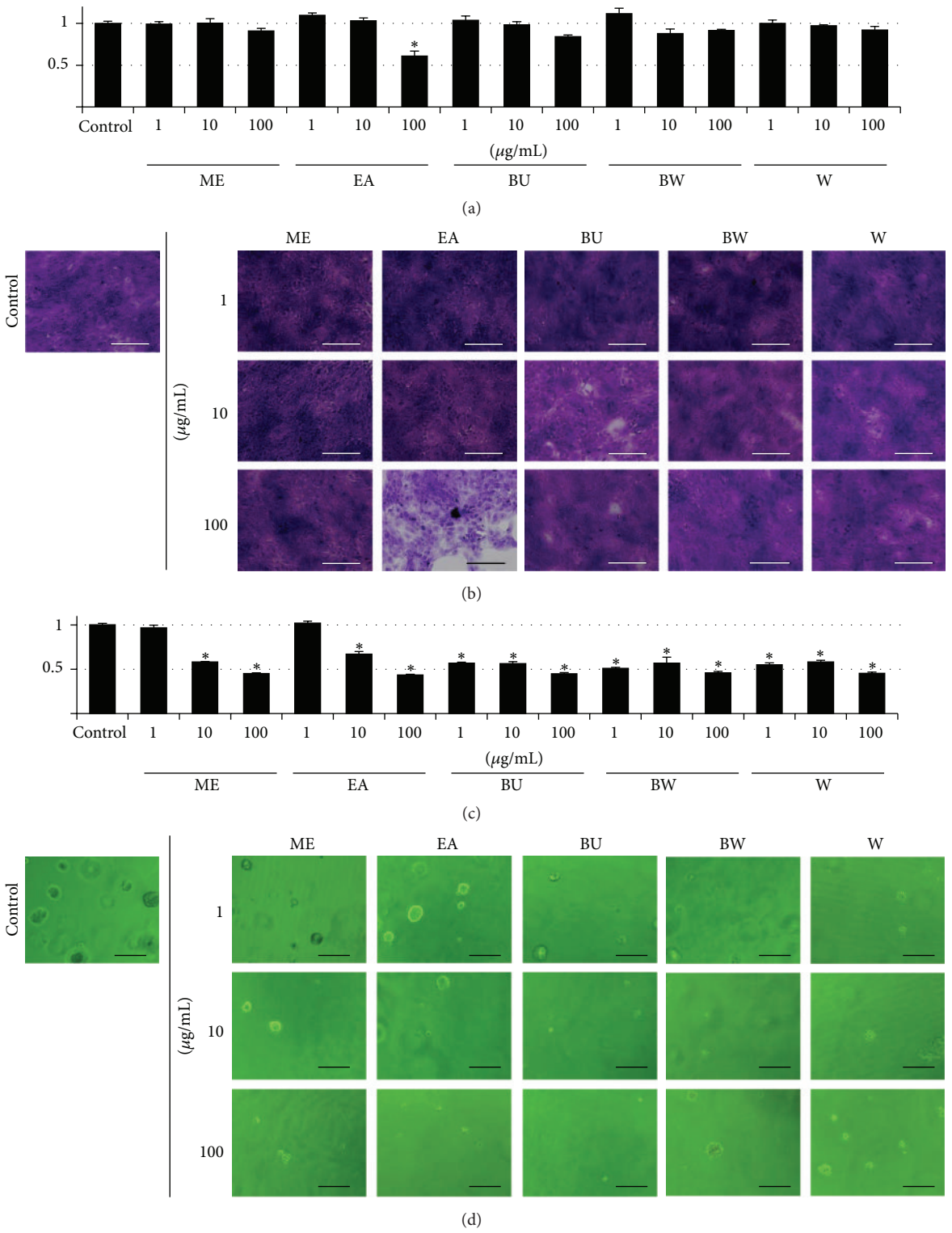

FIGURE 1: Growth-inhibitory effects of extracts of *P. lutea* leaves. SAS cells were grown in a monolayer ((a) and (b)) or on soft agar ((c) and (d)) culture. Methanol (ME), ethyl acetate (EA), butanol (BU), butanol-insoluble (BW), and water (W) extracts of *P. lutea* leaves were added to the culture medium at 0 (control) and 1, 10, or 100 μg/mL. After 7 d, the cells were subjected to MTT assay ((a) and (c)) and crystal violet staining (b) or examined under a phase-contrast microscope (d). Data in (a) and (c) are means ± standard deviations of 3 cultures; the mean of the control cultures is taken as "1." $^{*}p < 0.05$ versus control. Bars, 100 μm (b) and 200 μm (d).

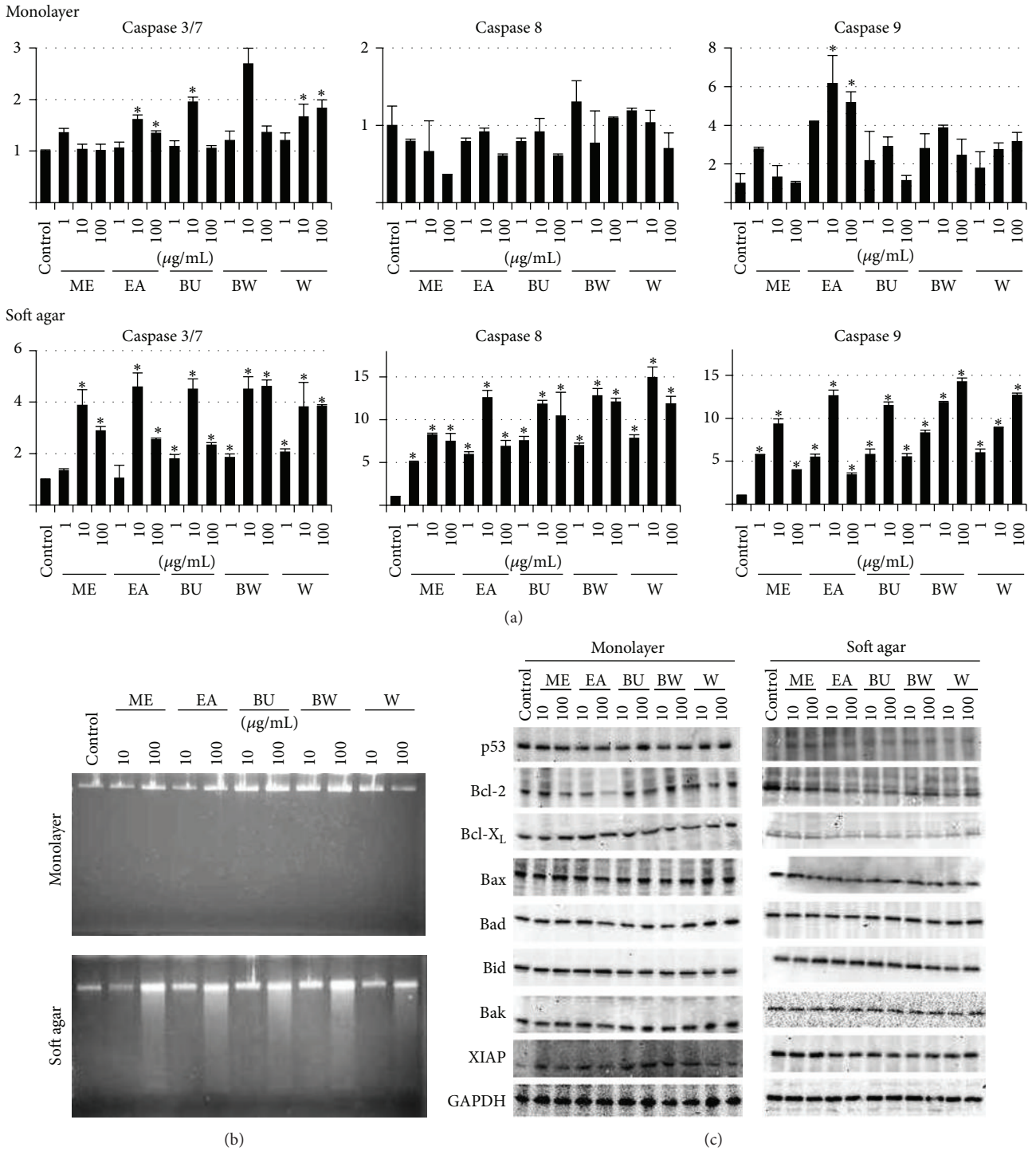

Figure 2: Apoptosis-induced effects of *P. lutea* leaf extracts. SAS cells were grown in a monolayer or on soft agar culture. Methanol (ME), ethyl acetate (EA), butanol (BU), butanol-insoluble (BW), and water (W) extracts of *P. lutea* leaves were added to the culture medium at 1 to 100 μg/mL ((a) and (b)), 10 to 100 μg/mL (c), or 0 μg/mL (control). After 3 d, the cells were subjected to caspase 3/7, 8, and 9 assays (a), a DNA ladder assay (b), or Western blotting analysis for apoptosis-related proteins (p53, Bcl-2, Bcl-X_L, Bax, Bad, Bid, Bak, and XIAP) using GAPDH as an internal control (c). Data in (a) are means ± standard deviations of 3 cultures; the mean of the control cultures is taken as "1." $^*P < 0.05$ versus control.

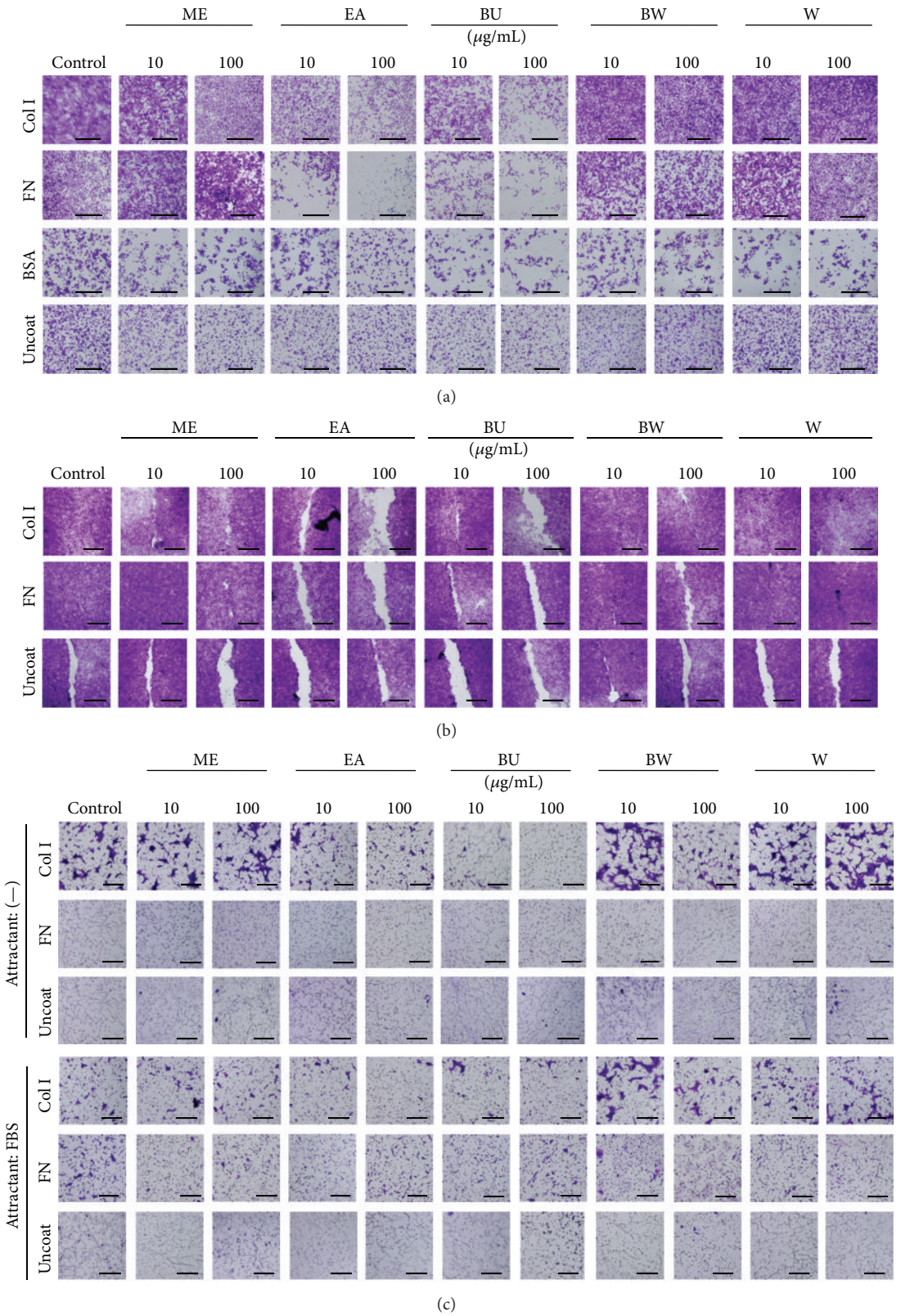

Figure 3: Effects of *P. lutea* leaf extracts on cell adhesion to ECMs. SAS cells were grown in a monolayer culture in the presence or absence (control) of methanol (ME), ethyl acetate (EA), butanol (BU), butanol-insoluble (BW), and water (W) extracts of *P. lutea* leaves at 10 to 100 μg/mL. After 3 d, the cells were subjected to adhesion (a), wound healing (b), and migration (c) assays for ECM (type I collagen (Col I), fibronectin (FN), and BSA) or an uncoated surface (Uncoat). 10% FBS was used as a chemoattractant or not (—) in the migration assay (c). Bars, 100 μm (a and c) and 1 mm (b).

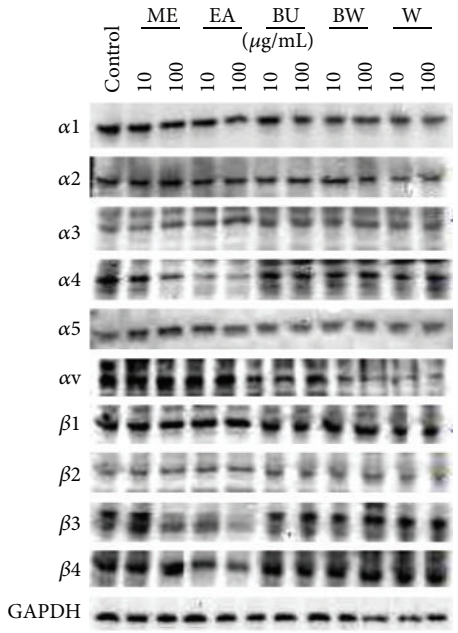

Figure 4: Effects of *P. lutea* leaf extracts on expression of integrin proteins. SAS cells were grown in a monolayer culture in the presence or absence (control) of methanol (ME), ethyl acetate (EA), butanol (BU), butanol-insoluble (BW), and water (W) extracts of *P. lutea* leaves at 10 to 100 μg/mL. After 3 d, total cellular proteins were purified and 20 μg aliquots were subjected to Western blotting for α1, α2, α3, α4, α5, αv, β1, β2, β3, and β4 integrins. GAPDH was used as an internal control.

4. Discussion

The Paeoniaceae family has been widely used in traditional Chinese medicine for thousands of years. Recent studies have revealed that extracts of *Paeoniaceae* may provide alternative anticancer therapeutics [18–23] and prompted us to investigate the extracts of *P. lutea* leaves for their anticancer potency. We first conducted *in vitro* studies to determine the effects of *P. lutea* leaf extract on proliferation (Figure 1) and apoptosis (Figure 2) of SCC cells. The extracts decreased proliferation and induced apoptotic cell death mainly by a mitochondrial signaling pathway, similar to Paeoniaceae root extracts [32]. Interestingly, the effects were more prominent in anchorage-independent cultures. Since proliferation and migration in an anchorage-independent manner reflect properties of malignant cancer cells [33], those results suggested that the extracts could be useful as an anticancer agent.

We next examined whether the extracts modulate adhesion to ECM and affect ECM-dependent migration, chemotaxis, and haptotaxis (Figure 3). EA and BU extracts significantly decreased adhesion to Col I and fibronectin. Several previous studies have reported that adhesion to ECM plays an important role in the invasion and metastasis of cancer cells [33, 34]. Thus, the present results suggest that the extracts might also decrease invasion and metastasis. Furthermore, adhesion between ECM and normal and cancer cells is supported by integrins, in particular $\alpha5\beta1$ integrin, a main component of the fibronectin receptor [35]. However, Western blotting analysis for various major integrin subunits (Figure 4) showed essentially no modulation of the expression of α5 or β1 subunits by the extracts, although α4, β3, β4, and β5 integrin subunit expression was suppressed by the EA and BU extracts. Further studies, for example, on integrin-dependent signaling pathways and on other adhesion molecules, are required to resolve this discrepancy. Nevertheless, the present study demonstrated that EA and BU extracts modulate the expression of several integrin subunits, thus decreasing the invasion and metastasis of SCC cells *in vitro*.

The potential utility of the extracts for clinical use was investigated by an animal experiment and subsequent histochemical examination. A dose of 100 mg/kg body weight was chosen based on our previous studies [36–38]. The extracts were orally administrated to SAS-cell-transplanted nude mice, and the survival and body weight of the mice and the volume of the primary tumor were measured (Figure 5). In contrast to the *in vivo* results, no antitumor effects were observed. HE staining and subsequent histochemical examination of the primary tumor, liver, and lung (Figure 6) showed no effect of the extracts. Cytokeratin 10/13 is highly expressed in SCC cells [39, 40], including SAS cells, and immunohistochemistry for cytokeratin 10/13 is indicative of metastasis of tumor cells in liver and lung. Mice given the extracts for 70 days showed positive cells in the organ (liver and lung). However, administration of EA and BU extracts significantly decreased the number and size of cytokeratin 10/13-positive tumor cells, suggesting that the extracts may have potency for reducing hepatic and pulmonary metastasis of epidermal SCC.

Our results demonstrate that EA and BU extracts of *P. lutea* have pharmacological effects of preventing the metastasis of SCC cells. The chemical composition, side effects, and minimum required dosage of the extracts of the extraction

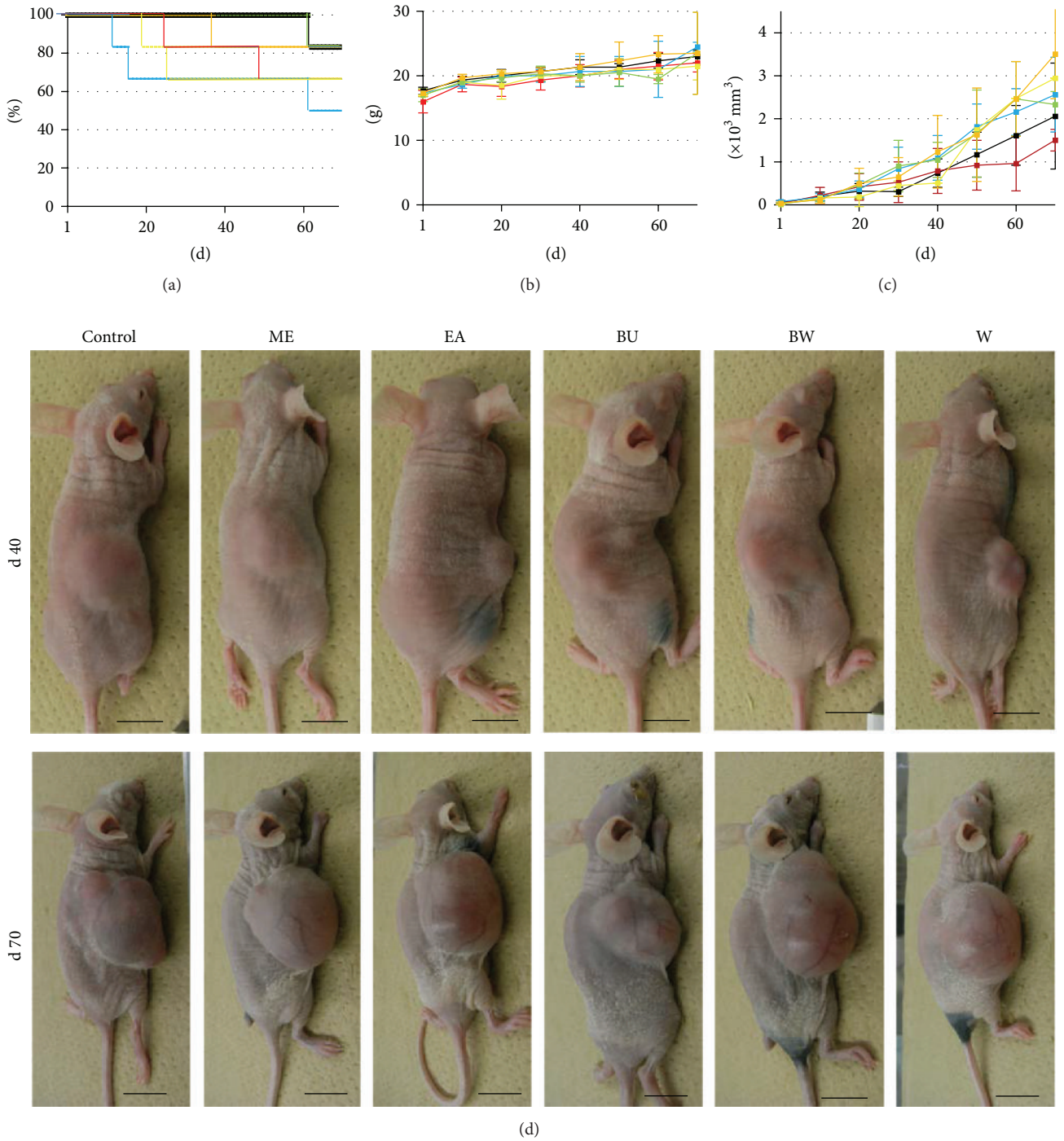

Figure 5: Effects of *P. lutea* leaf extracts on mouse survival and tumor growth in SAS-cell-xenograft nude mice. One million SAS cells were subcutaneously injected into the dorsal flank of nude mice (see Section 2). After 7 d, the mice were divided into 6 groups: vehicle (black lines in (a), (b), and (c) and control in (d)) methanol (red lines and ME), ethyl acetate (blue lines and EA), butanol (yellow lines and BU), butanol-insoluble (green lines and BW), and water (orange lines and W) extracts of *P. lutea* leaves were administrated once every three days at a concentration of 100 mg/kg body weight in PBS. Mouse survival Kaplan Meier plot in %, body weight in grams, and tumor volume in $\times 10^3$ mm^3 of each group are depicted in (a), (b), and (c), respectively; images of a representative mouse in each group were taken at d 40 and 70 (d). Bars, 1 cm.

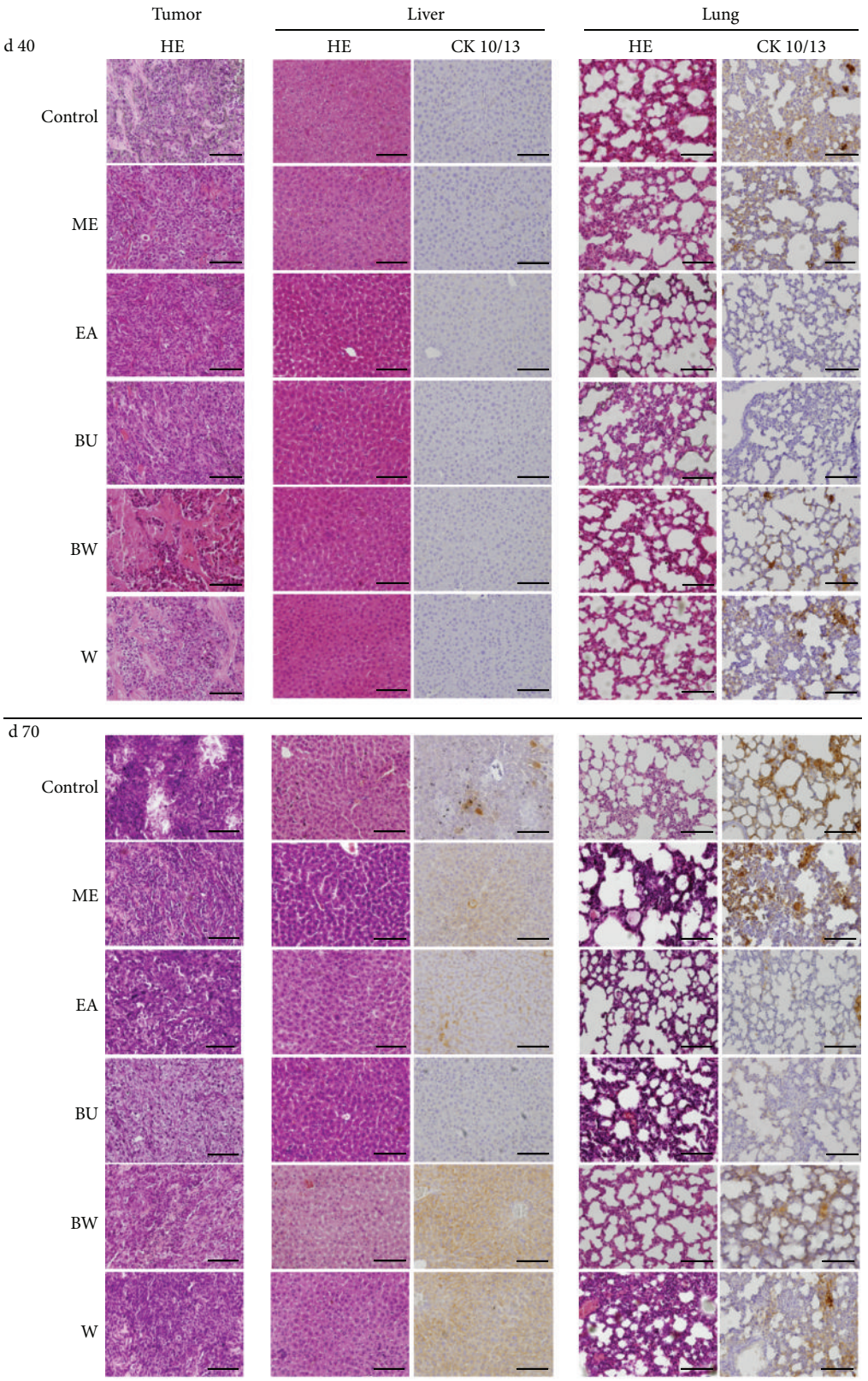

Figure 6: Effects of *P. lutea* leaf extracts on hepatic and pulmonary tumor-cell-metastasis in SAS-cell-xenograft nude mice. One million SAS cells were subcutaneously injected into the dorsal flank of nude mice, and vehicle (control), methanol (ME), ethyl acetate (EA), butanol (BU), butanol-insoluble (BW), and water (W) extracts of *P. lutea* leaves were administrated once every three days at 100 mg/kg body weight in PBS (see Section 2). After d 40 or 70, the mice were sacrificed, and the tumors, livers, and lungs were fixed and subjected to HE staining (HE) and immunohistochemistry for cytokeratin 10/13 (CK 10/13). Bars, 200 μm.

are currently being investigated in detail and will be reported in the near future.

Competing Interests

All authors have no competing interests.

Acknowledgments

This study was supported by Grants-in-Aid for Scientific Research (KAKENHI) from the Japan Society for the Promotion of Science (JSPS) (KAKENHI C to Yoshiki Mukudai, Seiji Kondo, and Tatsuo Shirota). The authors wish to thank all the doctors in the Department of Oral and Maxillofacial Surgery, School of Dentistry, Showa University, and Ms. Miho Yoshihara for secretarial assistance.

References

[1] J.-P. Machiels, M. Lambrecht, F.-X. Hanin et al., "Advances in the management of squamous cell carcinoma of the head and neck," *F1000Prime Reports*, vol. 6, article 44, 2014.

[2] Y.-C. Lin, H.-W. Chen, Y.-C. Kuo, Y.-F. Chang, Y.-J. Lee, and J.-J. Hwang, "Therapeutic efficacy evaluation of curcumin on human oral squamous cell carcinoma xenograft using multimodalities of molecular imaging," *American Journal of Chinese Medicine*, vol. 38, no. 2, pp. 343–358, 2010.

[3] N. A. G. dos Santos, M. A. C. Rodrigues, N. M. Martins, and A. C. dos Santos, "Cisplatin-induced nephrotoxicity and targets of nephroprotection: an update," *Archives of Toxicology*, vol. 86, no. 8, pp. 1233–1250, 2012.

[4] S. R. McWhinney, R. M. Goldberg, and H. L. McLeod, "Platinum neurotoxicity pharmacogenetics," *Molecular Cancer Therapeutics*, vol. 8, no. 1, pp. 10–16, 2009.

[5] J. Herrstedt, "Antiemetics: an update and the MASCC guidelines applied in clinical practice," *Nature Clinical Practice Oncology*, vol. 5, no. 1, pp. 32–43, 2008.

[6] L. P. Rybak, D. Mukherjea, S. Jajoo, and V. Ramkumar, "Cisplatin ototoxicity and protection: clinical and experimental studies," *Tohoku Journal of Experimental Medicine*, vol. 219, no. 3, pp. 177–186, 2009.

[7] A. D. Rapidis, M. Trichas, E. Stavrinidis et al., "Induction chemotherapy followed by concurrent chemoradiation in advanced squamous cell carcinoma of the head and neck: final results from a phase II study with docetaxel, cisplatin and 5-fluorouracil with a four-year follow-up," *Oral Oncology*, vol. 42, no. 7, pp. 675–684, 2006.

[8] A. Psyrri, M. Kwong, S. DiStasio et al., "Cisplatin, fluorouracil, and leucovorin induction chemotherapy followed by concurrent cisplatin chemoradiotherapy for organ preservation and cure in patients with advanced head and neck cancer: long-term follow-up," *Journal of Clinical Oncology*, vol. 22, no. 15, pp. 3061–3069, 2004.

[9] C. H. Lau, C. M. Chan, Y. W. Chan et al., "Pharmacological investigations of the anti-diabetic effect of Cortex Moutan and its active component paeonol," *Phytomedicine*, vol. 14, no. 11, pp. 778–784, 2007.

[10] H. Fujiwara, M. Tabuchi, T. Yamaguchi et al., "A traditional medicinal herb Paeonia suffruticosa and its active constituent 1,2,3,4,6-penta-O-galloyl-β-d-glucopyranose have potent anti-aggregation effects on Alzheimer's amyloid β proteins in vitro and in vivo," *Journal of Neurochemistry*, vol. 109, no. 6, pp. 1648–1657, 2009.

[11] J. Zhou, L. Zhou, D. Hou, J. Tang, J. Sun, and S. C. Bondy, "Paeonol increases levels of cortical cytochrome oxidase and vascular actin and improves behavior in a rat model of Alzheimer's disease," *Brain Research*, vol. 1388, pp. 141–147, 2011.

[12] H. S. Kim, A.-R. Kim, J. M. Lee et al., "A mixture of Trachelospermi caulis and Moutan cortex radicis extracts suppresses collagen-induced arthritis in mice by inhibiting NF-κB and AP-1," *Journal of Pharmacy and Pharmacology*, vol. 64, no. 3, pp. 420–429, 2012.

[13] T.-C. Chou, "Anti-inflammatory and analgesic effects of paeonol in carrageenan-evoked thermal hyperalgesia," *British Journal of Pharmacology*, vol. 139, no. 6, pp. 1146–1152, 2003.

[14] G. Li, C.-S. Seo, K.-S. Lee et al., "Protective constituents against sepsis in mice from the root cortex of *Paeonia suffruticosa*," *Archives of Pharmacal Research*, vol. 27, no. 11, pp. 1123–1126, 2004.

[15] C.-L. Hsieh, C.-Y. Cheng, T.-H. Tsai et al., "Paeonol reduced cerebral infarction involving the superoxide anion and microglia activation in ischemia-reperfusion injured rats," *Journal of Ethnopharmacology*, vol. 106, no. 2, pp. 208–215, 2006.

[16] C.-Y. Hsiang, C.-L. Hsieh, S.-L. Wu, L. Lu, T.-Y. Lai, and Ho, "Inhibitory effect of anti-pyretic and anti-inflammatory herbs on herpes simplex virus replication," *American Journal of Chinese Medicine*, vol. 29, no. 3-4, pp. 459–467, 2001.

[17] T. K. Au, T. L. Lam, T. B. Ng, W. P. Fong, and D. C. C. Wan, "A comparison of HIV-1 integrase inhibition by aqueous and methanol extracts of Chinese medicinal herbs," *Life Sciences*, vol. 68, no. 14, pp. 1687–1694, 2001.

[18] J.-Y. Hung, C.-J. Yang, Y.-M. Tsai, H.-W. Huang, and M.-S. Huang, "Antiproliferative activity of paeoniflorin is through cell cycle arrest and the Fas/Fas ligand-mediated apoptotic pathway in human non-small cell lung cancer A549 cells," *Clinical and Experimental Pharmacology and Physiology*, vol. 35, no. 2, pp. 141–147, 2008.

[19] H. S. Choi, H.-S. Seo, J. H. Kim, J.-Y. Um, Y. C. Shin, and S.-G. Ko, "Ethanol extract of paeonia suffruticosa Andrews (PSE) induced AGS human gastric cancer cell apoptosis via fas-dependent apoptosis and MDM2-p53 pathways," *Journal of Biomedical Science*, vol. 19, article 82, 2012.

[20] G. Xing, Z. Zhang, J. Liu, H. Hu, and N. Sugiura, "Antitumor effect of extracts from moutan cortex on DLD-1 human colon cancer cells in vitro," *Molecular Medicine Reports*, vol. 3, no. 1, pp. 57–61, 2010.

[21] S.-C. Wang, S.-W. Tang, S.-H. Lam et al., "Aqueous extract of Paeonia suffruticosa inhibits migration and metastasis of renal cell carcinoma cells via suppressing VEGFR-3 pathway," *Evidence-Based Complementary and Alternative Medicine*, vol. 2012, Article ID 409823, 9 pages, 2012.

[22] M.-Y. Lin, Y.-R. Lee, S.-Y. Chiang et al., "Cortex Moutan induces bladder cancer cell death via apoptosis and retards tumor growth in mouse bladders," *Evidence-Based Complementary and Alternative Medicine*, vol. 2013, Article ID 207279, 8 pages, 2013.

[23] C. Li, K. Yazawa, S. Kondo et al., "The root bark of Paeonia moutan is a potential anticancer agent in human oral squamous cell carcinoma cells," *Anticancer Research*, vol. 32, no. 7, pp. 2625–2630, 2012.

[24] Y. Mukudai, S. Kondo, T. Koyama et al., "Potential anti-osteoporotic effects of herbal extracts on osteoclasts, osteoblasts

and chondrocytes in vitro," *BMC Complementary and Alternative Medicine*, vol. 14, article 29, 2014.

[25] D. Sato, S. Kondo, K. Yazawa et al., "The potential anticancer activity of extracts derived from the roots of Scutellaria baicalensis on human oral squamous cell carcinoma cells," *Molecular and Clinical Oncology*, vol. 1, no. 1, pp. 105–111, 2013.

[26] Y. Mukudai, S. Kondo, S. Shiogama et al., "Root bark extracts of *Juncus effusus* and *Paeonia suffruticosa* protect salivary gland acinar cells from apoptotic cell death induced by cis-platinum (II) diammine dichloride," *Oncology Reports*, vol. 30, no. 6, pp. 2665–2671, 2013.

[27] K. Okumura, A. Konishi, M. Tanaka, M. Kanazawa, K. Kogawa, and Y. Niitsu, "Establishment of high- and low-invasion clones derived for a human tongue squamous-cell carcinoma cell line SAS," *Journal of Cancer Research and Clinical Oncology*, vol. 122, no. 4, pp. 243–248, 1996.

[28] Y. Mukudai, S. Kondo, A. Fujita, Y. Yoshihama, T. Shirota, and S. Shintani, "Tumor protein D54 is a negative regulator of extracellular matrix-dependent migration and attachment in oral squamous cell carcinoma-derived cell lines," *Cellular Oncology*, vol. 36, no. 3, pp. 233–245, 2013.

[29] H. Tsukamoto, S. Kondo, Y. Mukudai et al., "Evaluation of anticancer activities of benzo[c]phenanthridine alkaloid sanguinarine in oral squamous cell carcinoma cell line," *Anticancer Research*, vol. 31, no. 9, pp. 2841–2846, 2011.

[30] A. Yasuda, S. Kondo, T. Nagumo et al., "Anti-tumor activity of dehydroxymethylepoxyquinomicin against human oral squamous cell carcinoma cell lines in vitro and in vivo," *Oral Oncology*, vol. 47, no. 5, pp. 334–339, 2011.

[31] S. Shiogama, S. Yoshiba, D. Soga, H. Motohashi, and S. Shintani, "Aberrant expression of EZH2 is associated with pathological findings and P53 alteration," *Anticancer Research*, vol. 33, no. 10, pp. 4309–4317, 2013.

[32] D. Brenner and T. W. Mak, "Mitochondrial cell death effectors," *Current Opinion in Cell Biology*, vol. 21, no. 6, pp. 871–877, 2009.

[33] P. Paoli, E. Giannoni, and P. Chiarugi, "Anoikis molecular pathways and its role in cancer progression," *Biochimica et Biophysica Acta—Molecular Cell Research*, vol. 1833, no. 12, pp. 3481–3498, 2013.

[34] I. R. Indran, G. Tufo, S. Pervaiz, and C. Brenner, "Recent advances in apoptosis, mitochondria and drug resistance in cancer cells," *Biochimica et Biophysica Acta—Bioenergetics*, vol. 1807, no. 6, pp. 735–745, 2011.

[35] R. Rathinam and S. K. Alahari, "Important role of integrins in the cancer biology," *Cancer and Metastasis Reviews*, vol. 29, no. 1, pp. 223–237, 2010.

[36] M. Shirosaki, T. Koyama, and K. Yazawa, "Apple leaf extract as a potential candidate for suppressing postprandial elevation of the blood glucose level," *Journal of Nutritional Science and Vitaminology*, vol. 58, no. 1, pp. 63–67, 2012.

[37] M. Shirosaki, Y. Goto, S. Hirooka, H. Masuda, T. Koyama, and K. Yazawa, "Peach leaf contains multiflorin A as a potent inhibitor of glucose absorption in the small intestine in mice," *Biological and Pharmaceutical Bulletin*, vol. 35, no. 8, pp. 1264–1268, 2012.

[38] T. Koyama, C. Nakajima, S. Nishimoto, M. Takami, J.-T. Woo, and K. Yazawa, "Suppressive effects of the leaf of *Terminalia catappa* L. on osteoclast differentiation in vitro and bone weight loss in vivo," *Journal of Nutritional Science and Vitaminology*, vol. 58, no. 2, pp. 129–135, 2012.

[39] S. Soni, M. Mathur, N. K. Shukla, S. V. S. Deo, and R. Ralhan, "Stromelysin-3 expression is an early event in human oral tumorigenesis," *International Journal of Cancer*, vol. 107, no. 2, pp. 309–316, 2003.

[40] C. Qiu, H. Wu, H. He, and W. Qiu, "A cervical lymph node metastatic model of human tongue carcinoma: serial and orthotopic transplantation of histologically intact patient specimens in nude mice," *Journal of Oral and Maxillofacial Surgery*, vol. 61, no. 6, pp. 696–700, 2003.

microRNA expression profiles in oral squamous cell carcinoma

DAISUKE SOGA, SAYAKA YOSHIBA, SUNAO SHIOGAMA, HIROAKI MIYAZAKI, SEIJI KONDO and SATORU SHINTANI

Department of Oral and Maxillofacial Surgery, Showa University School of Dentistry, Ota-ku, Tokyo 145-8515, Japan

Received December 12, 2012; Accepted January 31, 2013

DOI: 10.3892/or.2013.2488

Abstract. microRNAs (miRNAs) are involved in cancer pathogenesis, apoptosis and cell growth, thereby functioning as both tumor suppressors and oncogenes. However, the expression patterns and roles of miRNAs in oral squamous cell carcinoma (OSCC) remain largely unknown. We hypothesized that oral cancer may have a unique miRNA profile, which in turn may play a critical role in oral cancer development, progression, diagnosis and prognosis. We, therefore, investigated the expression profiles of 29 OSCC tumors and 7 normal oral mucosal samples. The miRNA expression patterns in OSCC were examined by TaqMan-based microRNA assays. We were subsequently able to identify the candidates of cancer-related miRNAs through analysis of the miRNA expression profiles. In conclusion, OSCC tissues were shown to have a unique miRNA profile pattern when compared with that in normal tissues. The present study may provide useful information for further investigation of the functional roles of miRNAs in OSCC development, progression, diagnosis and prognosis.

Introduction

Oral cancer, which is occurring at an increasing frequency worldwide, is the sixth most common malignancy in humans. This year alone, it is estimated that ~600,000 new cases will arise, with only 40-50% of patients with oral squamous cell carcinoma (OSCC) likely to survive for 5 years. Despite combined surgery and radiation therapy, long-term survival of patients with oral cancer has shown no improvement over the past few decades (1,2). This is primarily due to the poor clinical prognosis of patients with lymph node metastasis. A deeper understanding of the molecular basis of the highly malignant properties of oral cancer combined with patient stratification is therefore needed.

Correspondence to: Dr Daisuke Soga, Department of Oral and Maxillofacial Surgery, Showa University School of Dentistry, 2-1-1 Kitasenzoku, Ota-ku, Tokyo 145-8515, Japan
E-mail: d-soga@dent.showa-u.ac.jp

Key words: microRNA, exhaustive analysis, abnormal expression, oral squamous cell carcinoma

microRNAs (miRNAs) are non-coding small RNAs (~22 nucleotides) that regulate post-transcriptional gene expression by interfering with the translation of target mRNAs. A single miRNA can regulate the expression of several genes, while more than one-third of all protein-coding genes are thought to be under translational control of miRNAs. miRNAs are involved in a variety of cellular processes, including the regulation of cellular differentiation, proliferation and apoptosis (3,4). In addition, aberrant expression of miRNAs is known to induce various human malignancies, clearly classified by their miRNA profiles (5,6). However, little is known about the miRNA expression patterns or function in oral cancer (7,8).

Specific overexpression or underexpression of miRNAs has been correlated with particular types of tumors (5,9,10). It has also been suggested that miRNA overexpression could result in downregulation of tumor-suppressor genes, while underexpression may lead to oncogene upregulation (9). Most importantly, it has been suggested that miRNA expression signatures could be used to predict the outcome in several tumor types, including lung cancer and chronic lymphocytic leukemia, as well as to predict the response to chemotherapy. miRNAs may therefore prove to be novel therapeutic targets for a wide range of diseases, including cancer (11).

In the present study, we examined the expression profiles of miRNAs in OSCC, revealing differential expression between normal and cancer tissues. These findings may further facilitate the potential therapeutic and diagnostic use of miRNAs in OSCC.

Materials and methods

Clinical samples and cell lines. Twenty-nine OSCC samples and 7 oral mucosal samples were obtained from oral cancer patients who underwent surgery at Showa University from April 2004 to November 2008. Written informed consent was obtained from all patients prior to sampling, and samples were maintained at -80˚C until use. OSCC samples were microscopically examined for determination of cancer cell content by two independent pathologists; they were dissected to enrich cancer cells when necessary. For molecular analysis, 29 samples containing ≥50% cancer cells were used. Normal oral mucosa was extracted at a sufficient margin from the cancer, and the absence of a muscle layer and cancer cells was confirmed microscopically. The present study was certified by the Ethics Committee of the Showa University.

RNA preparation. miRNA was prepared with the Recover All Total Nucleic Acid Isolation kit (Applied Biosystems, Darmstadt, Germany) according to the kit protocol. RNA yield and the A260/280 ratio were monitored with a NanoDrop ND-100 spectrometer (NanoDrop Technologies, Wilmington, DE, USA).

Reverse transcription. miRNAs were reverse transcribed with the TaqMan miRNA Reverse Transcription kit (Applied Biosystems), using 60 ng total RNA and pools of miRNA specific stem-loop primers (Megaplex RT Primers Pool A and B; Applied Biosystems). After reverse transcription, the cDNA was preamplified with Megaplex PreAmp Primers (Pool A and B) according to the recommendations of the supplier (Applied Biosystems).

TaqMan low density arrays. Differential expression of 768 miRNAs was determined using Taqman microRNA Array v2.0 (Applied Biosystems), with an A and B card for each. The array plate also included the RNU48 transcript as a normalization signal. Expression levels of each mature miRNA were evaluated using the comparative threshold cycle (Ct) method, with normalization to RNU48 ($2^{-\Delta\Delta Ct}$). The fold-change in each miRNA was calculated from the difference in expression levels between tumor tissues and normal tissues.

miRNA target prediction. TargetScan (http://www.targetscan.org/) was used to analyze potential target genes of the deregulated miRNAs.

Results

Differential expression of miRNAs between normal oral mucosa and oral cancer tissues. To define the role of miRNAs in OSCC, we investigated the expression profiles of 29 OSCC tumors and 7 normal oral mucosal samples. The 29 OSCC tissue samples were of various stages and histological grades (Table I). TaqMan-based microRNA assays of 768 different miRNA targets were performed, revealing a total of 177 detectable miRNAs. Volcano plots show differential expression between normal and cancer tissues (Fig. 1). We subsequently calculated the degree of differential expression, revealing that miRNAs >4-fold upregulated or downregulated could be considered as candidate miRNAs. miR-31*, miR-31, miR-135b, miR-193a-5p, miR-103, miR-224, miR-93, miR-200c, miR-183, miR203, miR-21 and miR-223 were shown to be upregulated, while miR-133a, miR-376c, miR-411, miR-30a-3p, miR-489, miR-139-5p, miR-483-5p, miR-30e-3p, miR-409-3p, let-7c and miR-486-5p were shown to be downregulated in OSCC (Tables II and III).

Differential expression of miRNAs between non-metastatic (-) and metastatic (+) OSCC. As cervical lymph node metastasis is directly correlated with oral cancer prognosis, we subsequently aimed to determine whether miRNA expression was associated with outcome in OSCC patients. Volcano plots show the differential expression of miRNAs in non-metastatic (-) and metastatic (+) OSCC (Fig. 2). We subsequently calculated the level of significance of the differential expression between these groups. miR-489, miR-483-5p and miR-1291 were shown to be downregulated in OSCC (Table IV). In addition, a decision tree model was used to classify the two groups (Fig. 3), doing so with 82% accuracy.

Table I. Demographic and clinical features of the OSCC patients.

Characteristic	n (%)
Gender	
Male	20 (69)
Female	9 (31)
Smoking habit	
Positive	8 (28)
Negative	21 (72)
Drinking habit	
Positive	9 (31)
Negative	20 (69)
WHO classification	
Well	10 (34)
Moderate	8 (28)
Poor	11 (38)
YK grade	
1	1 (4)
2	3 (10)
3	13 (45)
4	12 (41)
Local recurrence	
Positive	10 (34)
Negative	19 (66)
Age (years)	
>65	21 (72)
≤65	8 (28)
Stage	
I	6 (21)
II	9 (31)
III	3 (10)
IV	11 (38)
T status	
I	6 (21)
II	14 (48)
III	2 (7)
IV	7 (24)
N status	
N0	15 (51)
N1	4 (13)
N2	10 (36)

Discussion

miRNAs are a new class of non-coding small RNAs that regulate cell proliferation and various cellular functions by interfering with the translation of the target mRNAs (3,4,12,13). Recent studies have demonstrated that altered expression of miRNAs induces various human malignancies (14,15).

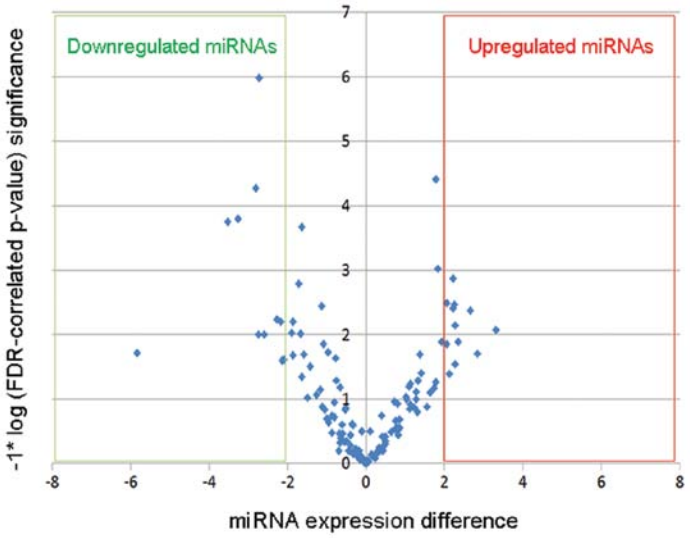

Figure 1. Comparison of miRNA expression between OSCC and normal oral mucosa. Volcano plots of 177 miRNAs analyzed for comparison between OSCC and normal oral mucosa. The level of differential miRNA expression between OSCC and normal oral mucosa is plotted on the x-axis, and the P-value of a FDR-corrected Wilcoxon signed-rank test of the differences (-1* log10 scale) is indicated on the y-axis. miRNAs significantly different between the two groups are boxed in red and green.

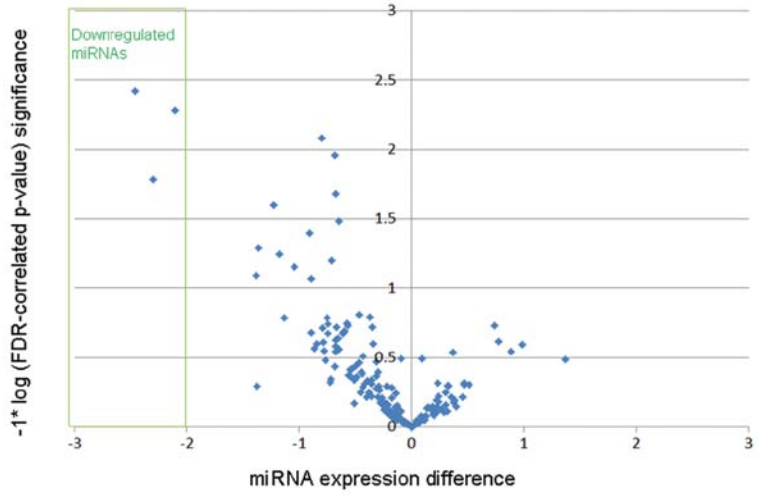

Figure 2. Comparison of miRNA expression between non-metastatic and metastatic OSCC. Volcano plots of 177 miRNAs analyzed for comparison between non-metastatic and metastatic OSCC. The level of differential miRNA expression between non-metastatic and metastatic OSCC is plotted on the x-axis, and the P-value of a FDR-corrected Wilcoxon signed-rank test of the differences (-1* log10 scale) is indicated on the y-axis. miRNAs significantly different between the two groups are boxed in green.

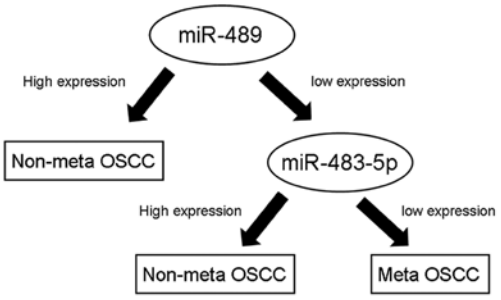

Figure 3. A decision making model was constructed to classify the oral cancer samples according to metastasis using miRNA expression using a training set of oral cancers (n=29). miR-489 (Ct-value ≤10.8; high expression) and miR-483-5p (Ct-value ≤12.1; high expression) resulted in the most accurate prediction (82% accuracy) for classifying the samples into the two corresponding groups.

However, little is known about the role of miRNAs in OSCC. In this study, we investigated the miRNA expression profiles of normal oral mucosa and OSCC tissues. miRNA profiling in B cell lymphoma (16), prostate (17), and colon cancer (18) was previously performed; however, to the best of our knowledge, this is the first comprehensive miRNA profiling study of oral cancer through exhaustive analysis.

miRNA analysis was performed using TaqMan microRNA Array v2.0, which consists of 768 candidate miRNA sites. A total of 177 miRNAs were detected in the oral cancer tissues and normal oral mucosa. Volcano plot analysis subsequently revealed aberrant expression of miRNAs in OSCC (Fig. 2). This result suggests that miRNA expression profiles differ between normal and abnormal cells.

Table II. Differentially expressed miRNAs showing increased expression in OSCC compared to normal mucosa.

microRNA	Fold-change (Ct-Ca/Ct-N)	FDR	Chromosome location	Putative target
hsa-miR-31*	0.60	0.008	9p21.3	RSBN1, ARHGEF2, IDE, NR5A2, SH2D1A
hsa-miR-31	0.29	0.020	9p21.3	RSBN1, ARHGEF2, IDE, NR5A2, SH2D1A
hsa-miR-135b	0.68	0.004	1q32.1	ANGPT2, GK5, NR3C2, GULP1, LOC221710
hsa-miR-193a-5p	0.77	0.013	17q11.2	HSPB6, ZNF385C, ITSN1, OLIG3, USO1
hsa-miR-103	0.76	0.007	5q34	DICER1, TMEM16C, NF1, FOXP1, HRB
hsa-miR-224	0.71	0.029	Xq28	ZDHHC20, AFF3, U2SURP, C8orf44, TTC3
hsa-miR-93	0.64	0.003	7q22.1	FGD4, PKD2, MAP3K2, ZNFX1, PDCD1LG
hsa-miR-200c	0.27	0.004	12p13.31	ZEB1, FAM122C, ZEB2, LRP1B, WIPF1
hsa-miR-183	0.82	0.001	7q32.2	ABAT, AKAP12, PIGX, PTPN4, REV1
hsa-miR-203	0.22	0.040	14q32.33	ZNF281, CAMTA1, B3GNT5, LIFR, ABCE1
hsa-miR-21	0.54	0.014	17q23.1	ANF367, GPR64, YOD1, PHF14, PLEKHA1
hsa-miR-223	0.27	0.003	Xq12	FBXW7, SP3, PAX6, C13orf31, PURB

Fold-changes are expressed as the ratio of OSCC Ct values vs. normal mucosa Ct values. FDR, false discovery rate. The top putative targets identified with TargetScan are included.

Table III. Differentially expressed miRNAs showing decreased expression in OSCC compared to normal mucosa.

microRNA	Fold-change (Ct-Ca/Ct-N)	FDR	Chromosome location	Putative target
hsa-miR-133a	3.13	0.019	18q.11.2	SYT2, LHFP, CCBL2, BRUNOL4, TTPAL
hsa-miR-376c	1.55	<1e-03	14q32.31	ARFGEF1, PAPSS2, GABRG2, SYF2, ARFGEF2
hsa-miR-411	1.52	<1e-03	14q32.31	ELFN1, SLC4A7, C16orf52, C21orf91, SPRY4
hsa-miR-30a-3p	1.75	<1e-03	6q13	NUFIP2, ZNF85, RUNDC2B, FIGN, POU4F1
hsa-miR-489	1.36	0.010	7q21.3	ETNK1, PARM1, CWC25, NRIP1, PNISR
hsa-miR-139-5p	1.65	<1e-03	11q13.4	TMF1, USP6NL, TBX1, SCAPER, NDRG2
hsa-miR-483-5p	1.33	0.010	11p15.5	SELO, MPZ, SRSF4, SLC12A5, RNF165
hsa-miR-30e-3p	1.54	0.006	1p34.2	NUFIP2, ZNF85, RUNDC2B, POU4F1, DSN
hsa-miR-409-3p	1.42	0.006	14q32.31	MRPL35, LRRN4CL, POMP, MTF2, TMEM65
hsa-let-7c	1.29	0.025	21q21.1	C14orf28, FIGNL2, HMGA2, LIN28B, TRIM71
hsa-miR-486-5p	1.49	0.025	8p11.21	FOXO1, GPX8, PTEN, TRAPPC6B, TWF1

Fold-changes are expressed as the ratio of OSCC Ct values vs. normal mucosa Ct values. FDR, false discovery rate. The top putative targets identified with TargetScan are included.

Table IV. Differentially expressed miRNAs showing decreased expression in non-metastatic and metastatic OSCC.

microRNA	Fold-change (Ct-Ca/Ct-N)	FDR	Chromosome location	Putative target
hsa-miR-489	1.27	0.004	7q21.3	ETNK1, ALS2CR13, HRH4, LONRF2, SFRS7
hsa-miR-1291	1.18	0.017	12q13.11	AQP1, ARID3B, MECP2, MAP3K9, PGM5
hsa-miR-483-5p	1.22	0.005	11p15.5	RAB3IP, ZBTB26, PGAM1, C5orf42, RBAK

Fold-changes are expressed as the ratio of OSCC Ct values vs. normal mucosa Ct values. FDR, false discovery rate. The top putative targets identified with TargetScan are included.

To identify candidate cancer-related miRNAs, we calculated the degree of differential expression of miRNAs between normal oral mucosa and OSCC tissues. Twelve miRNAs (miR-31*, miR-31, miR135b, miR-193a-5p, miR-103, miR-224, miR-93, miR-200c, miR-183, miR-203, miR-21 and miR-223) were significantly upregulated in most of the cancer tissue samples compared with the normal oral mucosa. Those showing >4-fold upregulation were considered candidate miRNAs; namely, miR-31*, miR-31, miR-135b, miR-193a-5p, miR-103, miR-224, miR-93, miR-200c, miR-183, miR-203, miR-21 and miR-223.

miR-21 has been investigated widely in various human malignancies including hematological malignancies and glioblastoma as a putative oncogenic miRNA (5,19-26). Moreover, aberrantly expressed miR-203 has been detected in colon (27), breast (28) and ovarian cancer (29-31), while miR-31 is also known to have oncogenic functions in esophageal cancer (32). Upregulation of both miR-31 and miR-31* by delivery of pre-miR-31 was also shown to enhance OSCC oncogenicity (33). Our results also indicated that miR-31 and miR-31* have a biological function in cancer development. However, a role in oral cancer has yet to be documented, and the function of these candidates in human cancer remains unclear. miR-133a, miR-376c, miR-411, miR-30a-3p, miR-489, miR-139-5p, miR-483-5p, miR-30e-3p, miR-409-3p, let-7c and miR-486-5p showed a >4-fold downregulation (Table III). Previously, miR-133a was shown to be downregulated in breast cancer tissues and correlated with poor prognosis (34), while let-7c is reportedly related to tumor growth inhibition in prostate cancer (35).

Cervical lymph node metastasis has a large impact on the prognosis of OSCC. We, therefore, performed volcano plot analysis according to the metastatic state. Three downregulated miRNAs (niR-489, miR-1291 and miR-483-5p) (Table IV) were detected, and subsequently, a decision tree model was constructed to classify non-metastatic and metastatic OSCC using Weka software. Our model divided the two groups with 82% accuracy (Fig. 3). This model may therefore have potential in determining the prognosis of OSCC patients, acting as a predictive marker of metastasis.

In summary, our findings identifying cancer-related miRNAs in OSCC suggest that oral cancer may have a unique miRNA expression pattern at the individual level. Further investigations are now required to determine the molecular functions and mechanisms of these miRNAs as well as their potential use as prognostic and/or diagnostic markers in oral cancer.

Acknowledgements

We thank Tomohide Isobe and Tetsuhiko Tachikawa for the diagnostic clinical oral cancer tissues.

References

1. Bernier J, Bentzen SM and Vermorken JB: Molecular therapy in head and neck oncology. Nat Rev Clin Oncol 6: 266-277, 2009.
2. Bozec A, Peyrade F, Fischel JL and Milano G: Emerging molecular targeted therapies in the treatment of head and neck cancer. Expert Opin Emerg Drugs 14: 299-310, 2009.
3. Hummel R, Maurer J and Haier J: MicroRNA: biogenesis, function and role in rancer. Curr Genomics 11: 537-561, 2010.
4. Wiemer EA: The role of microRNAs in cancer: no small matter. Eur J Cancer 43: 1529-1544, 2007.
5. Lu J, Getz G, Miska EA, *et al*: MicroRNA expression profiles classify human cancers. Nature 435: 834-838, 2005.
6. Calin GA and Croce CM: MicroRNA signatures in human cancers. Nat Rev Cancer 6: 857-866, 2006
7. Wu BH, Xiong XP, Jia J and Zhang WF: MicroRNAs: new actors in the oral cancer scene. Oral Oncol 47: 314-319, 2011.
8. Reis PP, Tomenson M, Cervigne NK, Machado J, Jurisica I and Pintilie M: Programmed cell death 4 loss increases tumor cell invasion and is regulated by miR-21 in oral squamous cell carcinoma. Mol Cancer 10: 238, 2010.
9. Gottardo F, Liu CG, Ferracin M, *et al*: Micro-RNA profiling in kidney and bladder cancers. Urol Oncol 25: 387-392, 2007.
10. Volinia S, Calin GA, Liu CG, *et al*: A microRNA expression signature of human solid tumors defines cancer gene targets. Proc Natl Acad Sci USA 103: 2257-2261, 2006.
11. Hammond SM: MicroRNA therapeutics: a new niche for antisense nucleic acids. Trends Mol Med 12: 99-101, 2006.
12. Lagos-Quintana M, Rauhut R, Lendeckel W and Tuschl T: Identification of novel genes coding for small expressed RNAs. Science 294: 853-858, 2001.
13. Bartel DP: MicroRNAs: genomics, biogenesis, mechanism, and function. Cell 116: 281-297, 2004.
14. Ruan K, Fang X and Ouyang G: MicroRNAs: novel regulators in the hallmarks of human cancer. Cancer Lett 285: 116-126, 2009.
15. Farazi TA, Spitzer JI, Morozov P and Tuschl T: miRNAs in human cancer. J Pathol 223: 102-115, 2011.
16. Calin GA, Liu CG, Sevignani C, *et al*: MicroRNA profiling reveals distinct signatures in B cell chronic lymphocytic leukemias. Proc Natl Acad Sci USA 101: 11755-11760, 2004.
17. Schaefer A, Jung M, Mollenkopf HJ, *et al*: Diagnostic and prognostic implications of microRNA profiling in prostate carcinoma. Int J Cancer 126: 1166-1176, 2010.
18. Schepeler T, Reinert JT, Ostenfeld MS, *et al*: Diagnostic and prognostic microRNAs in stage II colon cancer. Clin Chem 54: 1696-1704, 2008.
19. Zhang B, Pan X, Cobb GP and Anderson TA: microRNAs as oncogenes and tumor suppressors. Dev Biol 302: 1-12, 2007.
20. Papagiannakopoulos T, Shapiro A and Kosik KS: MicroRNA-21 targets a network of key tumor-suppressive pathways in glioblastoma cells. Cancer Res 68: 8164-8172, 2008.
21. Rossi L, Bonmassar E and Faraoni I: Modification of miR gene expression pattern in human colon cancer cells following exposure to 5-fluorouracil in vitro. Pharmacol Res 56: 248-253, 2007.
22. Cheng Y, Ji R, Yue J, *et al*: MicroRNAs are aberrantly expressed in hypertrophic heart: do they play a role in cardiac hypertrophy? Am J Pathol 170: 1831-1840, 2007.
23. Liu X, Cheng Y, Zhang S, Lin Y, Yang J and Zhang C: A necessary role of miR-221 and miR-222 in vascular smooth muscle cell proliferation and neointimal hyperplasia. Circ Res 104: 476-487, 2009.
24. Zhu S, Wu H, Wu F, Nie D, Sheng S and Mo YY: MicroRNA-21 targets tumor suppressor genes in invasion and metastasis. Cell Res 18: 350-359, 2008.
25. Meng F, Henson R, Wehbe-Janek H, Ghoshal K, Jacob ST and Patel T: MicroRNA-21 regulates expression of the PTEN tumor suppressor gene in human hepatocellular cancer. Gastroenterology 133: 647-658, 2007.
26. Löffler D, Brocke-Heidrich K, Pfeifer G, *et al*: Interleukin-6 dependent survival of multiple myeloma cells involves the Stat3-mediated induction of microRNA-21 through a highly conserved enhancer. Blood 15: 1330-1333, 2007.
27. Schetter AJ, Leung SY, Sohn JJ, Zanetti KA, Bowman ED and Yanaihara N: MicroRNA expression profiles associated with prognosis and therapeutic outcome in colon adenocarcinoma. JAMA 299: 425-436, 2008.
28. Iorio MV, Ferracin M, Liu CG, *et al*: MicroRNA gene expression deregulation in human breast cancer. Cancer Res 65: 7065-7070, 2005.
29. Nam EJ, Yoon H, Kim SW, Kim H, Kim YT and Kim JH: MicroRNA expression profiles in serous ovarian carcinoma. Clin Cancer Res 14: 2690-2695, 2008.
30. Saini S, Majid S, Yamamura S, *et al*: Regulatory role of mir-203 in prostate cancer progression and metastasis. Clin Cancer Res 17: 5287-5298, 2011.
31. Wellner U, Schubert J, Burk UC, *et al*: The EMT-activator ZEB1 promotes tumorigenicity by repressing stemness-inhibiting microRNAs. Nat Cell Biol 11: 1487-1495, 2009.
32. Alder H, Taccioli C, Chen H, *et al*: Dysregulation of miR-31 and miR-21 induced by zinc deficiency promotes esophageal cancer. Carcinogenesis 33: 1736-1744, 2012.
33. Chang KW, Kao SY, Wu YH, *et al*: Passenger strand miRNA miR-31(*) regulates the phenotypes of oral cancer cells by targeting RhoA. Oral Oncol 49: 27-33, 2013.
34. Wu ZS, Wang CQ, Xiang R, *et al*: Loss of miR-133a expression associated with poor survival of breast cancer and restoration of miR-133a expression inhibited breast cancer cell growth and invasion. BMC Cancer 12: 51, 2012.
35. Sugimura K, Miyata H, Tanaka K, *et al*: Let-7 expression is a significant determinant of response to chemotherapy through the regulation of IL-6/STAT3 pathway in esophageal squamous cell carcinoma. Clin Cancer Res 18: 5144-5153, 2012.

J Mol Neurosci (2014) 54:388–394
DOI 10.1007/s12031-014-0362-z

Comparison of Expression and Proliferative Effect of Pituitary Adenylate Cyclase-Activating Polypeptide (PACAP) and its Receptors on Human Astrocytoma Cell Lines

Tomoya Nakamachi · Kouichi Sugiyama · Jun Watanabe · Nori Imai · Nobuyuki Kagami · Motohide Hori · Satoru Arata · Seiji Shioda

Received: 4 May 2014 / Accepted: 24 June 2014 / Published online: 6 August 2014

Abstract Pituitary adenylate cyclase-activating polypeptide (PACAP) is a pleiotropic neuropeptide considered to be a potent regulator of astrocytes. It has been reported that PACAP also affects astrocytoma cell properties, but the proliferative effects of this peptide in previous reports were inconsistent. The purpose of this study was to search for correlations between malignant potential, PACAP/PACAP receptor expression, and the proliferative potential of four astrocytoma cell lines (KNS-81, KINGS-1, SF-126, and YH-13). Immunohistochemical observations were performed using astrocyte lineage markers with a view to establishing malignant potential, which is inversely correlated to differentiation status in astrocytoma cells. YH-13 showed the most undifferentiated astrocyte-like status, and was immunopositive to a cancer stem cell marker, CD44. These observations suggest that YH-13 is the most malignant of the astrocytoma cell lines tested. Moreover, the strongest PAC1-R immunoreactivity was observed in YH-13 cells. Using real-time PCR analysis, no significant differences among cell lines were detected with respect to PACAP mRNA, but PAC1-R and VPAC1-R mRNA levels were significantly increased in YH-13 cells compared with the other cell lines. Furthermore, when cell lines were treated with PACAP (10^{-11} M) for 3 days, the YH-13 cell line, but not of the other cell lines, exhibited a significantly increased cell number. These results suggest that PACAP receptor expression is correlated with the malignant and proliferative potential of astrocytoma cell lines.

Keywords PACAP · Astrocytoma · Proliferation · PAC1-R · VPAC1-R · Malignancy

Introduction

Astrocytoma is a form of primary tumor arising from astrocytes. Glioblastoma multiforme, the most aggressive astrocytoma, usually occurs more frequently in the adult brain than in the spinal cord. Because of this tumor's potential to grow quickly, the median survival time is only 12–15 months following diagnosis, even if the patient receives optimal medical treatment (Ahmed et al. 2014), keeping in mind that truly effective drugs have yet to be developed to treat high-grade astrocytomas. This is partly because our present understanding of the pathology of astrocytomas has limited the development of therapeutic interventions.

Pituitary adenylate-cyclase activating polypeptide (PACAP) is a neuropeptide that exists in 38- and 27-amino acid residue forms (Miyata et al. 1989, 1990). PACAP belongs to the vasoactive intestinal polypeptide (VIP)/secretin/glucagon family, and its closest paralog is VIP. PACAP and VIP share three types of receptors (PAC1-R, VPAC1-R, and VPAC2R), with both PACAP and its receptors widely expressed throughout the brain (Arimura and Shioda 1995; Shioda 2000). PACAP has a pleiotropic role in the central nervous system, functioning as a neurotransmitter, neuroprotectant, and promoting factors for neural stem cell

Presented at the 11th International Symposium on VIP, PACAP, and Related Peptides.

T. Nakamachi · K. Sugiyama · J. Watanabe · N. Imai · N. Kagami · M. Hori · S. Shioda (✉)
Department of Anatomy, Showa University School of Medicine, 1-5-8 Hatanodai, Shinagawa-Ku, Tokyo 142-8555, Japan
e-mail: shioda@med.showa-u.ac.jp

T. Nakamachi
Laboratory of Regulatory Biology, Graduate School of Science and Engineering, University of Toyama, Toyama, Toyama, Japan

J. Watanabe · S. Arata
Center for Biotechnology, Showa University, Shinagawa-Ku, Tokyo 142-8555, Japan

differentiation (Shioda et al. 2006; Watanabe et al. 2007; Ohtaki et al. 2008). Moreover, PACAP regulates astrocytes as well as neurons (Masmoudi-Kouki et al. 2007; Nakamachi et al. 2011a).

PACAP also affects glioma cells. Based on elevated cAMP levels, Robberecht et al. first suggested a role played by PACAP receptor expression in human glioma cells (Robberecht et al. 1994). Later, the effect of PACAP on the proliferation of astrocytoma cells was studied by several groups, but conflicting results were obtained (Vertongen et al. 1996; Dufes et al. 2003; Sokolowska and Nowak 2008; D'Amico et al. 2013). We believe that these differences were caused by variations in the malignancy levels of the astrocytoma cells used in the respective studies. As such, the purpose of the present study is to clarify the relation between astrocytoma malignancy and the proliferative effects of PACAP in vitro using a number of different ascytoma cell lines.

Materials and Methods

Human Astrocytoma Cell Lines

Four human astrocytoma cell lines (KNS-81, KINGS-1, SF-126, and YH-13) were obtained from the Health Science Research Resources Bank (Osaka, Japan). The KINGS-1 cell line was established from grade 3 astrocytoma tissue, while SF-126 and YH-13 were established from grade 4 astrocytoma tissue (or glioblastoma multiforme) according to the WHO classification of tumors of the central nervous system (Louis et al. 2007). The KNS-81 cell line was generated from astrocytoma tissue whose malignancy was not recorded.

Cell Culture

Stocks of the four cell lines were defrosted in a 37 °C water bath and then mixed with minimum essential medium (MEM) medium (Invitrogen, Carlsbad, CA, USA) supplemented with 20 % fetal bovine serum (FBS). After centrifugation at 1,500 rpm and 4 °C, the supernatant was removed, the pellet was dissolved in MEM medium with 20 % FBS and antibiotic-antimycotic agents (Invitrogen) and cells were incubated in a 5 % CO_2/air incubator at 37 °C. When the incubated cells reached subconfluence, they were detached by treatment with trypsin-EDTA (Invitrogen) for 5 min. The detached cells were collected and centrifuged at 1,500 rpm for 5 min at 4 °C. The pellet was suspended in the medium, and seeded on 100 mm culture dishes for passage, 60 mm dishes for immunocytochemistry, and 96-well plates for CyQUANT assay. Extra pellets were maintained at −80 °C for real-time PCR analysis.

Immunocytochemistry

Cultured cells were fixed with 4 % paraformaldehyde in 0.05 M phosphate buffer, pH 7.2 for 30 min at 4 °C. After washing with phosphate buffered saline (PBS), the cells were incubated in 5 % normal horse serum with 0.25 % Triton X-100 in PBS for penetration and blocking. The cells were then incubated with primary antibody in blocking buffer for 18 h at 4 °C. The antibodies used were: rat anti-CD44 (1:1000; TONBO Biosciences, San Diego, CA, USA), mouse antiglia fibrillary acidic protein (GFAP, 1:500; Sigma, St. Louis, MO, USA), mouse anti-A2B5 IgM (1:200, EMD Millipore Corporation, Billerica, MA, USA), mouse antiglutamate synthase (GS, 1:500, EMD Millipore Corporation), mouse antineuronal nuclei (NeuN, 1:1,000; EMD Millipore Corporation), rat antimyelin basic protein (MBP, 1:500; EMD Millipore Corporation), rat anti-CD11b (1:500; Serotec, Oxford, UK), or PAC1-R (Suzuki et al. 2003). After incubation with Alexa488-labeled secondary antibodies (Invitrogen), cells were treated for 10 min with 4′,6-diamidino-2-phenylindole (DAPI, 1:10,000). After mounting with aqueous mounting medium on cover slips, the immunoreactivity of cells was measured with the aid of a fluorescence microscope (AXIO Imager Z1, Carl Zeiss, Germany). All of the above procedures were carried out on three cells from three independently prepared cultures.

Real-Time PCR Analysis

Total RNA was isolated by TRIzol Reagent (Invitrogen) from cell pellets prepared from each of the cell lines, and complementary DNA was generated by reverse-transcriptase (PrimeScript RT reagent kit, TaKaRa BIO INC., Kyoto, Japan). PCR primer sets for human PACAP, PAC1-R, VPAC1-R, VPAC2R, and GAPDH mRNA sequences are listed in Table 1. Real-time PCR was performed using SYBR Premix Ex Taq II reagent (TaKaRa BIO INC) and an ABI PRISM 7900 instrument (Applied Biosystems, Lincoln, CA, USA). Relative gene expression was calculated using the comparative delta Ct method, and normalized with respect to the GAPDH housekeeping gene. The specificity of PCR products was confirmed by dissociation curve with a single peak at the final PCR step.

CyQUANT Assay

Astrocytoma cells were seeded at 100 cells/cm^2 on 96-well plates and treated with human PACAP38 (final concentration 10^{-13} to 10^{-7} M in PBS) or PBS as control. After 3 days of treatment, the medium was removed and plates were stored at −80 °C. The number of cells was measured by CyQUANT kit (Invitrogen) following the manufacturer's instructions.

Table 1 Primer sequences used for real-time PCR analyses

Oligo Name	Sequence (5′ to 3′)
Adcyap1-F	GTGAGGTAAGCAAGCTCCAACAGAC
Adcyap1-R	CTCGATCTGATTGCTGGGTGAA
Adcyap1r1-F	CTCACCACTGCCATGGTCATC
Adcyap1r1-R	GCCCTCAGCATGAACGACAC
Vipr1-F	CATTGCCTGTGGTTTGGATGAC
Vipr1-R	GGATAGCTGTGGCGACCAGAA
Vipr2-F	AGTGGCGTCTGGGACAACATC
Vipr2-R	AATCTGGGAACGTCTCTGACCATC
GAPDH-F	GCACCGTCAAGGCTGAGAAC
GAPDH-R	TGGTGAAGACGCCAGTGGA

Statistical Analysis

Data were expressed as mean±SEM. Multiple comparisons were made by ANOVA with Tukey-Kramer multiple-comparison tests. *P* values of less than 0.05 or less than 0.01 were considered to indicate statistical significance for all analyses.

Results

Characterization of Astrocytoma Cell Lines by Immunocytochemistry

We first checked the differentiation level of astrocytoma cells by immunostaining with astrocyte and glial progenitor markers given that malignant astrocytoma cell have been described to show an undifferentiated glial-like phenotype (Jellinger 1978; Piepmeier et al. 1993). Anti-GFAP (marker for mature astrocytes but not immature glial cells such as radial glia), anti-GS (marker for astrocytes and astrocytoma cells), and anti-A2B5 (glial progenitor cell marker) antibodies were used (Fig. 1). GFAP immunoreactivity was observed in the KNS-81 and KINGS-1 cell lines, but not in SF-126 or YH-13. On the other hand, GS immunoreactivity was detected in the KNS-81, KINGS-1, and SF-126 cell lines, but not in YH-13. In contrast, immunoreactivity to A2B5 was observed in SF-126 and YH-13, but not in KNS-81 and KINGS-1 cell lines. To confirm that these cells were derived from astrocytes, other cell markers, such as antibodies against NeuN (as a neuronal marker), MBP (as an oligodendrocyte marker), and CD11b (as a microglial marker) were also tested. Immunoreactivities against these antibodies were not observed in any of the cell lines (Fig. 2). CD44 is a receptor for hyaluronic acid and is used as a marker for cancer stem cells and as an indicator of high-invasive potential (Wiranowska et al. 2006; Anido et al. 2010). Only marginal CD44 immunoreactivity was observed in KNS-81 and KINGS-1 cells, but strong immunoreactivity was observed in SF-126 and YH-13 cells (Fig. 3). PAC1-R immunoreactivity was observed all cells, with the signal intensity increasing in the following order: KNS-81 < KINGS-1 < SF-126 < YH-13 (Fig. 3).

mRNA Levels of PACAP/PACAP Receptors in Astrocytoma

mRNA levels for PACAP and its receptor were measured in the four astrocytoma cell lines by real-time PCR analysis. While differences in ADCYAP1 (gene for PACAP) mRNA levels were not statistically significant between the cells lines (KINGS-1, 100 %; KNS-81, 82.1 %; SF-126, 111.3 %; and YH-13, 68.9 %) (Fig. 4a), large variations were seen for ADCYAP1R1 (gene for PAC1-R) mRNA levels, which in order of ranking were KINGS-1 < KNS-81 < SF-126 < YH-13, with normalized levels of 100, 130.3, 147.5, and 656.0 %, respectively. In this way, ADCYAP1R1 mRNA expression for the YH-13 cell line was significantly increased compared with the other astrocytoma cell lines (Fig. 4b). The VIPR1 mRNA level for YH-13 (4,720.3 %) was significantly higher than that for the other cell lines (KINGS-1, 100 %; KNS-81, 68.9 %; SF-126, 92.9 %) (Fig. 4c). VPAC2R mRNA was below the level of detection in all of the astrocytoma cell lines tested (data not shown).

CyQUANT Proliferation Assay

The effect of PACAP on the proliferative activity of the four astrocytoma cell lines was measured by CyQUANT assay. When employed at concentrations ranging from 10^{-13} to 10^{-7} M, PACAP did not affect the number of KNS-81, KINGS-1, or SF-126 cells in culture compared with the PBS control groups. However, for YH-13 cells in culture, treatment with 10^{-11} M PACAP significantly increased the number of cells compared with PBS treatment (Fig. 5) indicating a proliferative effect of PACAP on YH-13 cells at this concentration.

Discussion

This study was designed to compare the effects of PACAP and its receptor expression on the differentiation status of four human astrocytoma cell lines. GFAP is an intermediate filament protein that is expressed in mature astrocytes but not in immature glial cells such as radial glia (Pixley and de Vellis 1984). On the other hand, the A2B5 antibody binds to gangliosides and is used as glial progenitor marker (Fok-Seang and Miller 1992). Xia et al. (2003) suggested that astrocytoma cells share similar antigenicity with astrocytes, and that the A2B5-positive astrocytoma cells exhibited a higher

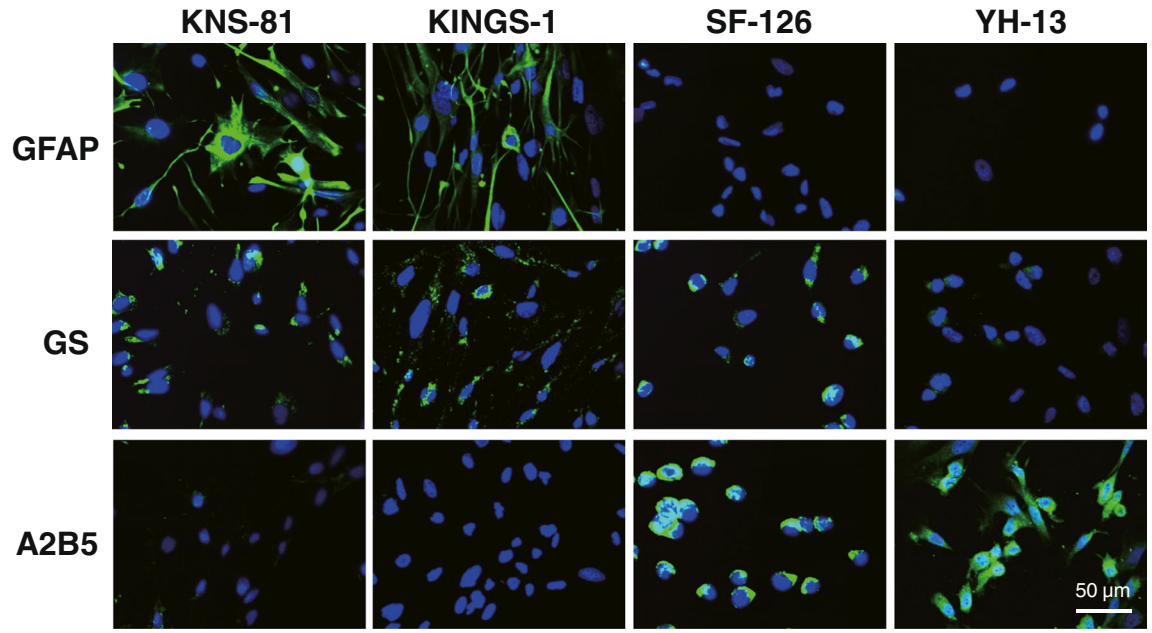

Fig. 1 Characterization of astrocytomas by immunostaining with astrocyte and glial progenitor markers. Cultured astrocytoma cells were immunostained with antibodies against GFAP, GS, and A2B5. *Green* shows immunoreactivity to antibodies. Nuclei counterstained with DAPI are shown in *blue*

recurrence rate than A2B5-negative astrocytoma. In our study, GFAP immunoreactivity was observed in KNS-81 and KINGS-1 cells, but not in SF126 or YH-13 cells. On the other hand, A2B5 immunoreactivity was observed in SF-126 and YH-13 cells, but not KNS-81 or KINGS-1 cells.

GS is a an enzyme that plays a key role in the metabolism of nitrogen. It is a commonly used marker for astrocytes and astrocytoma cells, where an inverse correlation between histological malignancy and degree of GS expression has been observed (Akimoto 1993; Anlauf and Derouiche 2013). Here, GS immunoreacitivty was observed in KNS-81, KINGS-1, and SF126 cells, but not in YH-13 cells (Fig. 1). Moreover, immunoreactivity for CD44, which is known as an astrocytoma stem cell marker, was weak in KINGS-1 cells, and stronger in SF-126 and YH-13 cells (Fig. 3). Taken together, these

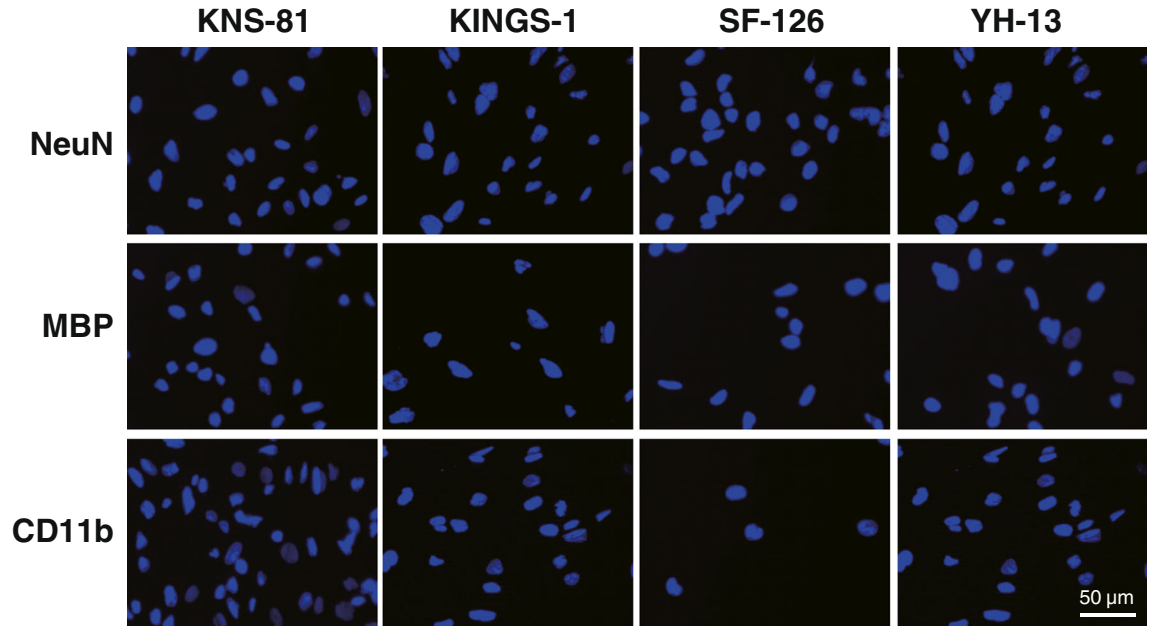

Fig. 2 Characterization of astrocytomas by immunostaining with neuronal cell markers. Cultured astrocytoma cells were immunostained with antibodies against *NeuN* (neuronal marker), *MBP* (oligodendrocyte marker), and *CD11b* (microglia marker). Evidence of any *green color* would be indicative of immunoreactivity against these antibodies. Nuclei counterstained with DAPI are shown in *blue*

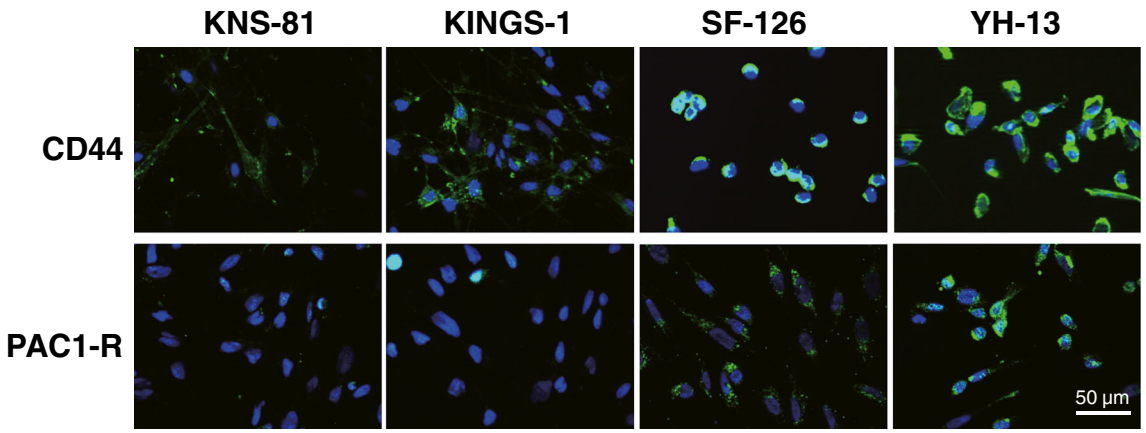

Fig. 3 Characterization of astrocytomas by immunostaining with anti-CD44 or anti-PAC1-R antibodies. Cultured astrocytoma cells were immunostained with antibodies against CD44 and PAC1-R. *Green* shows immunoreactivity to these antibodies. Nuclei counterstained with DAPI are shown in *blue*

immunohistochemistry observations suggest that the malignancy of the astrocytoma cell lines used here (in the order of strength) is YH-13, followed by SF-126, KINGS-1, and KNS-81. These findings also imply that the malignant character of the original astrocytoma tissue used to prepare these cell lines was maintained. Immunoreactivity for other neuronal cell markers (NeuN, MBP, and CD11b) was not observed in the four cell lines (Fig. 2), indicating that they are cells from astrocytomas and not other types of brain tumor cells.

PACAP mRNA levels were not significantly different among the astrocytoma cell lines, but PAC1-R and VPAC1-R mRNA levels in YH-13 were significantly greater than the others (Fig. 4). Similary, strong PAC1-R immunoreactivity was also observed in YH-13 cells (Fig. 3). In consideration of the character of the astrocytoma cell lines, PAC1-R and VPAC1-R mRNA levels of cells with high-malignant potential were greater than those of low-malignant potential.

The results of the CyQUANT assay, a highly sensitive, fluorescence-based microplate assay for determining numbers of cultured cells (Jones et al. 2001), showed that PACAP, employed at a concentration of 10^{-11} M, stimulated an increase in the number of YH-13 cells compared with control PBS-treated cells, but this effect was not seen in the other cell lines (Fig. 5). These differences in sensitivity to PACAP seem to correlate with PAC1-R and VPAC1-R expression levels. As such, conflicting results from previous reports on the effects of PACAP on astrocytoma proliferation and malignancy (see "Introduction" section) may be explained in part by differences in the expression levels of PACAP receptors.

We previously reported that PAC1-R immunoreactivity was increased in reactive astrocytes induced by brain ischemia or spinal cord injury (Tsuchikawa et al. 2012; Nakamachi et al. 2013). PACAP treatment of cultured reactive astrocytes induced by scratch injury significantly increased the number

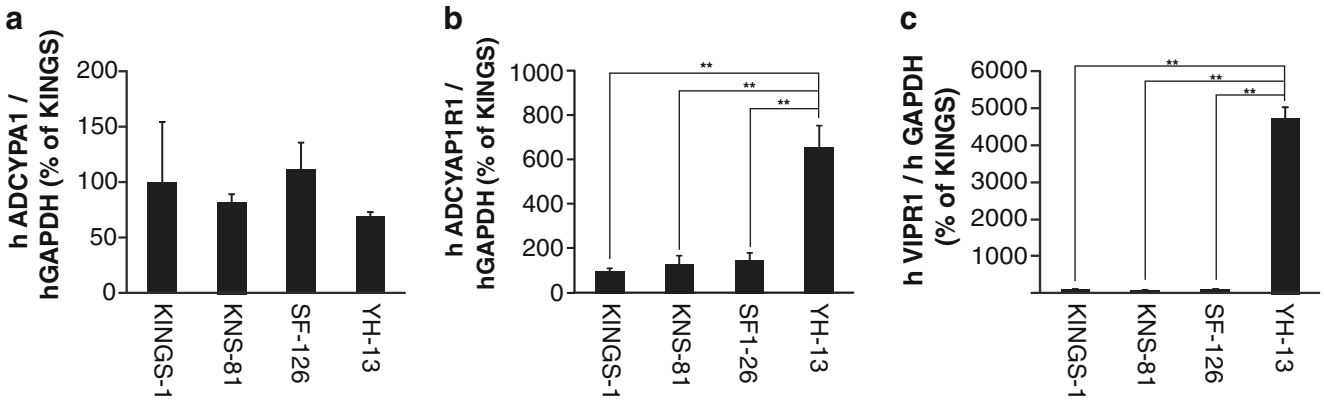

Fig. 4 mRNA levels of PACAP and its receptor in the four astrocytoma cell lines. mRNA level of ADCYAP1 (PACAP), ADCYAP1R1 (PAC1-R), and VIP1R in astrocytoma cell lines were measured by real-time PCR analysis with normalization to GAPDH mRNA level (n=3 cultures for each result). **P<0.01

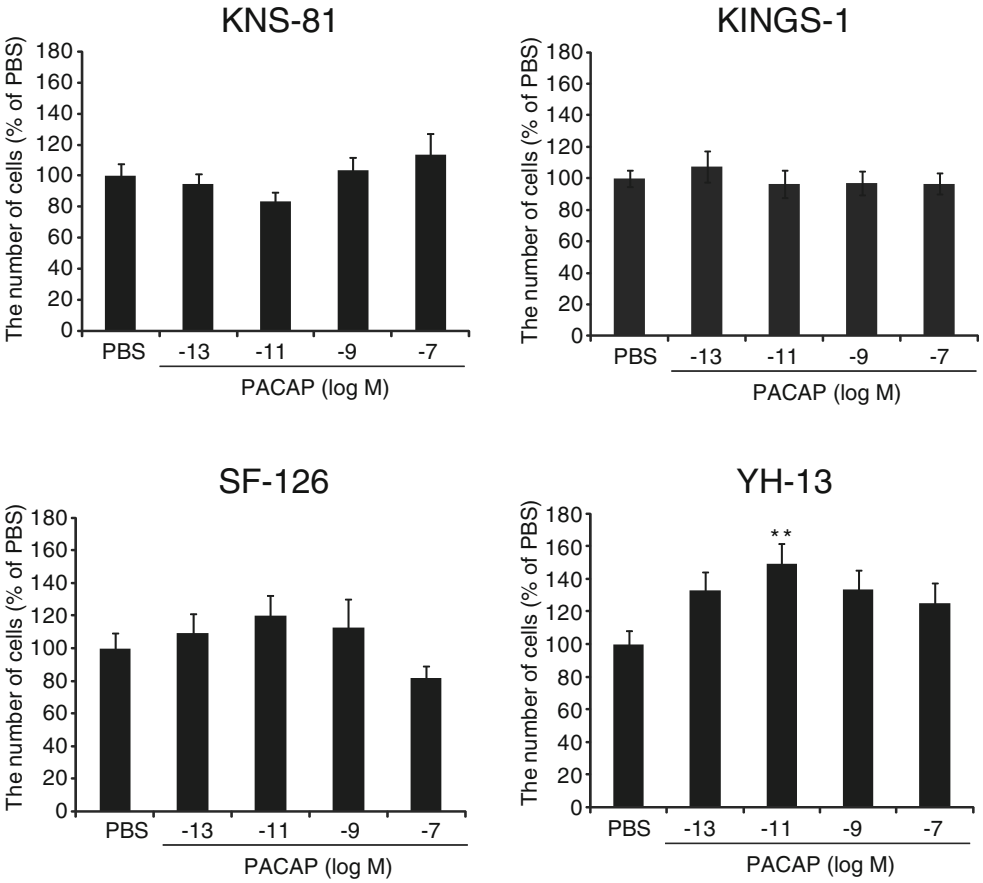

Fig. 5 Effect of PACAP on astrocytoma cell proliferation. Proliferation assays were performed with a CyQUANT kit after 3 days of PACAP treatment (10^{-13}, 10^{-11}, 10^{-9}, and 10^{-7} M). Each value was normalized to values obtained for cells maintained in PBS alone. $^{**}P<0.01$ vs. PBS

of Ki67-positive proliferating cells in vitro (Nakamachi et al. 2011b). These data imply that malignant astrocytes and reactive astrocytes display similar characteristics, making it possible therefore to choose between low-malignant type astrocytoma cell lines (e.g., KNS-81) and high-malignant type cell lines (e.g., YH-13) as models of resting and reactive astrocytes, respectively.

It has also been reported that PACAP protects astrocytes against oxidative stress-induced apoptosis (Masmoudi-Kouki et al. 2011). Although the results in this study provide some information showing that PACAP increased the number of highly malignant astrocytoma cells, it remains unclear whether PACAP stimulates proliferation or survival. In addition, it is known that PACAP induces the differentiation of neural stem cells into astrocytes (Watanabe et al. 2007; Nakamachi et al. 2011a), implying that PACAP may influence differentiation status or, in other words, the malignancy level of astrocytoma cells. Further studies focusing on the function of PACAP on astrocytoma cells is therefore warranted.

In conclusion, we have shown here that PACAP receptor expression is correlated with malignant potential, and that this effect may underlie differences in PACAP sensitivity exhibited by astrocytoma cell lines. Further study on the effects of PACAP on astrocytoma cells could help to elucidate characteristics of malignant astrocytoma cells, on their high proliferative and invasive potential, and on their resistance to chemotherapy.

Acknowledgments This work was supported by Grants-in Aid for Scientific Research (KAKENHI: 23249079, 24592681, and 24592680) and by the MEXT-Support Program for the Strategic Research Foundation at Showa University (2012-16).

References

Ahmed R, Oborski MJ, Hwang M, Lieberman FS, Mountz JM (2014) Malignant gliomas: current perspectives in diagnosis, treatment, and early response assessment using advanced quantitative imaging methods. Cancer Manag Res 6:149–170

Akimoto J (1993) [Immunohistochemical study of glutamine synthetase expression in normal human brain and intracranial tumors]. No to shinkei = Brain and nerve 45:362–368

Anido J, Saez-Borderias A, Gonzalez-Junca A et al (2010) TGF-beta receptor inhibitors target the CD44(high)/Id1(high) glioma-initiating cell population in human glioblastoma. Cancer Cell 18: 655–668

Anlauf E, Derouiche A (2013) Glutamine synthetase as an astrocytic marker: its cell type and vesicle localization. Front Endocrinol (Lausanne) 4:144

Arimura A, Shioda S (1995) Pituitary adenylate cyclase activating polypeptide (PACAP) and its receptors: neuroendocrine and endocrine interaction. Front Neuroendocrinol 16:53–88

D'Amico AG, Scuderi S, Saccone S, Castorina A, Drago F, D'Agata V (2013) Antiproliferative effects of PACAP and VIP in serum-starved glioma cells. J Mol Neurosci 51:503–513

Dufes C, Alleaume C, Montoni A, Olivier JC, Muller JM (2003) Effects of the vasoactive intestinal peptide (VIP) and related peptides on glioblastoma cell growth in vitro. J Mol Neurosci 21:91–102

Fok-Seang J, Miller RH (1992) Astrocyte precursors in neonatal rat spinal cord cultures. J Neurosci 12:2751–2764

Jellinger K (1978) Glioblastoma multiforme: morphology and biology. Acta Neurochir (Wien) 42:5–32

Jones LJ, Gray M, Yue ST, Haugland RP, Singer VL (2001) Sensitive determination of cell number using the CyQUANT cell proliferation assay. J Immunol Methods 254:85–98

Louis DN, Ohgaki H, Wiestler OD et al (2007) The 2007 WHO classification of tumours of the central nervous system. Acta Neuropathol (Berl) 114:97–109

Masmoudi-Kouki O, Douiri S, Hamdi Y et al. (2011). Pituitary adenylate cyclase-activating polypeptide protects astroglial cells against oxidative stress-induced apoptosis. J Neurochem 117(3):403–411. doi:10.1111/j.1471-4159.2011.07185.x

Masmoudi-Kouki O, Gandolfo P, Castel H et al (2007) Role of PACAP and VIP in astroglial functions. Peptides 28:1753–1760

Miyata A, Arimura A, Dahl RR et al (1989) Isolation of a novel 38 residue-hypothalamic polypeptide which stimulates adenylate cyclase in pituitary cells. Biochem Biophys Res Commun 164:567–574

Miyata A, Jiang L, Dahl RD et al (1990) Isolation of a neuropeptide corresponding to the N-terminal 27 residues of the pituitary adenylate cyclase activating polypeptide with 38 residues (PACAP38). Biochem Biophys Res Commun 170:643–648

Nakamachi T, Farkas J, Kagami N et al (2013) Expression and distribution of pituitary adenylate cyclase-activating polypeptide receptor in reactive astrocytes induced by global brain ischemia in mice. Acta Neurochir Suppl (Wien) 118:55–59

Nakamachi T, Farkas J, Watanabe J et al (2011a) Role of PACAP in neural stem/progenitor cell and astrocyte—from neural development to neural repair. Curr Pharm Des 17:973–984

Nakamachi T, Nakamura K, Oshida K et al (2011b) Pituitary adenylate cyclase-activating polypeptide (PACAP) stimulates proliferation of reactive astrocytes in vitro. J Mol Neurosci 43:16–21

Ohtaki H, Nakamachi T, Dohi K, Shioda S (2008) Role of PACAP in ischemic neural death. J Mol Neurosci 36:16–25

Piepmeier JM, Fried I, Makuch R (1993) Low-grade astrocytomas may arise from different astrocyte lineages. Neurosurgery 33:627–632

Pixley SK, de Vellis J (1984) Transition between immature radial glia and mature astrocytes studied with a monoclonal antibody to vimentin. Brain Res 317:201–209

Robberecht P, Woussen-Colle MC, Vertongen P et al (1994) Expression of pituitary adenylate cyclase activating polypeptide (PACAP) receptors in human glial cell tumors. Peptides 15:661–665

Shioda S (2000) Pituitary adenylate cyclase-activating polypeptide (PACAP) and its receptors in the brain. Kaibogaku Zasshi 75:487–507

Shioda S, Ohtaki H, Nakamachi T et al (2006) Pleiotropic functions of PACAP in the CNS: neuroprotection and neurodevelopment. Ann N Y Acad Sci 1070:550–560

Sokolowska P, Nowak JZ (2008) Effects of PACAP and VIP on cAMP-generating system and proliferation of C6 glioma cells. J Mol Neurosci 36:286–291

Suzuki R, Arata S, Nakajo S, Ikenaka K, Kikuyama S, Shioda S (2003) Expression of the receptor for pituitary adenylate cyclase-activating polypeptide (PAC1-R) in reactive astrocytes. Brain Res Mol Brain Res 115:10–20

Tsuchikawa D, Nakamachi T, Tsuchida M et al (2012) Neuroprotective effect of endogenous pituitary adenylate cyclase-activating polypeptide on spinal cord injury. J Mol Neurosci 48:508–517

Vertongen P, Camby I, Darro F, Kiss R, Robberecht P (1996) VIP and pituitary adenylate cyclase activating polypeptide (PACAP) have an antiproliferative effect on the T98G human glioblastoma cell line through interaction with VIP2 receptor. Neuropeptides 30:491–496

Watanabe J, Nakamachi T, Matsuno R et al (2007) Localization, characterization and function of pituitary adenylate cyclase-activating polypeptide during brain development. Peptides 28:1713–1719

Wiranowska M, Ladd S, Smith SR, Gottschall PE (2006) CD44 adhesion molecule and neuro-glial proteoglycan NG2 as invasive markers of glioma. Brain Cell Biol 35:159–172

Xia CL, Du ZW, Liu ZY, Huang Q, Chan WY (2003) A2B5 lineages of human astrocytic tumors and their recurrence. Int J Oncol 23:353–361

First International Journal of Andrology
ANDROLOGIA

ORIGINAL ARTICLE

Distribution of pituitary adenylate cyclase-activating polypeptide (PACAP) in the human testis and in testicular germ cell tumors

K. Nakamura[1,2], T. Nakamachi[1,3], K. Endo[1], K. Ito[1], T. Machida[2], T. Oka[4], M. Hori[1], K. Ishizaka[5] & S. Shioda[1]

1 Department of Anatomy, Showa University School of Medicine, Shinagawaku, Tokyo, Japan;
2 Department of Urology, Kanto Central Hospital, Setagayaku, Tokyo, Japan;
3 Center for Biotechnology, Showa University, Tokyo, Japan;
4 Department of Pathology, Kanto Central Hospital, Tokyo, Japan;
5 Department of Urology, Mizonokuchi University Hospital, Teikyo University School of Medicine, Kawasaki, Japan

Keywords
Embryonal carcinoma—immunostaining—PACAP—seminoma—testis

Correspondence
Seiji Shioda, PhD, Department of Anatomy, Showa University School of Medicine, 1-5-8 Hatanodai, Shinagawa-ku, Tokyo 142-8555, Japan.
Tel.: +81-3-3784-8103;
Fax: +81-3-3784-6815;
E-mail: shioda@med.showa-u.ac.jp

Accepted: March 4, 2013

doi: 10.1111/and.12102

Summary

Pituitary adenylate cyclase-activating peptide (PACAP) is a neuropeptide expressed in the central nervous system and peripheral organs. Previous studies revealed the role and distribution of PACAP in the rodent testis, however, its presence in the human testis and in testicular germ cell tumors is not known. We used RT-PCR and immunohistological observations to investigate whether human testicular tissue and testicular germ cell tumors contain PACAP. The mRNAs for PACAP and its receptors were detected in total RNA extracted from human testes. PACAP immunoreactivity was observed in spermatogonia and spermatids from normal testes. In contrast, diffuse PACAP immunopositivity was observed in seminoma tumor cells, while only faint immunoreactivity was observed in embryonal carcinoma cells. Our data suggest that PACAP may play a role in human spermatogenesis and in testicular germ cell tumor development.

Introduction

Pituitary adenylate cyclase-activating peptide (PACAP) is a neuropeptide that was initially isolated from the ovine hypothalamus (Miyata *et al.*, 1989). PACAP belongs to the vasoactive intestinal polypeptide (VIP)/secretin/glucagon family, with VIP being its closest analogue. PACAP and VIP share three types of receptors: the PAC1 receptor (PAC1R), and the VPAC1 and VPAC2 receptors (VPAC1R, VPAC2R). The affinity of PAC1R for PACAP is more than 1000 times higher than its affinity for VIP, indicating that PAC1R is a relatively selective receptor for PACAP (Harmar *et al.*, 2012). PACAP has pleiotropic functions that contribute to neurotransmission, neuroprotection, vasodilatation, immunomodulation and neural development (Shioda *et al.*, 2006; Vaudry *et al.*, 2009; Nakamachi *et al.*, 2011). In rodents, PACAP and its receptors are widely distributed in the central nervous system and peripheral organs including the testis (Arimura *et al.*, 1991). While histological studies have shown that PACAP immunoreactivity is present in the developing acrosome of the rat spermatid (Shioda *et al.*, 1994; Li *et al.*, 2004), no studies as yet have examined the nature of PACAP expression in the human testis.

Testicular germ cell tumors are common in young men (Boujelbene *et al.*, 2011). Their prevalence is increasing steadily, although the underlying causes of such tumors are still poorly understood. PACAP and its receptors are widely expressed in cancer cells such as human malignant tumors (Reubi *et al.*, 2000; Moretti *et al.*, 2006). To be more specific, malignant tumors of the lung and colon have been shown to expresses PACAP (Godlewski and Lakomy, 2010; Szanto *et al.*, 2012). This could also be the case with respect to testicular tumors, however, no such report of the fact has been made. The purpose of this study, therefore, was to describe the distribution of PACAP and its receptors in normal human testicular tissue and in testicular germ cell tumors.

Material and method

Patients and tissue preparation

Human testicular tumor samples were obtained from patients undergoing high orchiectomy as a surgical therapy for testicular tumor. Single sample of normal testicular tissue was obtained from testicular biopsy procedure. Twenty-two cases (age range: 35–55) underwent operative therapy from July 2006 to June 2012. Of these, 15 cases involved seminomas, three cases were embryonal carcinomas and four other cases were malignant lymphoma or mixed types. Eight cases of testicular tumor (five seminomas and three embryonal carcinomas) and a single case of normal testis were enrolled in this study. The Institutional Review Board of Kanto Central Hospital approved the use of tissue specimens for further study (approval number: 23-2-002).

Tissues were embedded in paraffin after fixation with 6% paraformaldehyde for pathological diagnosis. Five micro meter thick paraffin sections stained with Hematoxylin and eosin (HE) were used for routine pathological examination and tumor grading. Tumors were classified according to the TNM classification (Eble, 2004). Table 1 shows the characteristics of patients and tumors. Testicular tumor markers in blood serum were assessed using kits to measure lactate dehydrogenase (LDH; Wakojunyaku, Osaka, Japan), α-fetoprotein (AFP; Abbott Japan, Chiba, Japan) and beta-human chorionic gonadotrophin (β-hCG; Siemens Healthcare Diagnostics Japan, Tokyo, Japan) as a routine aspect of the clinical diagnosis.

Reverse transcription polymerase chain reaction (RT-PCR)

Reverse transcription polymerase chain reaction (RT-PCR) was performed according to the methods outlined in a previous report (Nakamachi *et al.*, 2012) with minor modification. Briefly, human brain and testis total RNA were purchased from Clontech Laboratories, Inc. (#636530 and # 636533, Mountain View, CA, USA). The total RNAs were reverse transcribed into cDNA using the PrimeScript RT reagent kit (TaKaRa BIO INC., Kyoto, Japan). As a negative control, the RT reaction was performed without reverse transcriptase (RT-). PCR was performed with SYBR Premix Ex Taq II reagent (TaKaRa BIO INC) using a GeneAmp PCR system 2700 (Applied Biosystems; Lincoln, CA, USA) with primer sets for human Adcyap1 (PACAP), Vip, Adcyap1r (PAC1R), Vpac1r, Vpac2r and two housekeeping genes, Actb (β-actin) and Gapdh (Table 2). The PCR products were visualised by electrophoresis on a 2.5% agarose XP gel (Nippon gene, Toyama, Japan) with added ethidium bromide.

Immunostaining of PACAP

Immunostaining was performed according to a previous report (Nakamachi *et al.*, 2008) to detect the expression of PACAP in testicular and tumor tissue. Briefly, 5 micro meter sections were deparaffinised and boiled with citrate buffer (10 mmol l^{-}, pH 6.0 for 30 min). Sections were then quenched with H_2O_2 with absolute methanol for 30 min. After blocking with 5% normal horse serum for 60 min, sections were incubated overnight at 4 °C with rabbit anti-PACAP antibody (1 : 200, Bachem/Peninsula Laboratories; T-4473, San Carlos, CA, USA). Biotinylated anti-rabbit IgG antibody and Avidin-Biotin enzyme Complex (Vector Laboratories, Burlingame, CA, USA) were used. The immunolabelling was developed with 3,3'-diaminobenzidine (DAB; Sigma-Aldrich, St. Louis, MO, USA). The antigen pre-absorption test was performed as negative control. PACAP antibody was mixed with 10^{-7} mol/L of PACAP and incubated overnight. After centrifugation at 15000 × g for 10 minutes, sections were treated with supernatant instead of PACAP antibody.

Table 1 Characteristics of patients and testicular tumor tissue samples

No	Age	Side	Pathological diagnosis	AFP (ng ml^{-1})	LDH (IU l^{-1})	β-hCG (mIU ml^{-1})	TNM stage
1	43	Bilateral	Normal	–	–	–	–
2	37	Left	Seminoma	2.3	222	62.2	pT1N0M0
3	35	Right	Seminoma	2.1	258	0	pT2N0M0
4	39	Left	Seminoma	3.6	337	6.5	pT2N1M0
5	55	Right	Seminoma	5.15	694	3.7	pT1N0M0
6	39	Left	Seminoma	2.7	148	2.9	pT1N0M0
7	36	Right	Embryonal ca.	3.4	454	0	pT2N1M0
8	39	Left	Embryonal ca.	8.4	232	0	pT2N0M0
9	40	Right	Embryonal ca.	22.07	264	0	pT1N0M0

AFP, alpha fetoprotein; LDH, lactate dehydrogenase; βHCG, beta subunit of human chorionic gonadotrophin.

Table 2 Primer sequences and PCR conditions

Gene	Encoding protein		Sequence	Amplicon length (bp)	Cycle
Adcyap1	PACAP	Forward	GTGAGGTAAGCAAGCTCCAACAGAC	149	28
		Reverse	CTCGATCTGATTGCTGGGTGAA		
Adcyap1r1	PAC1R	Forward	CTCACCACTGCCATGGTCATC	98	28
		Reverse	GCCCTCAGCATGAACGACAC		
Vip	VIP	Forward	ACCCTGTACCAGTCAAACGTCACTC	198	28
		Reverse	GAAGTTGTCATCAGCTTTGCTCCA		
Vipr1	VPAC1R	Forward	CATTGCCTGTGGTTTGGATGAC	134	28
		Reverse	GGATAGCTGTGGCGACCAGAA		
Vipr2	VPAC2R	Forward	AGTGGCGTCTGGGACAACATC	157	28
		Reverse	AATCTGGGAACGTCTCTGACCATC		
Actb	β-actin	Forward	TGGCACCCAGCACAATGAA	186	20
		Reverse	CTAAGTCATAGTCCGCCTAGAAGCA		
Gapdh	GAPDH	Forward	GCACCGTCAAGGCTGAGAAC	138	20
		Reverse	TGGTGAAGACGCCAGTGGA		

PACAP, pituitary adenylate cyclase-activating polypeptide; VIP, vasoactive intestinal polypeptide.

Results

Expression of PACAP, VIP and its receptors mRNA in human testis

We first evaluated by RT-PCR the mRNA expression of PACAP, VIP and their receptors in normal human testicular tissue. The mRNAs of all PACAP-related genes were detected in human brain tissue which was used as a positive control (Fig. 4). Two housekeeping genes, Actb and Gapdh, were detected at similar levels in the total mRNA of control brain and testis. PACAP levels in the testis were similar to that in brain, while levels of VIP mRNA were much lower or absent. Weak signals for all three types of PACAP receptors were observed in the testis. The reverse transcriptase-free negative control (RT-) showed no signal at all in the brain and testis total mRNA, suggesting that the PACAP, VIP and receptor signals were derived from mRNA, not genomic DNA.

Localization of PACAP immunoreactivity in testis

Tissue sections of normal human testis subjected to HE staining indicated the presence of normal spermatozoa in the seminiferous tubules (Fig. 1a–b). In sections immunostained with PACAP antibody, immunoreactivity was observed on the round spermatids and spermatogonia in the seminiferous tubules (Fig. 1e–f). Spermatogonia near the basal membrane of the seminiferous tubules were mostly PACAP immunopositive (Fig. 1f). Negative control sections showed no detectable signal in the spermatids or spermatogonia (Fig. 1c).

Localization of PACAP immunoreactivity in testicular germ cells

Seminoma tumor cells were immunopositive for PACAP (Fig. 2). HE staining showed typical patterns of seminoma with an eosinophilic cytoplasm, but syncytiotrophoblastic cells were not observed (Fig. 2a). PACAP immunoreactivity was observed in the nuclei, cytoplasm, and plasma membrane of seminoma tumor cells (Fig. 2c–d). In the case of embryonal carcinoma tumor cells, a typical histological pattern, with irregular nuclei and eosinophilic granular cytoplasm, was observed with HE staining (Fig. 3a). Low-intensity PACAP immunoreactivity was observed in embryonal carcinoma tumor cells compared with the seminoma tumor cells (Fig. 3c–d). No immunoreactivities were observed in negative control seminoma (Fig. 2b) and embryonal carcinoma (Fig. 3b) sections.

Discussion

The testes express many bioactive peptides which are typically associated with the nervous system. For example, the PACAP/VIP/secretin/glucagon family was shown to be expressed in the rodent reproductive system (Li & Arimura, 2003). We have shown here that the mRNA for PACAP and its receptors is expressed in human testicular tissue, which is the first time PACAP expression in the human testis has been described. In rodent, PACAP and PAC1R expression and localization has been demonstrated. PACAP immunoreactivity in adult rodent testis was observed in round/elongated spermatids, and its mRNA was detected in spermatogonia, spermatocytes and spermatids; in contrast, expression was decreased in the

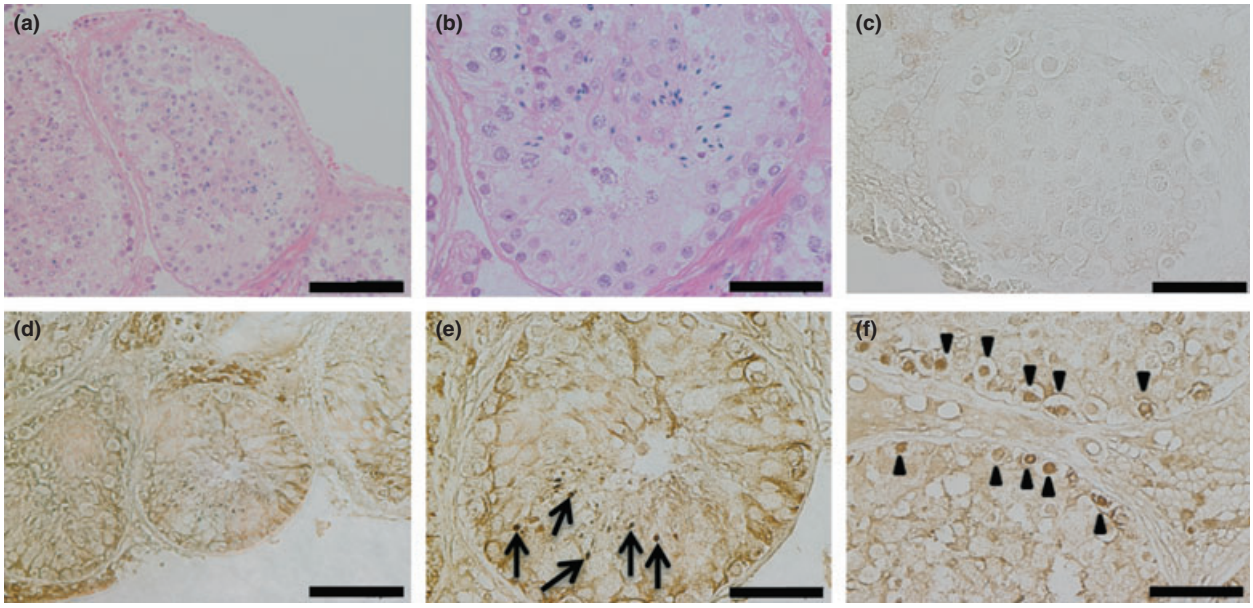

Fig. 1 Distribution of pituitary adenylate cyclase-activating polypeptide (PACAP) immunoreactivity in the normal human testis. Representative images of Hematoxylin and eosin (HE)-stained sections of human testicular tissue (a, b), negative control section stained using the antigen pre-absorption test (c) and immunostained with PACAP antibody (d–f). Black arrows indicate spermatids and arrow heads shows spermatogonia (d–f). Images are shown at low (a, d) and high (b, c, e, f) magnification. Scale bar represents 100 μm (a, d) and 40 μm (b, c, e, f).

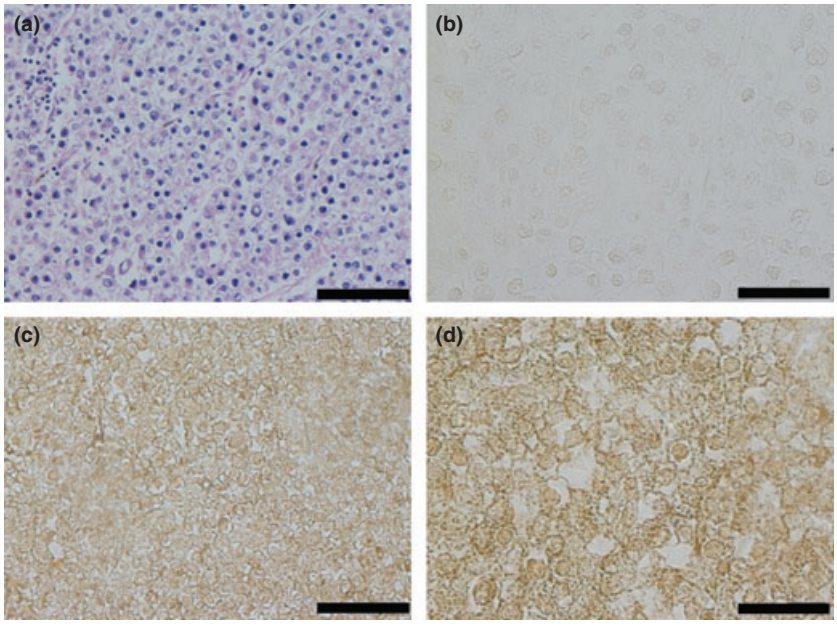

Fig. 2 Distribution of pituitary adenylate cyclase-activating polypeptide (PACAP) immunoreactivity in seminoma tumor cells. Series of photomicrographs of Hematoxylin and eosin (HE)-stained seminoma tumor cells(a), negative control section stained using the antigen pre-absorption test (b) and immunostained with PACAP antibody (c, d). Images are shown at low (a – c) and high (d) magnification. Scale bar represents 100 μm (a – c) and 40 μm (d).

spermatozoa (Arimura & Shioda, 1995; Li & Arimura, 2003). PACAP immunoreactivity was also observed here in human spermatogonia and round spermatids (Fig. 1) in a similar manner to that in rodents, suggesting that PACAP is associated with spermatogenesis and spermiogenesis in the human testis.

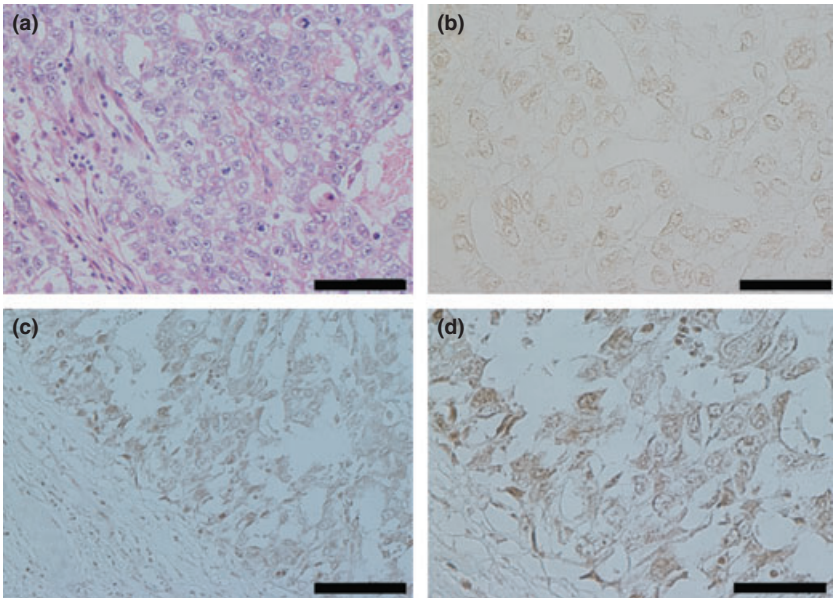

Fig. 3 Distribution of pituitary adenylate cyclase-activating polypeptide (PACAP) immunoreactivity in embryonal carcinoma tumor cells. Series of photomicrographs of Hematoxylin and eosin (HE)-stained embryonal carcinoma cells (a), negative control section stained using the antigen pre-absorption test (b) and immunostained with PACAP antibody (c, d). Images are shown at low (a–c) and high magnification (d). Scale bar represents 100 μm (a–c) and 40 μm (d).

In relation to PACAP receptor expression, PAC1R immunoreactivity and mRNA were detected in the spermatid acrosomes in rodent seminiferous tubules (Li & Arimura, 2003; Li *et al.*, 2004). Although all three types of PACAP receptor mRNAs were detected in human testicular tissue samples (Fig. 4), a precise localization of PACAP receptors in the seminiferous tubule is necessary if a proper understanding of PACAP function in the testis is to be gained.

The function of PACAP in spermatogenesis and fertilisation was recently reported by Brubel and colleagues (Brudel *et al.* 2012), who showed that PACAP increases sperm motility in human spermatozoa and that PACAP-deficient mice have an abnormal sperm morphology. Furthermore, it has been reported that sperm penetration through the oocyte investment, cumulus cell layer and zona pellucida was enhanced by PACAP treatment (Tanii *et al.*, 2011). These reports indicate that PACAP contributes to spermatogenesis and sperm motility. PACAP could also be associated with male infertility, and serve as a candidate to increase fertility potential.

Testicular germ cell tumors are classified broadly into seminoma and non-seminomatous tumors based on diagnosis by the HE staining of testicular tissue sections. Non-seminomatous tumors, however, have various or mixed histological patterns, and in some cases are difficult to diagnose with HE staining only (Young, 2008). Non-seminomatous tumors also show a poor prognosis in comparison with seminoma (International Germ Cell Cancer Collaborative Group, 1997), making a precise diagnosis is essential for their proper management. In the past, only a few classical tumor markers such as placental alkaline phosphatase (PLAP), AFP and hCG were available to

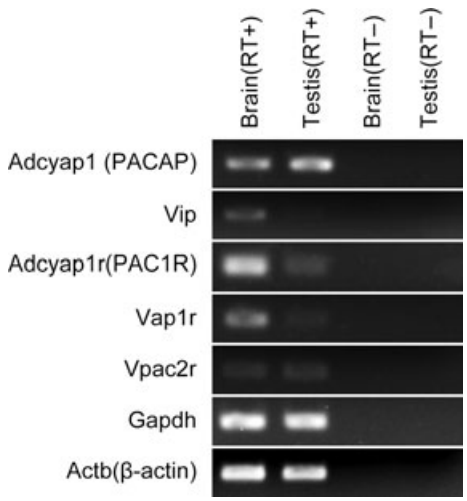

Fig. 4 Expression of pituitary adenylate cyclase-activating polypeptide (PACAP), VIP and their receptors in human testis and brain. Equivalent amounts of total mRNA (25 ng lane^{-1}) were used for RT-PCR. PCR primer sequences and the PCR conditions used are given in Table 2. RT+, RT reaction with reverse transcriptase; RT-, RT reaction without reverse transcriptase.

detect testicular tumors. Several novel tumor markers such as OCT4 (Jones *et al.*, 2004), SOX2 and SOX17 (de Jong *et al.*, 2008) have now been identified. However, their specificities and sensitivities are sometimes inadequate for a differential diagnosis to be made of non-seminomatous germ cell tumors. The intracrine function of cytosolic PACAP and a strong PAC1R signal in the nuclear fraction of rodent testicular germ cells were demonstrated by Li *et al.*, (2004). It has reported that PACAP treatment of isolated testicular nuclei stimulates calcium release from these nuclei (Doan *et al.*, 2012). In our study, the cytoplasm and nuclei of testicular tumor cells were immunoreactive for PACAP, suggesting that a similar function or potency of PACAP may also occur in human testicular tumor cells.

PACAP expression in human cancer differs between primary organs(Reubi *et al.*, 2000). We showed here that PACAP immunoreactivity was positive in both types of testicular tumors analyzed. The intensity of PACAP immunoreactivity in seminoma sections was greater than that in embryonal carcinoma cells. This observation suggests that PACAP may serve as a new candidate in the differential diagnosis of testicular germ cell tumor pathologies.

In conclusion, PACAP is expressed in the normal human testis, as well as in human seminoma and embryonal carcinoma tumor cells. Our results suggest that PACAP may play a role in spermatogenesis and testicular germ tumor development. Evaluation of the function and distribution of PACAP in the testis may contribute to the development of new approaches to treat male infertility. Moreover, while the observation of PACAP immunoreactivity in testicular tumor cells is an important one, further investigation is however required to develop a new diagnostic procedure to detect testicular germ cell tumors based on PACAP expression.

Acknowledgements

We would like to thank the technicians at the Kanto Central Hospital who provided technical support concerning specimen preparation. This work was supported by Grants-in-Aid for Scientific Research (KAKENHI: 23249079, 24592680), by the MEXT – Support Program for the Strategic Research Foundation at Showa University (2008–2012, 2012–16).

References

Arimura A, Shioda S (1995) Pituitary adenylate cyclase activating polypeptide (PACAP) and its receptors: neuroendocrine and endocrine interaction. *Front Neuroendocrinol* 16:53–88.

Arimura A, Somogyvari-Vigh A, Miyata A, Mizuno K, Coy DH, Kitada C (1991) Tissue distribution of PACAP as determined by RIA: highly abundant in the rat brain and testes. *Endocrinology* 129:2787–2789.

Boujelbene N, Cosinschi A, Khanfir K, Bhagwati S, Herrmann E, Mirimanoff RO, Ozsahin M, Zouhair A (2011) Pure seminoma: a review and update. *Radiat Oncol* 6:90.

Brubel R, Kiss P, Vincze A, Varga A, Varnagy A, Bodis J, Mark L, Jambor E, Maasz G, Hashimoto H, Helyes Z, Toth G, Tamas A, Koppan M, Reglodi D (2012) Effects of pituitary adenylate cyclase activating polypeptide on human sperm motility. *J Mol Neurosci : MN* 48: 623–630.

Eble JNSG, Epstein JI, Sesterhenn IA (eds). (2004) World Health Organization Classification of Tumours: Pathology and Genetics of Tumours of the Urinary System and Male Genital Organs. IARC Press, Lyon, France.

Group IGCCC (1997) International germ cell consensus classification: a prognostic factor-based staging system for metastatic germ cell cancers. *J Clin Oncol* 15: 594–603.

Harmar AJ, Arimura A, Gozes I, Journot L, Laburthe M, Pisegna JR, Rawlings SR, Robberecht P, Said SI, Sreedharan SP, Wank SA, Waschek JA (1998) International union of pharmacology. XVIII. Nomenclature of receptors for vasoactive intestinal peptide and pituitary adenylate cyclase-activating polypeptide. *Pharmacol Rev* 50:265–270.

Jones TD, Ulbright TM, Eble JN, Baldridge LA, Cheng L (2004) OCT4 staining in testicular tumors: a sensitive and specific marker for seminoma and embryonal carcinoma. *Am J Surg Pathol* 28:935–940.

de Jong J, Stoop H, Gillis AJ, Van Gurp RJ, Van de Geijn GJ, Boer M, Hersmus R, Saunders PT, Anderson RA, Oosterhuis JW, Looijenga LH (2008) Differential expression of SOX17 and SOX2 in germ cells and stem cells has biological and clinical implications. *J Pathol* 215:21–30.

Li M, Arimura A (2003) Neuropeptides of the pituitary adenylate cyclase-activating polypeptide/vasoactive intestinal polypeptide/growth hormone-releasing hormone/secretin family in testis. *Endocrine* 20:201–214.

Li M, Funahashi H, Mbikay M, Shioda S, Arimura A (2004) Pituitary adenylate cyclase activating polypeptide-mediated intracrine signaling in the testicular germ cells. *Endocrine* 23:59–75.

Miyata A, Arimura A, Dahl RR, Minamino N, Uehara A, Jiang L, Culler MD, Coy DH (1989) Isolation of a novel 38 residue-hypothalamic polypeptide which stimulates adenylate cyclase in pituitary cells. *Biochem Biophys Res Commun* 164:567–574.

Moretti C, Mammi C, Frajese GV, Mariani S, Gnessi L, Arizzi M, Wannenes F, Frajese G (2006) PACAP and type I PACAP receptors in human prostate cancer tissue. *Ann N Y Acad Sci* 1070:440–449.

Nakamachi T, Ohtaki H, Yofu S, Dohi K, Watanabe J, Hayashi D, Matsuno R, Nonaka N, Itabashi K, Shioda S

(2008) Pituitary adenylate cyclase-activating polypeptide (PACAP) type 1 receptor (PAC1R) co-localizes with activity-dependent neuroprotective protein (ADNP) in the mouse brains. *Regul Pept* 145:88–95.

Nakamachi T, Farkas J, Watanabe J, Ohtaki H, Dohi K, Arata S, Shioda S (2011) Role of PACAP in neural stem/progenitor cell and astrocyte–from neural development to neural repair. *Curr Pharm Des* 17:973–984.

Nakamachi T, Tsuchida M, Kagami N, Yofu S, Wada Y, Hori M, Tsuchikawa D, Yoshikawa A, Imai N, Nakamura K, Arata S, Shioda S (2012) IL-6 and PACAP Receptor Expression and Localization after Global Brain Ischemia in Mice. *J Mol Neurosci* 48:518–525.

Reubi JC, Laderach U, Waser B, Gebbers JO, Robberecht P, Laissue JA (2000) Vasoactive intestinal peptide/pituitary adenylate cyclase-activating peptide receptor subtypes in human tumors and their tissues of origin. *Cancer Res* 60:3105–3112.

Shioda S, Legradi G, Leung WC, Nakajo S, Nakaya K, Arimura A (1994) Localization of pituitary adenylate cyclase-activating polypeptide and its messenger ribonucleic acid in the rat testis by light and electron microscopic immunocytochemistry and *in situ* hybridization. *Endocrinology* 135:818–825.

Shioda S, Ohtaki H, Nakamachi T, Dohi K, Watanabe J, Nakajo S, Arata S, Kitamura S, Okuda H, Takenoya F, Kitamura Y (2006) Pleiotropic functions of PACAP in the CNS: neuroprotection and neurodevelopment. *Ann N Y Acad Sci* 1070:550–560.

Tanii I, Aradate T, Matsuda K, Komiya A, Fuse H (2011) PACAP-mediated sperm-cumulus cell interaction promotes fertilization. *Reproduction* 141:163–171.

Vaudry D, Falluel-Morel A, Bourgault S, Basille M, Burel D, Wurtz O, Fournier A, Chow BK, Hashimoto H, Galas L, Vaudry H (2009) Pituitary adenylate cyclase-activating polypeptide and its receptors: 20 years after the discovery. *Pharmacol Rev* 61:283–357.

Young RH (2008) Testicular tumors–some new and a few perennial problems. *Arch Pathol Lab Med* 132: 548–564.

nature COMMUNICATIONS

ARTICLE

Received 4 Jun 2015 | Accepted 22 May 2016 | Published 27 Jun 2016

DOI: 10.1038/ncomms12034 OPEN

PACAP suppresses dry eye signs by stimulating tear secretion

Tomoya Nakamachi[1,2], Hirokazu Ohtaki[2], Tamotsu Seki[2], Sachiko Yofu[2], Nobuyuki Kagami[2], Hitoshi Hashimoto[3,4,5], Norihito Shintani[3], Akemichi Baba[6], Laszlo Mark[7,8,9,10], Ingela Lanekoff[11], Peter Kiss[12], Jozsef Farkas[2,12], Dora Reglodi[12] & Seiji Shioda[13]

Dry eye syndrome is caused by a reduction in the volume or quality of tears. Here, we show that pituitary adenylate cyclase-activating polypeptide (PACAP)-null mice develop dry eye-like symptoms such as corneal keratinization and tear reduction. PACAP immunoreactivity is co-localized with a neuronal marker, and PACAP receptor (PAC1-R) immunoreactivity is observed in mouse infraorbital lacrimal gland acinar cells. PACAP eye drops stimulate tear secretion and increase cAMP and phosphorylated (p)-protein kinase A levels in the infraorbital lacrimal glands that could be inhibited by pre-treatment with a PAC1-R antagonist or an adenylate cyclase inhibitor. Moreover, these eye drops suppress corneal keratinization in PACAP-null mice. PACAP eye drops increase aquaporin 5 (AQP5) levels in the membrane and pAQP5 levels in the infraorbital lacrimal glands. AQP5 siRNA treatment of the infraorbital lacrimal gland attenuates PACAP-induced tear secretion. Based on these results, PACAP might be clinically useful to treat dry eye disorder.

[1] Laboratory of Regulatory Biology, Graduate School of Science and Engineering, University of Toyama, 3190-Gofuku, Toyama-shi, Toyama 930-8555, Japan. [2] Department of Anatomy, Showa University School of Medicine, Shinagawa-Ku, Tokyo 142-8555, Japan. [3] Laboratory of Molecular Neuropharmacology, Graduate School of Pharmaceutical Sciences, Osaka University, 1-6 Yamadaoka, Suita, Osaka 565-0871, Japan. [4] iPS Cell-based Research Project on Brain Neuropharmacology and Toxicology, Graduate School of Pharmaceutical Sciences, Osaka University, 1-6 Yamadaoka, Suita, Osaka 565-0871, Japan. [5] Molecular Research Center for Children's Mental Development, United Graduate School of Child Development, Osaka University, Kanazawa University, Hamamatsu University School of Medicine, Chiba University and University of Fukui, 2-2 Yamadaoka, Suita, Osaka 565-0871, Japan. [6] Hyogo University of Health Sciences, 1-3-6 Minatojima, Chuo-ku, Kobe, Hyogo 650-8530, Japan. [7] Department of Analytical Biochemistry, Institute of Biochemistry and Medical Chemistry, Medical School, University of Pécs, Szigeti u 12, Pécs 7624, Hungary. [8] Imaging Center for Life and Material Sciences, University of Pécs, Szigeti u 12, Pécs 7624, Hungary. [9] János Szentágothai Research Center, University of Pécs, Szigeti u 12, Pécs 7624, Hungary. [10] PTE-MTA Human Reproduction Research Group, Szigeti u 12, Pécs 7624, Hungary. [11] Department of Chemistry-BMC, Uppsala University, PO Box 599, Uppsala 751 24, Sweden. [12] Department of Anatomy, MTA-PTE PACAP Lendulet Research Group, Centre for Neuroscience, University of Pécs, Szigeti u 12, Pécs 7624, Hungary. [13] Innovative Drug Discovery, Global Research Center for Innovative Life Science, Hoshi University, 4-41 Ebara 2-chome, Shinagawa-ku, Tokyo 142-8501, Japan. Correspondence and requests for materials should be addressed to S.S. (email: shioda@hoshi.ac.jp)

Dry eye syndrome, also known as keratoconjunctivitis sicca, is a common eye disease caused by a reduction in the volume or quality of tears. Tear components are secreted from the main lacrimal gland, accessory lacrimal gland (Krause and Wolfring glands), meibomian gland, and the corneal and conjunctival epithelia in humans. A thin layer of tear film containing water, lipid electrolytes and $\sim 10\,mg\,ml^{-1}$ protein comprising different tear proteins, covers the ocular surface, thereby maintaining and protecting the eye. The major categories of dry eye are the aqueous tear-deficient type, in which the lacrimal glands fail to produce enough of the watery component of tears to maintain a tear film, and the evaporative type, in which impaired lipid secretion from the meibomian glands destabilizes the tear film[1]. Dry eye syndrome correlates with old age and affects females to a larger degree[2]. The number of patients diagnosed with the condition has increased in recent years, which could be due to the popularity of video display use (computer vision syndrome) or the wearing of contact lenses[3,4]. The orthodox strategy for the treatment of dry eye syndrome is symptomatic therapy, such as tear replacement using artificial tears. Although artificial tears provide temporary symptomatic relief, they do not address the underlying pathophysiology of dry eye syndrome, and the outcome is not always satisfactory[5].

Pituitary adenylate cyclase-activating polypeptide (PACAP; encoded by the gene *Adcyap1*), which exists in 27- or 38-amino-acid isoforms, was originally discovered in extracts of ovine hypothalamus[6,7]. The amino-acid sequence of PACAP—a member of the vasoactive intestinal polypeptide (VIP)/secretin/growth hormone-releasing hormone family of peptides—shows a 68% sequence homology with VIP. PACAP and VIP share three different receptors: the VPAC1 and VPAC2 receptors (VPAC1-R and VPAC2-R; gene names: *Vipr1* and *Vipr2*) and the PAC1-receptor (PAC1-R; encoded by the gene: *Adcyap1r1*) with different splice variants[8,9]. The affinity of PAC1-R for PACAP is more than 1,000 times higher than its affinity for VIP, indicating that PAC1-R is a relatively selective receptor for PACAP (ref. 10). The amino-acid sequences of PACAP27 and PACAP38 are highly conserved among mammals, and those of mouse and human are identical. PACAP is distributed mainly in the central nervous system, but it is also detected in the testis, adrenal gland, digestive tract and other peripheral organs[10]. The amino-acid sequence of PAC1-R is conserved with a 96.6% homology between mouse and human. *Adcyap1r1* mRNA is widely detected in the central nervous system and peripheral organs, including the adrenal gland, testis, anterior pituitary gland, pancreas and placenta[10].

PACAP is a multi-functional peptide that can act as a neurotrophic factor, neuroprotectant, neurotransmitter, immunomodulator and vasodilator[10–13]. During the past 10 years, PACAP-null ($Adcyap1^{-/-}$) mice have been generated by several laboratories and their phenotypes have been analysed[14–16]. Recently, we observed that corneal keratinization, associated with a decreased tear volume, frequently occurs in $Adcyap1^{-/-}$ mice. It has been reported that PACAP immunopositive nerve fibres were observed in cat lacrimal gland[17], but PACAP and PACAP receptor expression and function in lacrimal glands has not been well studied to date. To address this interesting finding, we investigate the effects and underlying mechanism of action of PACAP on lacrimal gland tear secretion in PACAP-null mice, as well as in mice treated with topical eye drops.

Results

Dry eye-like signs in the $Adcyap1^{-/-}$ mouse. During the routine housing of $Adcyap1^{-/-}$ mice in our animal facility, we unexpectedly discovered that some mice exhibited cloudiness of the cornea (Fig. 1a). The ocular surface appeared white and sandy, and blood vessels could be seen in the cornea (Fig. 1b). Based on fluorescein staining, which is commonly used to visualize corneal injury, strong fluorescence was observed in the central part of the cornea in these mice (Fig. 1c). On examination of this pathology, we discovered that the corneal epithelial cells were hypertrophied and the surface was keratinized (Fig. 1d). To quantify the degree of corneal keratinization, corneas were classified into four grades with the aid of a dissecting microscope (from Grade 0, denoting normal, to Grade 3 signifying hypertrophy of the surface and keratinization, as shown in Supplementary Fig. 1). Wild-type and $Adcyap^{+/-}$ male mice over the age of 20 weeks had normal corneas, whereas about 40% of $Adcyap1^{-/-}$ male mice over 30 weeks of age had Grade 3 corneas (Fig. 1e). In female mice, all groups showed a higher frequency of keratinization than that observed in male mice (Fig. 1f). In female $Adcyap1^{-/-}$ mice, the percentage of animals showing corneal keratinization was $<20\%$ in animals younger than 10 weeks of age, but increased with age to 90% of animals over 30 weeks of age (Fig. 1f). These data indicate that corneal keratinization frequently occurs in older $Adcyap1^{-/-}$ mice, and particularly in female animals.

Because keratinization is a common feature of dry eye disorder, we postulated that the corneal keratinization was caused by a reduction in tear fluid or quality. To test this, the tear secretion level in $Adcyap1^{-/-}$ mice was measured using the cotton thread method. As expected, tear secretion levels of male and female $Adcyap1^{-/-}$ mice were reduced compared with those of wild-type mice aged 10 weeks or younger (Fig. 1g,h). The tear volume in eyes with corneal keratinization was significantly reduced compared with that of Grade 0 eyes (Fig. 1i,j), while the tear volume and the corneal grade were weakly though significantly inversely correlated ($r=-0.242$, $P=0.007$, two-tailed Spearman's correlation test). On histological examination, the infraorbital lacrimal gland, conjunctiva and corneal neural network of $Adcyap1^{-/-}$ mice were found to be morphologically normal (Supplementary Fig. 2a–c). Taken together, these observations suggest that $Adcyap1^{-/-}$ mice exhibit a dry eye-like phenotype with a reduction in tear volume and corneal damage, despite the structure of the infraorbital lacrimal gland, conjunctiva and neural network of the cornea remaining normal.

Distribution and function of PACAP in the lacrimal gland. Based on the above data, we hypothesized that the PACAP/PAC1-R system was associated with altered tear secretion by the lacrimal gland, the major source of tear secretion. To test this, we first examined PACAP/PAC1-R expression and distribution in the mouse infraorbital lacrimal gland. Using the RT-PCR method, *Adcyap1* and *Adcyap1r1* mRNAs were detected in gland extracts, producing a signal with the same band size as that obtained from an eye ball sample that was used as a positive control (Fig. 2a). PACAP immunoreactivity was observed around acinar cells, and co-localized with immunoreactivity for the neuronal marker NeuN (Fig. 2b,c), and the parasympathetic neuronal marker choline acetyltransferase (ChAT) (Fig. 2d). The PACAP antibody recognized PACAP38 but not VIP (Supplementary Fig. 3a). PAC1-R immunoreactivity was observed on the basal side of acinar cells and ducts, but did not co-localize with smooth muscle actin as a myoepithelial cell marker (Fig. 2e,f). The PACAP and PAC1-R immunoreactivities were abolished by pre-absorption of the antibody with antigen (Supplementary Fig. 3b,c). PACAP38 was detected in wild-type, but not $Adcyap1^{-/-}$ mouse tears by matrix-assisted laser desorption/ionization (MALDI) time-of-flight (TOF) mass spectrometry (MS), and nanospray desorption electrospray ionization (nano-DESI) Orbitrap MS/MS (Supplementary Figs 4 and 5).

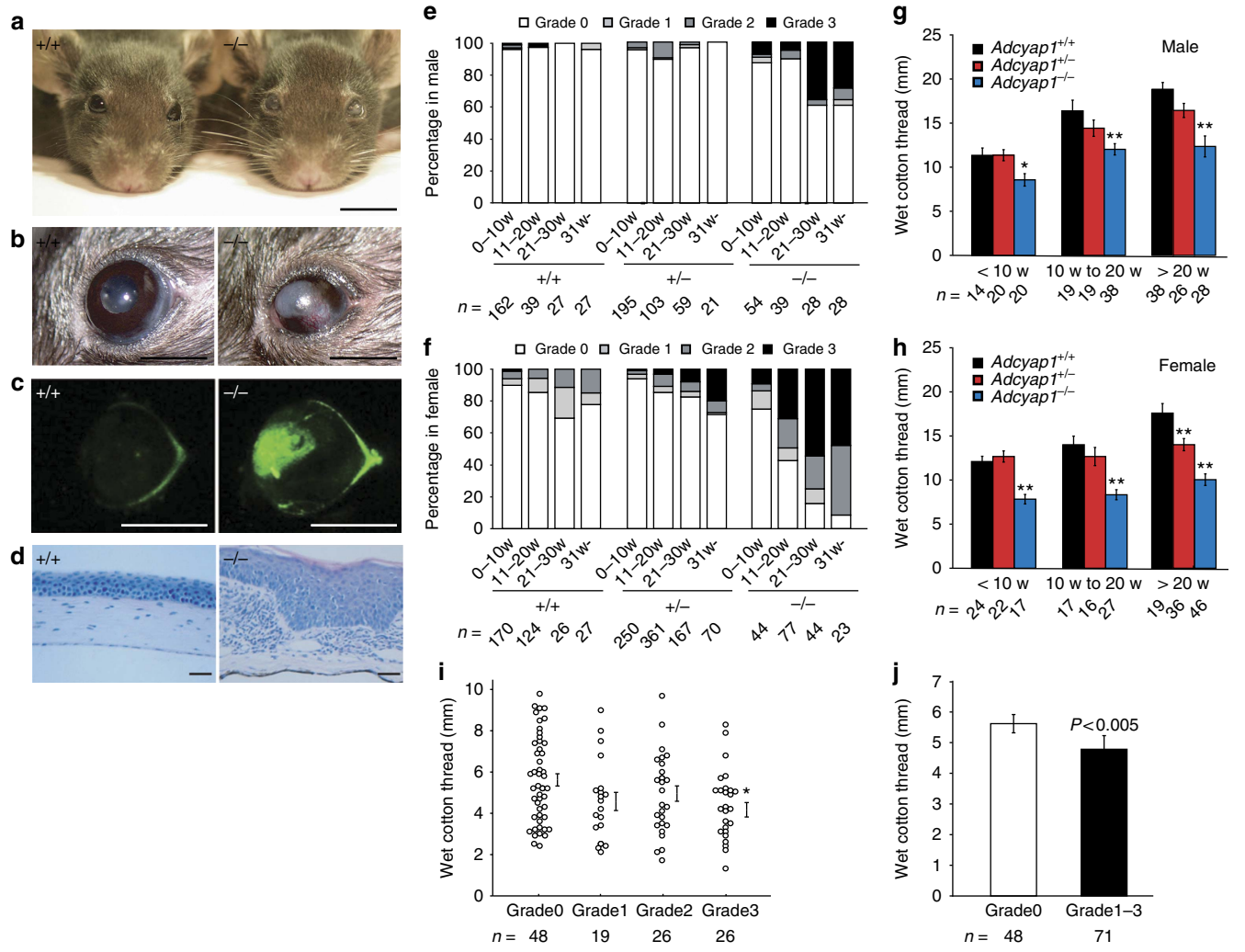

Figure 1 | Corneal keratinization and reduction of tear volume in *Adcyap1*$^{-/-}$ mice. (**a**–**d**) Low- and high-power images of the corneal surface showing pathological changes. Scale bars, 10 mm in **a**, 2 mm in **b** and **c**, and 50 μm in **d**. (**e**,**f**) Scoring of corneal keratinization in wild-type, *Adcyap1*$^{+/-}$ and *Adcyap1*$^{-/-}$ mice as described in Supplementary Fig. 1. The classification was evaluated on both sides, and the highest grade was used for the grading of male (**e**) and female (**f**) mice at different ages. (**g**,**h**) Tear volume measured with the cotton thread method in wild-type, *Adcyap1*$^{+/-}$ and *Adcyap1*$^{-/-}$ mice at different ages. The total wet cotton thread length from both eyes is shown for male (**g**) and female (**h**) mice. *$P<0.05$, **$P<0.01$ versus wild-type mice. (**i**,**j**) Relationship between the wet cotton thread length and the corneal grade in female *Adcyap1*$^{-/-}$ mice. The dot plot graph shows the wet thread length for each eye of each grade expressed in terms of the mean ± s.e. value (**i**). *$P<0.05$ versus Grade 0. The bar graph (**j**) shows the wet thread length of Grade 0 and Grades 1–3, based on the data in Fig. 1i.

To investigate the function of PACAP in the lacrimal gland, PACAP38 was delivered in the form of eye drops to wild-type mice, and the level of tear secretion was measured using the cotton thread method (Fig. 3a). Eye drops containing 10^{-10} to 10^{-8} M PACAP38 significantly increased tear secretion from 15 to 45 min after treatment, with levels returning to baseline by 120 min (Fig. 3b). The basal tear secretion level and PACAP-induced tear secretion level did not differ significantly between males and females (Supplementary Fig. 6). PACAP27-containing eye drops also stimulated lacrimation, whereas the structurally related peptide VIP did not (Fig. 3c,d). Given that it has been reported that PACAP38, rather than PACAP27, is predominantly expressed in mammalian tissues[10], PACAP38 was used in the following experiments. When PACAP was administered unilaterally, tear secretion was only induced on the PACAP-treated side (Supplementary Fig. 7). When corneas were pre-treated with the topical anaesthetic Benoxil to suppress the corneal reflex, the basal lacrimation level decreased, but PACAP still elicited a significant increase in tear secretion (Supplementary Fig. 8). PACAP can thus induce tear secretion under topical anaesthesia, showing that it has a direct effect on the infraorbital lacrimal gland in the absence of the corneal/conjunctival reflex. Moreover, when the acute to semi-acute toxicological effect of PACAP38 (10^{-7} M) eye drops was evaluated at a concentration 1,000 times higher than an effective dose of PACAP38 (10^{-10} M) 48 h after the eye drop treatment, no morphological changes were observed in the corneas or in the infraorbital lacrimal glands (Supplementary Fig. 9). In addition, we examined the effect of PACAP on angiogenesis *in vitro* using human endothelial cells and fibroblasts in co-culture systems. No changes were observed in either the PACAP38 or PACAP6–38 (a PAC1-R and VPAC2-R antagonist)-treated groups (Supplementary Fig. 10). These data suggest that PACAP eye drops act locally to stimulate lacrimation without causing acute to semi-acute toxicity or eliciting a corneal reflex. Mice have two lacrimal glands (the infraorbital and exorbital glands) (Supplementary Fig. 11a), both of which were found to express PAC1-R and VPAC1-R (Supplementary

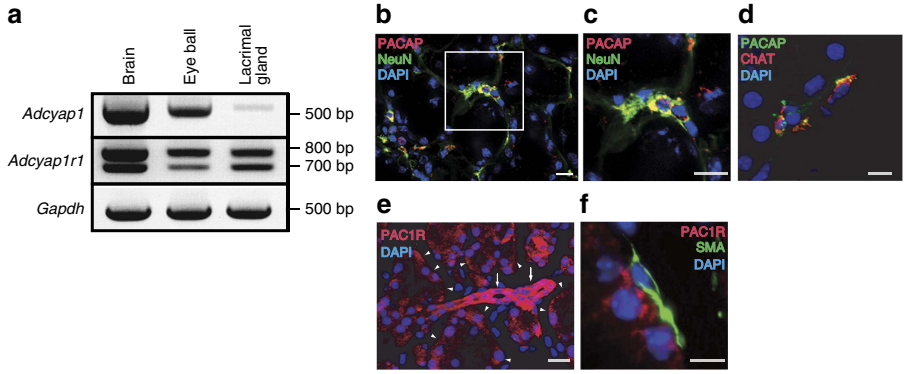

Figure 2 | PACAP and PAC1-R expression in wild-type male mouse infraorbital lacrimal gland. (**a**) Reverse transcriptase PCR analysis to detect *Adcyap1* and *Adcyap1r1* mRNA in the infraorbital lacrimal gland. The eye ball was used as a positive control. (**b**–**d**) PACAP immunoreactivity in the mouse infraorbital lacrimal gland with NeuN immunoreactivity as a neuronal marker (**b**,**c**), and ChAT immunoreactivity as a marker of parasympathetic neurons (**d**). The white square in **b** is expanded in **c**. Scale bar, 20 μm in **b** and **c** and 10 μm in **d**. (**e**,**f**) PAC1-R immunoreactivity in the infraorbital lacrimal gland identified with single immunostaining in the acinus (arrow head) and in the duct (arrow) (**e**), and with smooth muscle actin (SMA) immunoreactivity as a myoepithelial cell marker (**f**). Scale bar, 20 μm in **e** and 5 μm in **f**. DAPI was used as a nuclear marker (**e**,**f**).

Fig. 11b). Although PACAP still significantly stimulated lacrimation in a mouse model in which the exorbital lacrimal gland had been removed, it could not stimulate tear secretion in a second model in which both lacrimal glands had been removed (Fig. 3e,f). These findings indicate that the target organ for PACAP administered in an eye drop formulation is the infraorbital lacrimal gland.

We next examined the signalling cascade associated with PACAP-induced lacrimation. Pre-treatment with PACAP6–38 significantly suppressed PACAP-induced tear secretion (Fig. 3g), whereas VIP6–28 (a VPAC1-R and VPAC2-R antagonist) did not suppress tear secretion (Fig. 3h). Moreover, a single drop of PACAP6–38 (10^{-8} M) to the ocular surface reduced the level of normal lacrimation at the 15 and 60 min time points post-administration (Fig. 3g). The intravenous infusion of PACAP also increased tear secretion in a manner that could be inhibited by co-treatment with PACAP6–38 (Supplementary Fig. 12). These results indicate that PACAP eye drops stimulate lacrimation via an action on PAC1-R.

PACAP eye drops to *Adcyap1*$^{-/-}$ mice. We also used PACAP-containing eye drops on *Adcyap1*$^{-/-}$ mice. PACAP38 (10^{-10} M) drops increased tear secretion in these mice as well as in their wild-type counterparts, suggesting that PACAP transiently restores tear secretion in *Adcyap1*$^{-/-}$ mice (Fig. 4a). We subsequently tested the effects of repeated administration of PACAP38 on the eyes of *Adcyap1*$^{-/-}$ mice (one eye treated with PACAP38, the other with saline) with a view to preventing corneal keratinization. After 3 weeks of treatment, the injury score had increased in saline-treated eyes, but was still at the pre-treatment level in PACAP-treated eyes (Fig. 4b,c). Angiogenesis and ocular hyperaemia were not observed in PACAP-treated eyes (Fig. 4b).

Signalling associated with PACAP-induced tear secretion. To determine the pathway related to PACAP-induced tear secretion, we next investigated the signalling pathways downstream of PAC1-R, focusing on the adenylate cyclase (AC)-cAMP-dependent pathway. As determined by ELISA, the cAMP level in mouse infraorbital lacrimal glands was increased at 15 min and peaked 30 min after the application of PACAP38-containing eye drops (Fig. 5a). The signal for phosphorylated (p) protein kinase A (PKA), a cAMP-dependent protein kinase, was significantly increased at 30 min (Fig. 5b), while pre-treatment with the AC inhibitor SQ22536 or with PACAP6–38 7.5 min before the administration of PACAP eye drops significantly suppressed the PACAP-induced phosphorylation of PKA (Fig. 5c). Pre-treatment with the AC inhibitor dramatically suppressed PACAP-induced tear secretion (Fig. 5d).

Aquaporin expression in wild-type and *Adcyap1*$^{-/-}$ mice. The aquaporins (AQPs) are a family of water channel proteins that are expressed in numerous tissues and organs, with expression of the AQP4 and AQP5 subtypes being reported in the lacrimal gland[18]. To evaluate the relationship between PACAP-induced tear secretion and AQPs, we examined AQP4 and AQP5 immunoreactivities in the infraorbital lacrimal gland in wild-type and *Adcyap1*$^{-/-}$ mice. AQP5 immunoreactivity was identified on the apical side of acinar cells in wild-type mice, but only weak immunoreactivity was observed in these cells in *Adcyap1*$^{-/-}$ mice (Fig. 6a). AQP4 immunoreactivity was observed on the basal side of acinar cells in both wild-type and *Adcyap1*$^{-/-}$ mice, without any obvious difference between the two (Fig. 6a). The specificity of the AQP4 and AQP5 immunoreactivities was confirmed using an antigen pre-absorption test for AQP5 antibody or comparison with a primary antibody-free (AQP4 antibody) negative control (Supplementary Fig. 3d,e). On immunoblotting, the AQP5 signal was found to be significantly lower in the infraorbital lacrimal glands of *Adcyap1*$^{-/-}$ mice than in those of wild-type animals, but the AQP4 signal was almost the same in both cases (Fig. 6b).

The trafficking of AQP5 protein from the cytosol to the membrane contributes to increased water permeability[19]. After fractionation and immunoblotting, the AQP5 signal in the membrane fraction was significantly lower in *Adcyap1*$^{-/-}$ mice than in wild-type mice, but was not significantly different in the cytosolic fraction (Fig. 6c). In contrast, the APQ4 signals in the cytosolic and membrane fractions were similar for the two groups (Fig. 6c).

AQP5 expression and distribution after PACAP eye drops. The phosphorylation of AQP5 has been postulated to initiate its trafficking to the membrane[20,21]. On this basis, the cellular localization and degree of phosphorylation of AQP5 was evaluated in PACAP-treated infraorbital lacrimal glands. Thirty minutes after treatment with 10^{-10} M PACAP, AQP5 immunoreactivity on the apical side of acinar cells was greater

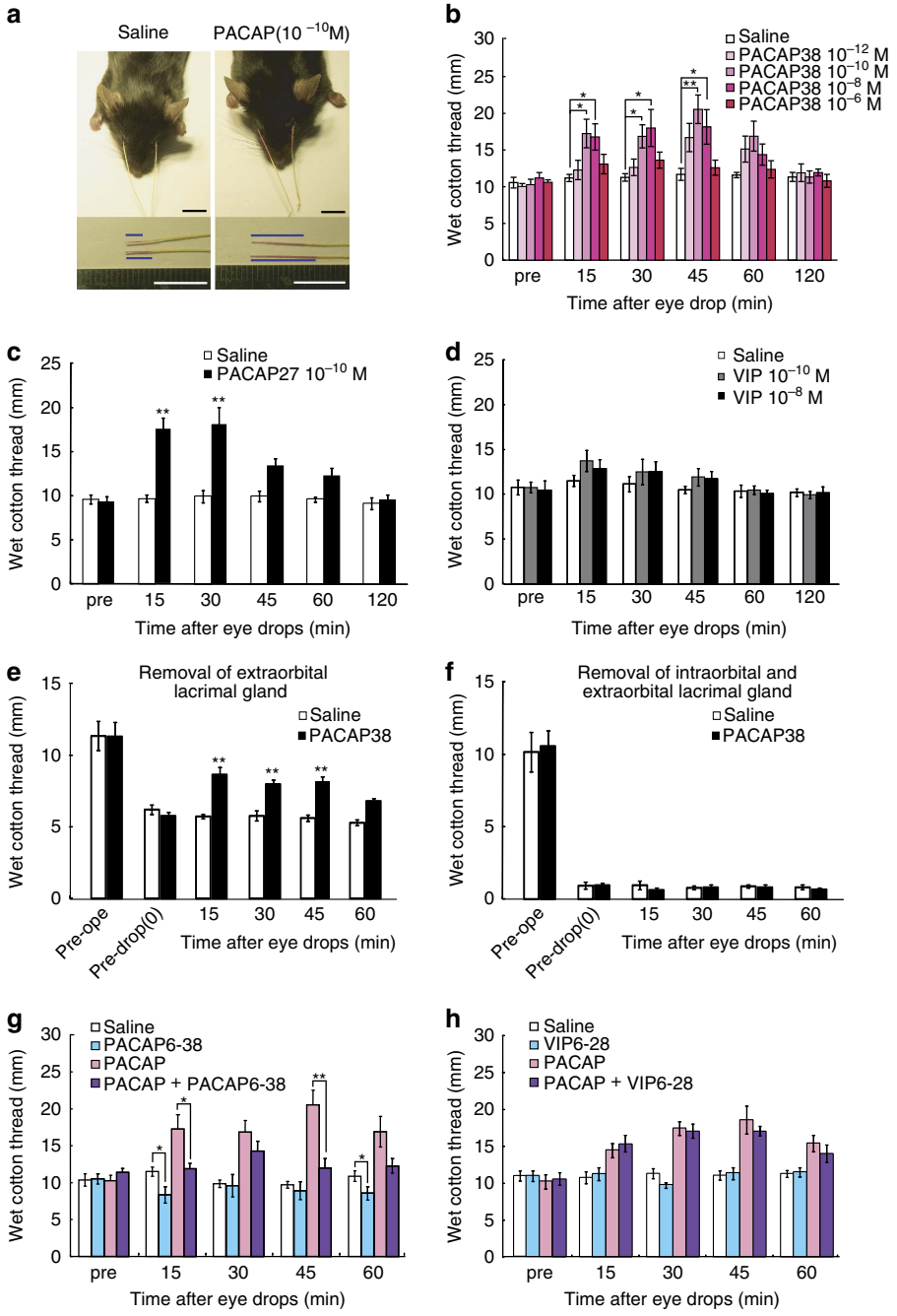

Figure 3 | Effect of PACAP eye drops on tear secretion in male mice. (**a**) Representative images of the cotton thread measurements 30 min after administration of 10^{-10} M PACAP38 or saline eye drops with a 30 s insertion of the thread into both lower eyelids. The blue bar in the lower pictures shows the length of the tear-absorbed thread that changed colour from yellow to red. Scale bar, 10 mm. (**b**) Dose-response effect of PACAP38 eye drops on tear secretion in mice. Test solution eye drops were applied to both eyes. The sum of the wet length of cotton from the two eyes is shown on the *Y*-axis ($n=10$ per group). $^{*}P<0.05$, $^{**}P<0.01$. (**c**,**d**) Effect of PACAP27 (**c**) and VIP (**d**) eye drops on tear secretion ($n=9$–10 per group). $^{**}P<0.01$ versus the saline-treated group. (**e**,**f**) Effect of 10^{-10} M PACAP38 eye drops on two lacrimal gland-deficient models: removal of the exorbital lacrimal gland (**e**) and removal of both the infraorbital and exorbital lacrimal glands (**f**) ($n=10$ per group). $^{**}P<0.01$ versus the saline-treated group. (**g**,**h**) Effect of PAC1-R and VPAC2-R antagonist, PACAP6-38 (**g**) and VPAC1-R and VPAC2-R antagonist, VIP6-28 (**h**) treatments on PACAP-induced tear secretion ($n=10$ per group). $^{*}P<0.05$, $^{**}P<0.01$.

than that in the saline-treated, SQ22536-pre-treated or PACAP6–38-pre-treated groups (Fig. 7a,b). The AQP5 levels in the total lysates of the infraorbital lacrimal gland extracts showed no difference between the groups at 30 min (Fig. 7c). However, the AQP5 signal in infraorbital lacrimal gland extracts immunoprecipitated with a pan-phospho antibody was clearly detectable in the PACAP-treated group, but was less obvious in the other groups (Fig. 7c). An AQP4 signal was not detected in the sample immunoprecipitated with the pan-phospho antibody (Supplementary Fig. 13). The AQP5 signals in the membrane fractions were increased 30 min after treatment with PACAP compared with the other groups (Fig. 7d,e). To elucidate the contribution of AQP5 to PACAP-induced tear secretion, an AQP5 gene-silencing experiment was

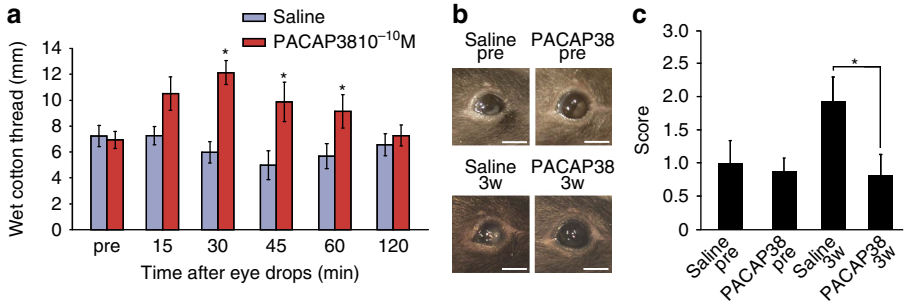

Figure 4 | Effect of PACAP eye drops on female *Adcyap1*$^{-/-}$ mice. (**a**) Tear secretion level in *Adcyap1*$^{-/-}$ mice after application of saline or 10^{-10} M PACAP38 eye drops ($n=9$ per group). *$P<0.05$ versus saline-treated group. (**b**,**c**) Corneal scoring before and after the repeated application of PACAP eye drops to *Adcyap1*$^{-/-}$ mice over a 3-week period. (**b**) Representative images of the corneal surface before and after eye drop application. Scale bar, 2 mm. (**c**) Eighteen female *Adcyap1*$^{-/-}$ mice were given saline or PACAP eye drops unilaterally. The classification of each side of the cornea was evaluated separately before, and 3 weeks after eye drop treatment commenced. *$P<0.05$.

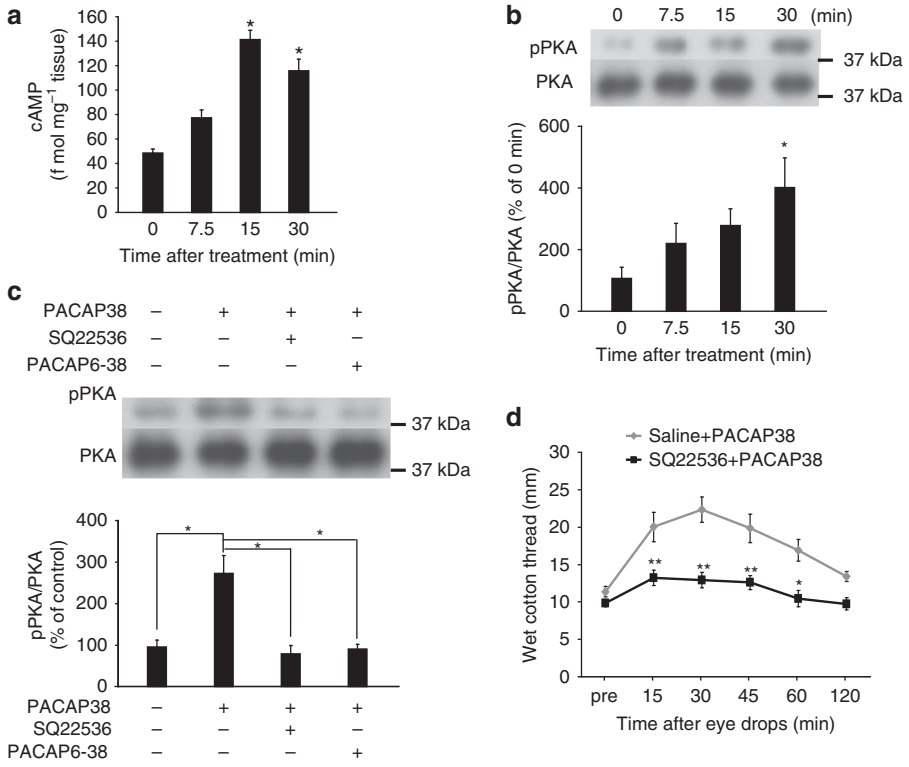

Figure 5 | Contribution of the cAMP/PKA pathway to PACAP-induced tear secretion. (**a**) cAMP content in infraorbital lacrimal gland extracts after application of 10^{-10} M PACAP eye drops ($n=8$ per group). *$P<0.05$ versus 0 min. (**b**) Phosphorylated PKA (pPKA) levels in the mouse infraorbital lacrimal gland after PACAP eye drop application ($n=6$ per group). *$P<0.05$ versus 0 min. (**c**) Pre-treatment with the adenylate cyclase inhibitor SQ22536 or the PACAP receptor antagonist PACAP6-38 suppressed PKA phosphorylation 30 min after PACAP eye drop administration ($n=6$ per group). *$P<0.05$. (**d**) Effect of SQ22536 pre-treatment on PACAP-induced tear secretion in male mice ($n=10$ per group). A single drop of test solution was applied to each ocular surface. The sum of the wet lengths of thread from both eyes is shown. *$P<0.05$, **$P<0.01$ versus saline + PACAP group.

designed (Fig. 8a). When infraorbital lacrimal glands were treated with AQP5 siRNAs, the *Aqp5* mRNA level was significantly decreased by about 70%, whereas the *Aqp4* mRNA level remained almost the same 24 h after the siRNA treatment compared with the control group (Fig. 8b,c). AQP5 siRNA treatment reduced AQP5 immunoreactivity in the infraorbital lacrimal glands, but not AQP4 immunoreactivity (Fig. 8d). The AQP5 siRNA treatment significantly decreased the basal level of tear secretion, and PACAP-induced tear secretion was attenuated 24 h after the siRNA treatment (Fig. 8e).

Taken together, these findings suggest an underlying mechanism whereby PACAP and its receptor are expressed in mouse infraorbital lacrimal glands. PACAP stimulates tear secretion via an AC/cAMP/PKA cascade, which in turn stimulates AQP5 translocation from the cytosol to the membrane of lacrimal acinar cells to bring about an increase in water permeability (Fig. 8f).

Discussion

Dry eye syndrome is more common in women than in men, particularly in older patients[2]. This study has made use of the

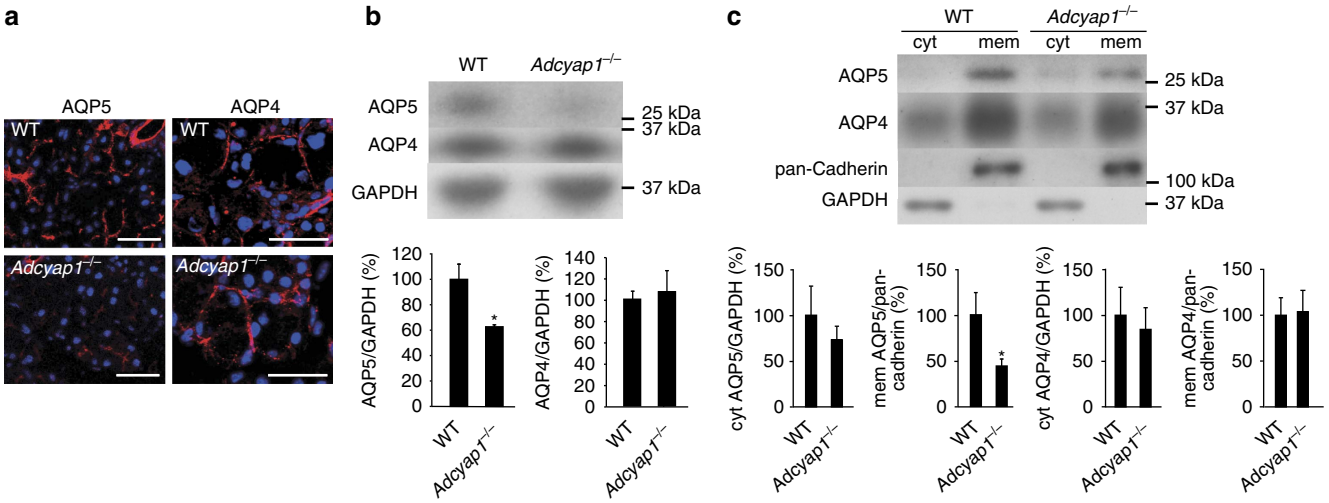

Figure 6 | AQP4 and AQP5 levels in the infraorbital lacrimal glands of male wild-type and *Adcyap1*$^{-/-}$ mice. (**a**) AQP4 and AQP5 immunoreactivities in wild-type and *Adcyap1*$^{-/-}$ mouse infraorbital lacrimal glands. Scale bar, 50 μm. (**b**) AQP4 and AQP5 signals in infraorbital lacrimal gland total lysates from wild-type and *Adcyap1*$^{-/-}$ mice detected by western blot analysis and expressed as semi-quantified results ($n=6$ per group). *$P<0.05$ versus wild-type mice. (**c**) AQP4 and AQP5 signals from fractionated infraorbital lacrimal glands and the semi-quantified results for wild-type and *Adcyap1*$^{-/-}$ mice ($n=6$ per group). *$P<0.05$ versus wild type. GAPDH and pan-cadherin signals were used as internal controls for cytosolic and membrane protein, respectively.

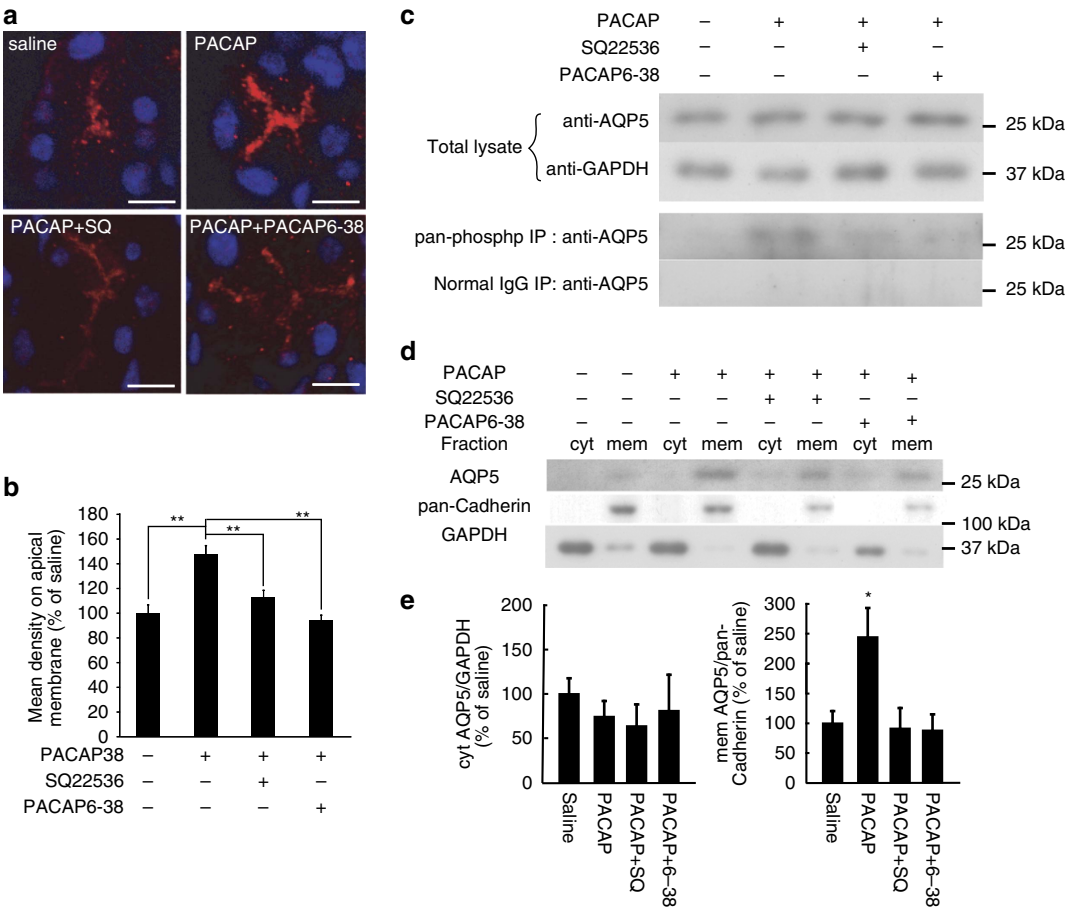

Figure 7 | PACAP eye drop-induced phosphorylation and trafficking of AQP5. (**a**) Representative images of AQP5 immunoreactivities in infraorbital lacrimal gland acinar cells after the application of saline, PACAP38, PACAP38 + SQ22536 (SQ) or PACAP38 + PACAP6–38 eye drops. Scale bar, 10 μm. (**b**) AQP5 signals in fractionated infraorbital lacrimal glands and the semi-quantified results ($n=11$ per group). **$P<0.01$. (**c**) AQP5 signals in total lysate and immunoprecipitation with a pan-phospho antibody. Immunoprecipitation with a normal IgG antibody was used as a negative control. (**d**,**e**) AQP5 signals in fractionated infraorbital lacrimal glands (**d**) and semi-quantified results (**e**) ($n=11$ animals per group). *$P<0.05$

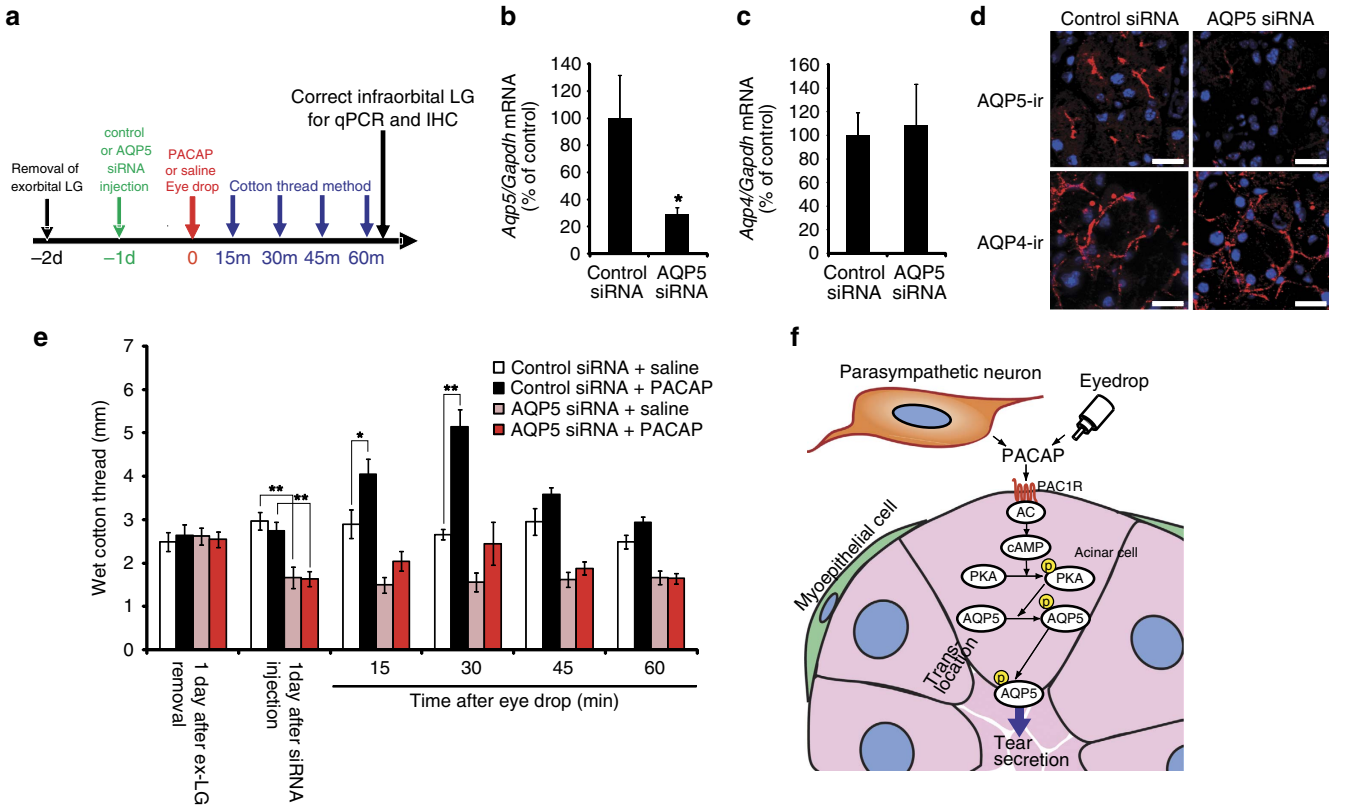

Figure 8 | Contribution of AQP5 to PACAP-induced tear secretion in mice. (**a**) Experimental design of AQP5 siRNA study. (**b**–**d**) AQP4 and AQP5 levels in the infraorbital lacrimal glands of male wild-type mice 1 day after AQP5 siRNA treatment. *Aqp4* (**b**) and *Aqp5* (**c**) mRNA levels were measured by real-time PCR ($n=12$ per group). $^{*}P<0.05$ (**d**) Representative pictures of AQP4 and AQP5 immunoreactivities in the infraorbital lacrimal gland after control and AQP5 siRNA injection. Scale bar, 20 μm. (**e**) Effect of AQP5 siRNA treatment of infraorbital lacrimal glands on PACAP-induced tear secretion ($n=12$). $^{*}P<0.05$, $^{**}P<0.01$. (**f**) Schema of proposed mechanisms of PACAP-induced tear secretion.

discovery of a new *Adcyap1*$^{-/-}$ mouse phenotype, namely the manifestation of corneal keratinization, which was particularly apparent in female mice as a function of age, the overall implication being that *Adcyap1*$^{-/-}$ mice manifest dry eye-like signs. The tear-secreting response to PACAP eye drops and the basal level of tear secretion were, nevertheless, similar between male and female wild-type mice (Supplementary Fig. 6). It has been suggested that the sex difference in dry eye syndrome in humans is due to the influence of female sex hormone levels[22]. Given that female *Adcyap1*$^{-/-}$ mice exhibit decreased serum progesterone levels[23], dry eye-like symptoms in these animals may be due to an imbalance in their sex hormone levels.

Animal models that mimic dry eye disorder have been established by several groups[24,25]. One type of dry eye is the aqueous-deficient model, which mimics the dry eye symptoms caused by autoimmune diseases such as Sjögren's syndrome, removal or irradiation of the lacrimal gland, or neuronal pathway dysfunction. Another type is the evaporative dry eye model, as seen with meibomian gland dysfunction, environmental stress such as exposure to a dry environment, and pharmaceutically induced tear film instability caused by a decrease in oil or mucin secretion in the tears as evidenced by dry eye symptoms[1]. However, a dry eye model arising from a specific endocrine imbalance has not been reported to date. We have shown that *Adcyap1*$^{-/-}$ mice exhibit (1) reduced lacrimation when left untreated, (2) increased lacrimation upon PACAP administration and (3) a morphologically normal lacrimal gland. These findings suggest that the impairment of lacrimal secretion in *Adcyap1*$^{-/-}$ mice results from lacrimal gland dysfunction rather than developmental or structural abnormalities. Moreover, *Adcyap1*$^{-/-}$ mice spontaneously develop corneal keratinization with aging, implying that this mouse phenotype could serve as a novel non-Sjögren's type aqueous-deficient dry eye model arising from lacrimal gland dysfunction.

AQP family genes and proteins are expressed in the eye and its accessory organs[26,27]. It has been reported that AQP5 immunoreactivity is markedly decreased in the lacrimal acinar cells of people with Sjögren's syndrome, a chronic autoimmune disorder with impairment of the moisture-producing glands[28]. The reduced expression of AQP5 suggests that this protein may be related to the decrease in tear secretion in this disease. On the other hand, Verkman's group reported that AQP5 KO mice do not exhibit an altered tear volume[29]. However, the same group recently published data showing that the Na^{+} content of tears from AQP5 KO mice is significantly higher than that of wild-type mice[30], suggesting that the ion concentration in AQP5 KO mouse tears is elevated due to decreased water secretion into the tear fluid. In our study, AQP5 gene silencing-attenuated PACAP-induced tear secretion, as well as the basal level of tear secretion. Taken together, we propose that AQP5 is associated with water secretion into the tear.

It has been reported that the activation of cAMP/PKA can induce the translocation of AQP5 from the cytosol to the apical membrane[31,32]. Moreover, X-ray analysis of the structure of human AQP5 has revealed that phosphorylation at the C-terminal is required for the conformational change for trafficking[21]. Although the relationship between membrane trafficking and phosphorylation of AQP5 is not yet fully understood, in the case of AQP2, the closest paralog of AQP5,

a key event for membrane trafficking is the phosphorylation of a C-terminal site by PKA (refs 33,34). Here, we demonstrate that PACAP eye drops induce an elevation of cAMP, pPKA and pAQP5 levels and membrane trafficking of AQP5 in the mouse infraorbital lacrimal gland, suggesting that PACAP is a regulator of AQP5 trafficking in this gland.

Gilbard and collaborators reported that topical administration of a cAMP inducer such as VIP stimulates tear secretion in a rabbit model of keratoconjuctivitis sicca[35] and in patients with dry eye disease[36]. However, they did not further study the nature of the target organ, or how reagents stimulate tear secretion. Here, we have demonstrated that PACAP stimulates tear secretion from the infraorbital lacrimal gland via a PAC1-R/cAMP/PKA/AQP5 cascade. Moreover, PACAP had a much greater effect on tear secretion than VIP. It should be noted that the Gilbard study used a high concentration of VIP (2×10^{-6} M) as eye drops in their rabbit model, whereas we used 10^{-10} M and 10^{-8} M, the same as our effective doses of PACAP in mice. We also found that PAC1-R is the main receptor for PACAP-induced tear secretion. The affinity of PACAP for PAC1-R is 1,000 times higher than that of VIP, implying that the higher concentration of VIP may be able to stimulate tear secretion via PAC1-R. Taken together, these results suggest that cAMP signalling is an important step for tear secretion, and that PACAP is an endogenous tear regulator in the lacrimal gland, with much greater potential than VIP to stimulate lacrimation.

Tear fluid includes several antibacterial proteins, growth factors and secretary mucin for corneal maintenance[37,38]. As it has been reported that systemic infusion of PACAP alters the composition of tears, especially the keratin family of proteins in rats[39], PACAP may regulate tear protein secretion as well as tear fluid secretion. It is also well known that tear secretion is important for corneal healing[40], and for this reason we postulated that a reduction in tear fluid would be an important factor underlying corneal keratinization in the *Adcyap1*$^{-/-}$ mouse, and that PACAP could protect the corneal surface by stimulating tear secretion. Moreover, we used MALDI-TOF MS and nano-DESI MS/MS to identify the presence of PACAP in mouse tear fluid, a finding that may imply that PACAP is secreted from the lacrimal gland into the tear fluid, thereby directly affecting the cornea. However, it remains questionable from which tissues in tear fluid PACAP is derived. The PACAP could be coming from corneal and conjunctival nerve endings released by dromic (parasympathetic or sympathetic nerves) or anti-dromic (sensory nerves) stimulation, conjunctival goblet cells or stratified squamous cells, or the meibomian glands. If the corneal keratinization in *Adcyap1*$^{-/-}$ mice is due to evaporative water loss caused by a reduced volume of tears, it could be postulated that lid closure (for example, reversible closure, using cyanoacrylate glue) in *Adcyap1*$^{-/-}$ mice would inhibit the development of this phenotype. Future studies will be needed to clarify the source of PACAP in tear fluid and the corneal healing effects of PACAP.

Although our findings indicate the potential of PACAP as a stimulator of tear production in mice, there are still problems that would need to be resolved in relation to drug development. First, the human and mouse lacrimal apparatuses are structurally different. In mice, the exorbital lacrimal glands are located near the ear on the lateral side of the skull, and connect with the excretory ducts into the eyelid. The infraorbital lacrimal glands and the lipid-secreting Harderian glands are found in the orbit of the eye. In humans, one main lacrimal gland is located in the lacrimal fossa of each orbit next to the eye ball; this connects with excretory ducts in the upper fornix. However, over 50 accessory lacrimal glands are scattered over the inner surfaces of the lower and upper eyelids, and the lipid-secreting meibomian gland is located in the tarsal plate of the upper and lower eyelids[41]. We anticipate that PACAP eye drops will not reach the main lacrimal gland in humans because of its location, making the target of PACAP the accessory lacrimal glands. However, it is still an open question whether PACAP only affects the lacrimal gland, or whether the corneal and conjunctival epithelia, and the intraorbital lipid-secreting gland are also involved. In any future clinical trials of PACAP on dry eye patients, it will be important to clarify the expression of PACAP and PACAP receptors in tear-secreting tissue, including the lacrimal glands, as well as the effect and target of PACAP eye drops in humans. Moreover, we showed that PACAP eye drops did not cause any adverse reaction in acute to semi-acute phase at a concentration of 10^{-7} M (Supplementary Fig. 9), or in chronic eye drop treatment at a concentration of 10^{-10} M for 3 weeks in *Adcyap1*$^{-/-}$ mice (Fig. 4). However, these toxicological evaluations may not be sufficient for safety trials of PACAP eye drops to proceed on healthy volunteers. Further suitable toxicological tests will be required before a clinical trial.

In this study, PACAP38 eye drops at the lower dose of 10^{-10} M stimulated mouse lacrimation for <1 h. Even if the effects of PACAP are similar in mice and humans, this short period of action would pose a problem in a clinical setting. We believe that the short-acting effect of PACAP in our study was due to the PACAP eye drops being washed from the ocular surface by lacrimation. One solution could be to formulate an ointment to provide sustained release. However, low doses of bioactive peptides have both advantages and disadvantages in terms of drug development. A low dose of peptide-based medicine offers good efficacy, safety and high selectivity and potency. In contrast, there are issues in relation to instability, short half-life and rapid elimination[42]. These problems would need to be overcome if PACAP were to be developed as an effective stimulator of lacrimation.

In conclusion, our results highlight a new function of PACAP as a stimulator of tear production initiated via the PAC1-R/AC/cAMP/PKA/AQP5 cascade. We found that PACAP eye drops induce tear secretion and suppress the progression of corneal keratinization in *Adcyap1*$^{-/-}$ mice. Topical administration of cyclosporine has been developed for dry eye patients to provide an anti-inflammatory effect; however, eye drops focusing on tear-stimulating mechanisms are still in the developmental stage. The findings from our work are encouraging and should provide the impetus for further preclinical and clinical studies on the efficacy of PACAP eye drops to treat dry eye patients.

Methods

Animals. All experimental procedures involving animals were approved by the Institutional Animal Care and Use Committee of Showa University (08116, 09110, 50021, 51033, 510043, 52007, 52013, 53020, 53025). The *Adcyap1*$^{-/-}$ mice on the C57BL/6 background were established by Dr Akemichi Baba[15] and were bred and maintained under specific pathogen-free conditions in the animal facility of Showa University. Animals were housed in a facility with a 12-h/12-h light/dark cycle and were given free access to water and standard rodent chow. Eight to twelve weeks old mice were used, excepting Figs 1 and 4, and Supplementary Figs 1 and 2 with 8 to over 30 weeks old mice. In this study, both male and female mice were used as described in the figure legends.

Evaluation of corneal scoring. Keratinization of the cornea was classified into four grades (Grades 0–3) by visual observation under a dissecting microscope as follows: Grade 0 (normal) = no observable abnormality; Grade 1 = clouded cornea; Grade 2 = angiogenesis; and Grade 3 = hypertrophy of the corneal epithelium as shown in Supplementary Fig. 1a–d. The evaluation of corneal score was performed in a blinded fashion. The corneal keratinization of wild-type, *Adcyap1*$^{+/-}$, and *Adcyap1*$^{-/-}$ mice was evaluated on both sides, and the higher grade was used for the grading of the animals in Fig. 1e,f.

Corneal fluorescein staining. Corneal injuries were visualized with fluorescein staining. *Adcyap1*$^{-/-}$ and wild-type mice were anaesthetized with an

intraperitoneal (i.p.) injection of pentobarbital, and 2 µl of fluorescein solution (1 µg µl^{-1}) dissolved in saline were dropped on the cornea. After letting the animal blink five times, excess drops were wiped off with a cotton swab. Photographs were taken with a digital camera (CAMEDIA C5050, Olympus, Tokyo, Japan) connected to a stereoscopic microscope.

PACAP-containing eye drops and cotton thread tear test. The rate of lacrimal secretion was determined with the cotton thread test using standardized phenol red-impregnated cotton threads (Zone-Quick; Menicon Co. Ltd, Nagoya, Japan). Mice were anaesthetized with an i.p. injection of pentobarbital to suppress autonomic nervous system reflexes that could have affected tear secretion. The basal level of tear secretion was evaluated by insertion of the thread under the lower eyelid for 30 s, after which the bilateral length of the colour-changed thread that had absorbed the tear fluid was measured in millimeters. The test solution, PACAP38 (10^{-6}–10^{-12} M (Peptide Institute, Osaka, Japan), PACAP27 (10^{-10} M, Peptide Institute), VIP (10^{-8} M or 10^{-10} M, Peptide Institute) or saline was then applied to both ocular surfaces. The mice were forced to blink their eyes five times, and their eyes were then kept closed during all subsequent steps to prevent drying of the surface of the cornea.

Excess drops were wiped off with a swab 7.5 min after application of the eye drops, and tear secretion was checked at 15-min intervals from 15 to 120 min after the eye drops had been administered. At each measurement time, the thread was kept on the lower conjunctival sac of each eye for 30 s. The tear volume in the no eye drop study (Fig. 1; Supplementary Fig. 12) was performed without anaesthesia. The total length of wet cotton thread was measured for both sides (Figs 1d,e, 3, 4 and 5;; Supplementary Figs 8 and 12), and in other specific experiments (Figs 1f,g and 8; Supplementary Fig. 7), the length was evaluated on each side. The PACAP receptor antagonist PACAP6–38 (Peptide Institute), VIP receptor antagonist VIP6–28 (Sigma, St Louis, MO, USA), adenylate cyclase inhibitor SQ22536 (Sigma-Aldrich) or topical anaesthetic 0.4% oxybuprocaine hydrochloride (Benoxil; Santen Pharmaceutical Co., Ltd., Osaka, Japan) was applied 7.5 min before the administration of eye drops containing 10^{-10} M PACAP38 or saline. When Benoxil was pre-administered, the loss of the corneal reflex was confirmed by stimulating the corneal surface with a blunt plastic tip before PACAP or saline treatment.

Histology. Adult C57BL/6 mice (Charles River Japan, Kanagawa, Japan) were anaesthetized with sodium pentobarbital (50 mg kg^{-1}, i.p.) and perfused with phosphate-buffered saline (PBS) followed by 2% paraformaldehyde in PBS. Immediately afterwards, the infraorbital lacrimal glands were removed and fixed in the same fixative for 24 h at 4 °C. Fixed tissues were embedded in paraffin for histopathological studies with hematoxylin and eosin staining, or frozen sections were used for double-labelling immunofluorescence staining.

Toxicology of the PACAP eye drops. In acute to semi-acute toxicology experiments, 2 µl of 10^{-7} M PACAP or saline were applied as eye drops, and the eye ball and accessory organs of treated animals were fixed with formaldehyde 48 h later. The acute to semi-acute toxicological effects of PACAP on the cornea and infraorbital lacrimal gland were evaluated based on hematoxylin and eosin staining.

Double-labelling immunofluorescent staining. The following primary antibodies were used according to standard protocols[43]. Eight-µm-thick frozen sections were blocked in 5% normal horse serum for 1 h and incubated overnight at 4 °C in mixtures of the following primary antibodies: rabbit anti-PACAP antibody (1:2000; Peninsula Laboratories, Inc., Belmont, CA, USA), rabbit anti- PAC1-R antibody (1:200; raised by using the N-terminal residue as an antigen[44]), mouse anti-smooth muscle actin antibody (1:200; R&D Systems, Inc. Minneapolis, MN, USA), mouse anti-NeuN antibody (1:1000; Millipore, Billerica, MA, USA), goat anti-ChAT antibody (1:100; Millipore), rabbit anti-AQP4 antibody (1:250; Millipore) and rabbit anti-AQP5 antibody (1:100; Millipore). Immunoreactivity was detected using an Alexa 488- or 546-labelled goat anti-mouse IgG, goat anti-rabbit IgG or donkey anti-goat IgG antibodies (1:800; Invitrogen) following a 90-min incubation at room temperature. After washing with PBS, the sections were incubated for 5 min with 4',6-diamidine-2-phenylindole dihydrochloride (DAPI, 1:10,000; Roche Diagnostics, Indianapolis, IN, USA) to stain cell nuclei. Labelling was imaged with a fluorescence microscope (Axio Imager Z1 with Apotome, Carl Zeiss, Oberkochen, Germany). In the antigen absorption test, PACAP, PAC1-R or AQP5 antibody solution was incubated with a final concentration of 1 µM of antigens in 5% normal horse serum in PBS overnight at 4 °C. After centrifugation at 10,000*g* for 20 min, the supernatant was used instead of the primary antibody.

Reverse transcriptase PCR. Total RNA was isolated from mouse infraorbital lacrimal glands with an RNAeasy kit (Qiagen, Hilden, Germany). Reverse transcription was performed with random primers. Mouse *Adcyap1* primers, forward; 5′-ATG ACC ATG TGT AGC GGA GCA AGG CTG G-3′, reverse; 5′-CTA CAA GTA TGC TAT TCG GCG TCC-3′ (product size 525 bp), and mouse *Adcyap1r1* primers, forward; 5′-CCT GTC GGT GAA GGC CCT CTA CAC A-3′, reverse; 5′- CCC AGC CCA AGC TCA AAC ACA AGT C-3′ (798–801 bp product for the hip or hop form, and 717 bp product for the short form), mouse *Vpacr1* primers, forward; 5′- GTA TGG ATG AGC AGC AAC AGA CTG-3′, reverse; 5′- TTG ATG ATG GTG TCC CAG CAC-3′ (product size 487 bp), mouse *Vpacr2* primers, forward; 5′-CAT CTC TGT GCT GGT CAA GGA C-3′, reverse; 5′- CGC CAT CTT CTT TTC AGT TCA C-3′ (product size 654 bp), mouse *Gapdh* primers, forward; 5′- GCC AAG GTC ATC CAT GAC AAC-3′, reverse; 5′-GTC CAC CAC CCT GTT GCT GTA-3′ (product size 498 bp), and mouse *Actb* primers, forward; 5′-GTG GGC CGC TCT AGG CAC CAA-3′, reverse; 5′-CTC TTT GAT GTC ACG CAC GAT TTC-3′ (product size 540 bp) were mixed with the EX taq kit (TAKARA Bio, Otsu, Japan) with the PCR conditions of penetration for 15 s at 95 °C, annealing at 50 °C for 30 s, elongation at 72 °C for 1 min with a final extension at 72 °C for 10 min. The PCR products were separated by gel electrophoresis on an agarose gel and visualized with an illuminometer. Image of the gel have been cropped for presentation. The uncropped images in Fig. 2a are shown in Supplementary Fig. 14.

Real-time PCR. RNA isolation was followed by the reverse transcriptase PCR method. Reverse transcription into complementary DNA was achieved using the reagents and protocol of the PrimeScript RT reagent kit (TaKaRa BIO, Kyoto, Japan). The PCR primer set was as follows: mouse *Aqp4* primers, forward; 5′-CTT TCT GGA AGG CAG TCT CAG-3′, reverse; 5′-CCA CAC CGA GCA AAA CAA AGA T-3′, mouse *Aqp5* primers, forward; 5′-GGG TAA CCT GGC CGT CAA TG-3′, reverse; 5′-TGA CCG ACA AGC CAA TGG ATA A-3′, and mouse *Gapdh* primers, forward; 5′-TGT GTC CGT CGT GGA TCT GA-3′, reverse; 5′-TTG CTG TTG AAG TCG CAG GAG-3′. Real-time PCR was performed using SYBR Premix Ex Taq II reagent (TaKaRa BIO Inc.) and an ABI PRISM 7900 instrument (Applied Biosystems, Lincoln, CA, USA). Relative gene expression was calculated using the comparative delta Ct method with the Ct values of the housekeeping gene, *Gapdh*. mRNA levels were normalized, with the percentage for control groups taken as 100%.

Repeated eye drop study. *Adcyap1*$^{-/-}$ female mice were given eye drops containing 10^{-10} M PACAP or saline, 2 µl per eye (unilaterally), 2 times per day, 6 days per week for 3 weeks. We selected 18 female *Adcyap1*$^{-/-}$ mice based on similar average pre-treatment corneal keratinization scores on both sides. The scoring method was the same as the previous evaluation for each side separately.

cAMP enzyme immunoassay. Enzyme-linked immunoassays for cAMP were performed using a cAMP enzyme immunoassay (EIA) kit (Cayman Chemicals, Grand Rapids, MI, USA) following the manufacturer's instructions. In brief, C57/BL6 mice were anaesthetized, and 2 µl of 10^{-10} M PACAP was applied to both ocular surfaces. Both infraorbital lacrimal glands were removed at 0, 7.5, 15 or 30 min after the application of the eye drops ($n = 8$). They were then homogenized in 200 µl of 5% trifluoroacetic acid on ice. After centrifugation at 1,500*g* for 10 min, the lysate was mixed with 1 ml of ether for 10 s. After removal of the ether, the aqueous layer was acetylated according to the EIA kit manufacturer's instructions and used for the EIA assay. The absorption in each well was measured with a plate reader (POLARstar Omega; BMG LABTECH GmbH, Offenburg, Germany).

Immunoblotting. For western blot analysis, mice were euthanized by decapitation and their infraorbital lacrimal glands were immediately removed. The infraorbital lacrimal glands were then homogenized in cold lysis buffer (10 mM Tris-HCl, 0.15 M NaCl and 1% Triton X-100) with a protease inhibitor cocktail (Sigma). Homogenates were centrifuged at 12,000*g* for 30 min at 4 °C and the resultant supernatant was collected as the total cell lysate, which was subsequently diluted with SDS sample buffer (250 mM Tris-HCl (pH 6.8), 4% SDS, 40% glycerol, 4% 2-mercaptoethanol and 0.002% bromophenol blue) and incubated for 12 h at 4 °C. This lysate sample (30 µg) was electrophoresed on a 7.5% polyacrylamide gel containing 0.1% SDS at 100 V. The protein bands were then transferred from the gel to polyvinylidinene fluoride membranes (Bio-Rad Laboratories, Inc. Hercules, CA, USA) for 3 h at 100 mA. The membrane was initially blocked with 2% Blockace (Dainihon Pharmaceutics, Osaka, Japan) in Tris- buffered saline with Tween 20 (TBS-T) for 1 h at room temperature and probed overnight with a mouse monoclonal antibody for PKA (1:1,000, Cell Signaling Technology, Danvers, MA), pPKA (1:1,000, Cell Signaling Technology), AQP4 (1:2,000, Millipore), AQP5 (1:4,000, Millipore), GAPDH (1:2,000, Millipore), or pan-cadherin (1:4,000, Abcam, Cambridge, UK) at 4 °C. After incubation with a sheep anti-mouse IgG HRP-conjugated antibody (1:2,000; GE Healthcare Bioscience, Little Chalfont, UK) for 1 h at room temperature, protein bands were revealed using a SuperSignal West Dura Extended Duration Substrate (Thermo Fisher Scientific Pierce Biotechnology, Rockford, IL, USA) and exposed onto X-ray Film. Subcellular protein fractionation (cytosolic and membrane fractions) was performed using the ProteoExtract Subcellular Proteome Extraction Kit according to the manufacturer's instructions (Calbiochem, Hessen, Darmstadt, Germany). The fractions were precipitated using a ProteoExtract Protein Precipitation Kit (Calbiochem). Precipitated protein was then dissolved in lysis buffer and the protein content was measured. Equivalent amounts of proteins (5 µg) for each fraction of subcellular fractionation were used for immunoblotting. GAPDH and pan-cadherin signals were used as the internal controls for cytosolic and membrane proteins, respectively. Image of the membrane have been cropped for presentation. The uncropped images in Figs 5–7 are shown in Supplementary Fig. 14.

Immunoprecipitation. All immunoprecipitations were carried out using the immunoprecipitation kit Catch and Release v2.0 (Millipore) following the manufacturer's instructions. In brief, mouse infraorbital lacrimal gland lysate was obtained 30 min after the application of eye drops. Four-hundred microgram protein from the cell lysate, 1 μg of a mouse anti-pThy, -pSer, or -pThr (pan-phospho) IgG antibody (AnaSpec Inc, San Jose, CA, USA) for the capture antibody or a normal mouse IgG (Millipore) as the control antibody, and 10 μl of the antibody capture affinity ligand (total 500 μl) were mixed and placed in a Catch and Release v2.0 spin column containing prepacked immunprecipitation capture resin. After end-over-end shaking for 16 h at 4 °C, the column was centrifuged, washed 3 times and then eluted with 70 μl of the elution buffer. The eluent was analysed by immunoblotting.

Removal of lacrimal glands. Under inhalation anaesthesia with sevoflurane, the hair from under the ear to the outer canthus of the eyes was shaved, and a 15 mm incision was made. In the exorbital lacrimal gland removal model, the exorbital lacrimal gland, which is located under the ear, was exposed and removed. In the infraorbital and exorbital lacrimal gland removal model, the exorbital lacrimal gland and the lacrimal duct were first isolated. The infraorbital lacrimal gland was exposed by pulling the lacrimal duct, after which both lacrimal glands were removed. The skin was then sutured and the animals were kept warm during their recovery from anaesthesia. The tear secretion level was checked before and after surgery.

Semi-quantification of AQP5 immunoreactivity in lacrimal acini. The densities of AQP5 immunoreactivity in the mouse infraorbital lacrimal gland 30 min after administration of eye drops containing saline, PACAP38, PACAP38 + SQ22536, or PACAP38 + PACAP6–38 was evaluated. AQP5 immunostaining was performed following the above method. One hundred pictures of acini from 10 infraorbital lacrimal glands (10 acinus pictures/lacrimal gland) from five wild-type mice in each group were cut out with grey scale. Using Image J software (ver. 1.44p), the average density in the apical membrane, and in four spots of 1 μm^2 in the cytosolic area were measured. The value of the apical membrane density was determined using the cytosolic density value as background. The quantification was performed with a blinded test, masking sample data for another person who used image J.

AQP5 siRNA treatment *in vivo*. An HPLC grade of non-target negative control and three types of mouse AQP5 siRNAs (sequence was shown in Supplementary Table 1) were designed and purchased from BONAC Corporation (Fukuoka, Japan). Mouse AQP5 siRNAs (10 μM × 3 siRNAs) or negative control siRNA (30 μM) were mixed with an equal volume of atelogene local use (KOKEN, Tokyo, Japan) and gently incubated for 1 h at 4 °C. One day after the removal of the exorbital lacrimal gland, the siRNA was applied to surround the infraorbital lacrimal gland. AQP5 siRNA and control siRNA were used on opposite sides. The next day, mice were anaesthetized with pentobarbital, after which PACAP38 (10^{-10} M) or saline eye drops were administered. At the 15, 30, 45 and 60 min time points, the tear secretion level was measured using the cotton thread method. The infraorbital lacrimal gland was then removed and the AQP4 and AQP5 levels were checked by real-time PCR and immunostaining.

Whole-cornea immunostaining. After euthanasia, the epithelial layer of the cornea was scraped off under a stereoscopic microscope. The eye ball was excised, then fixed in 4% paraformaldehyde for 2 h at room temperature. The cornea was dissected and washed 3 times with phosphate-buffered saline (PBS), after which it was incubated with blocking buffer (1% Triton X-100 and 10% normal horse serum in PBS) for 1 h. The cornea was then incubated with primary antibody (Neurofilament 200, 1:500, Sigma, St Louis, MO) diluted in blocking buffer for 3 days at 4 °C, washed four times in PBS, and incubated with a secondary antibody (alexa546-labelled anti-rabbit IgG, 1:500) diluted in the blocking buffer for 4 h at room temperature. After final washing in PBS, the cornea was mounted surface side up on a glass slide with aqueous mounting medium. Labelling was imaged with a fluorescence microscope (Axio Imager Z1 with Apotome, Carl Zeiss, Oberkochen, Germany).

Dot blotting. PACAP38 or VIP (1 μl of 0.2 to 25 pmol μl^{-1}) was dropped on a nitrocellulose membrane. After drying, the membrane was washed in Tris buffered saline with Tween 20 and blocking buffer, followed by immunoblotting as described above. A primary anti-PACAP antibody (1:4,000; Peninsula Laboratories, Belmont, CA, USA) was used in the dot blotting study.

MALDI-TOF mass spectrometry of intact PACAP38 in tear samples. Tear samples were collected from mice by application of sterile filter paper strips ($n = 5$, Schirmer paper), and PACAP38 was measured using MALDI-TOF mass spectrometry. Aqueous solutions of the standard and tear samples were loaded onto the target plate (MTP 384 massive target T, Bruker Daltonics, Bremen, Germany) by mixing 1.0 μl of each solution with the same volume of a saturated matrix solution, prepared fresh every day by dissolving α-cyano-4-hydroxycinnamic acid in acetonitrile/0.1% trifluoroacetic acid (1/2, v/v). The mass spectrometer used in this work was an Autoflex II TOF/TOF (Bruker Daltonics) operated in the linear mode. Ions were accelerated under delayed extraction conditions (140 ns) in the positive ion mode with an acceleration voltage of 20.00 kV. The instrument uses a 337 nm pulsed nitrogen laser, model MNL-205MC (LTB Lasertechnik Berlin GmbH, Berlin, Germany). External calibration was performed in each case using the average masses of the Bruker Peptide Calibration Standard (#206195, Bruker Daltonics). Protein masses were acquired within a range of 1,000–8,000 *m/z*. Each spectrum was produced by accumulating data from 800 consecutive laser shots. Bruker FlexControl 2.4 software was used for control of the instrument and Bruker FlexAnalysis 2.4 software for spectrum evaluation.

Nanospray desorption electrospray ionization Orbitrap MS/MS analyses of PACAP38 in tear samples. Nanospray desorption electrospray ionization (nano-DESI) was used to acquire MS/MS spectra directly from Schirmer paper containing tears ($n = 6$). The nano-DESI probe consisted of two fused silica capillaries (ID 50 μm, OD 150 μm, Polymicro Technologies, Molex, Lisle, IL) positioned at an angle to each other[45]. A solvent, consisting of methanol/water (9/1, v/v) with 2% formic acid, was propelled, at 0.5 μl min^{-1}, through the primary capillary, forming a liquid bridge to the secondary capillary. The secondary capillary transported the solvent to the mass spectrometer inlet for nanospray ionization. The filter paper was soaked with 10 μl 0.1% trifluoroacetic acid (99%, Sigma-Aldrich) on a regular glass slide. The glass slide was placed on a motorized *x*,*y*,*z*-stage (Newport Corporation, Irvine, CA, USA) to position the sample under the nano-DESI probe[46,47]. Material was extracted from the wet surface of the Schirmer paper by the nano-DESI probe and analysed using a QExactive Plus Orbitrap mass spectrometer (Thermo Fisher Scientific, Bremen, Germany). The instrument mass resolving power was set to 70,000 ($m/\Delta m$) and a high voltage of 3 kV was applied to the primary capillary. Selective ion monitoring was set to m/z 648.5 ± 2, corresponding to PACAP38 ($z = 7$) and tandem mass spectrometry was performed at m/z 648.5 ± 1 Da, using higher energy collision-induced dissociation with a normalized collision energy of 20 applied. The same settings were used for the PACAP38 standard, wild-type mouse samples and $PACAP^{-/-}$ mouse samples.

Effect of PACAP on angiogenesis. The experiments on endothelial cell tube formation were conducted in 24-well dishes using an angiogenesis kit (Kurabo, Okayama, Japan), according to the manufacturer's instructions. Human umbilical vein endothelial cells and fibroblasts were co-cultured in medium containing vascular endothelial growth factor (final 10 μg l^{-1}) with various concentrations of PACAP38 (10^{-9}, 10^{-6} M) and PACAP6–38 (10^{-8}, 10^{-6} M), with the medium exchanged on days 4, 7 and 9. On day 11, the cells were washed and directly fixed in the wells with 70% ice-cold ethanol for 30 min. The fixed cells were serially incubated with 1% bovine serum albumin (BSA) in the buffer, a mouse monoclonal antibody against human CD31, an alkaline phosphatase-conjugated goat anti-mouse IgG, and a nitro-blue tetrazolium chloride (NBT)/5-bromo-4-chloro-3′-indolylphosphatase p-toluidine salt from the kit, and then washed and photographed. The images were analysed using Angiogenesis Image Analyzer software (Kurabo) to measure the gross area of the CD31-positive tubes (the area of endothelial tubes) and the length of CD31-positive tubes in culture. Data are shown as a percentage of the area of the endothelial cell tubes in the untreated cultures.

Systemic infusion of PACAP38. Systemic infusion of PACAP was done as in our previous study[48]. Briefly, PACAP38 (5 nmol kg^{-1}) or PACAP38 plus PACAP6–38 (50 nmol kg^{-1}) was injected into the jugular vein with vehicle (0.1% BSA in saline) under inhalation anaesthesia with sevoflurane. A PE10 polyethylene tube connected to an Alzet osmotic pump (0.5 μl h^{-1}; DURECT Corporation, Cupertino, CA, USA) that was filled with the vehicle, PACAP38 (32 pmol μl^{-1}), or PACAP plus PACAP6–38 (320 pmol μl^{-1}) was then inserted for continuous administration. Tear volume was measured with the cotton thread method four days after the infusion commenced.

Statistical analyses. Data are presented as the mean ± s.e. (n = sample size). The effects of treatments were analysed with the Mann–Whitney *U*-test (Figs 1i,j and 4c), the two-tailed Student's *t*-test (Figs 6b,c and 8b,c), one-way ANOVA followed by the Dunnett test (Figs 3b, 5a–c and Fig. 7e) or a one-way ANOVA followed by the Tukey test (Figs 1g,h, 3c–h, Figs 5d and7b and Fig. 8e and Supplementary Figs 6–8, 10 and 12). The two-tailed Spearman's correlation test was used to identify correlations between corneal grade and tear volume in $Adcyap1^{-/-}$ mice. Differences due to the treatments were considered as significant for values of $P < 0.05$.

Data availability. The authors declare that the data supporting the findings of this study are available within the article and its Supplementary Information Files.

References

1. The definition and classification of dry eye disease: report of the Definition and Classification Subcommittee of the International Dry Eye WorkShop (2007). *Ocul. Surf.* **5,** 75–92 (2007).
2. Kastelan, S., Tomic, M., Salopek-Rabatic, J. & Novak, B. Diagnostic procedures and management of dry eye. *Biomed. Res. Int.* **2013,** 309723 (2013).
3. Blehm, C., Vishnu, S., Khattak, A., Mitra, S. & Yee, R. W. Computer vision syndrome: a review. *Surv. Ophthalmol.* **50,** 253–262 (2005).
4. Chen, Q. *et al.* Lower volumes of tear menisci in contact lens wearers with dry eye symptoms. *Invest Ophthalmol. Vis. Sci.* **50,** 3159–3163 (2009).
5. O'Brien, P. D. & Collum, L. M. Dry eye: diagnosis and current treatment strategies. *Curr. Allergy Asthma Rep.* **4,** 314–319 (2004).
6. Miyata, A. *et al.* Isolation of a neuropeptide corresponding to the N-terminal 27 residues of the pituitary adenylate cyclase activating polypeptide with 38 residues (PACAP38). *Biochem. Biophys. Res. Commun.* **170,** 643–648 (1990).
7. Miyata, A. *et al.* Isolation of a novel 38 residue-hypothalamic polypeptide which stimulates adenylate cyclase in pituitary cells. *Biochem. Biophys. Res. Commun.* **164,** 567–574 (1989).
8. Harmar, A. J. *et al.* Pharmacology and functions of receptors for vasoactive intestinal peptide and pituitary adenylate cyclase-activating polypeptide: IUPHAR review 1. *Br. J. Pharmacol.* **166,** 4–17 (2012).
9. Spengler, D. *et al.* Differential signal transduction by five splice variants of the PACAP receptor. *Nature* **365,** 170–175 (1993).
10. Vaudry, D. *et al.* Pituitary adenylate cyclase-activating polypeptide and its receptors: 20 years after the discovery. *Pharmacol. Rev.* **61,** 283–357 (2009).
11. Nakamachi, T. *et al.* Role of PACAP in neural stem/progenitor cell and astrocyte—from neural development to neural repair. *Curr. Pharm. Des.* **17,** 973–984 (2011).
12. Shioda, S. & Nakamachi, T. PACAP as a neuroprotective factor in ischemic neuronal injuries. *Peptides* **72,** 202–207 (2015).
13. Gonzalez-Rey, E., Varela, N., Chorny, A. & Delgado, M. Therapeutical approaches of vasoactive intestinal peptide as a pleiotropic immunomodulator. *Curr. Pharm. Des.* **13,** 1113–1139 (2007).
14. Sherwood, N. M., Adams, B. A., Isaac, E. R., Wu, S. & Fradinger, E. A. Knocked down and out: PACAP in development, reproduction and feeding. *Peptides* **28,** 1680–1687 (2007).
15. Hashimoto, H. *et al.* Altered psychomotor behaviors in mice lacking pituitary adenylate cyclase-activating polypeptide (PACAP). *Proc. Natl Acad. Sci. USA* **98,** 13355–13360 (2001).
16. Reglodi, D. *et al.* PACAP is an endogenous protective factor-insights from PACAP-deficient mice. *J. Mol. Neurosci.* **48,** 482–492 (2012).
17. Elsas, T., Uddman, R. & Sundler, F. Pituitary adenylate cyclase-activating peptide-immunoreactive nerve fibers in the cat eye. *Graefes Arch. Clin. Exp. Ophthalmol.* **234,** 573–580 (1996).
18. Ishida, N., Hirai, S. I. & Mita, S. Immunolocalization of aquaporin homologs in mouse lacrimal glands. *Biochem. Biophys. Res. Commun.* **238,** 891–895 (1997).
19. Ishikawa, Y. *et al.* Identification of AQP5 in lipid rafts and its translocation to apical membranes by activation of M3 mAChRs in interlobular ducts of rat parotid gland. *Am. J. Physiol. Cell Physiol.* **289,** C1303–C1311 (2005).
20. Woo, J. *et al.* Membrane trafficking of AQP5 and cAMP dependent phosphorylation in bronchial epithelium. *Biochem. Biophys. Res. Commun.* **366,** 321–327 (2008).
21. Horsefield, R. *et al.* High-resolution x-ray structure of human aquaporin 5. *Proc. Natl Acad. Sci. USA* **105,** 13327–13332 (2008).
22. Truong, S., Cole, N., Stapleton, F. & Golebiowski, B. Sex hormones and the dry eye. *Clin. Exp. Optom.* **97,** 324–336 (2014).
23. Isaac, E. R. & Sherwood, N. M. Pituitary adenylate cyclase-activating polypeptide (PACAP) is important for embryo implantation in mice. *Mol. Cell Endocrinol.* **280,** 13–19 (2008).
24. Barabino, S. & Dana, M. R. Animal models of dry eye: a critical assessment of opportunities and limitations. *Invest. Ophthalmol. Vis. Sci.* **45,** 1641–1646 (2004).
25. Schrader, S., Mircheff, A. K. & Geerling, G. Animal models of dry eye. *Dev. Ophthalmol.* **41,** 298–312 (2008).
26. Castle, N. A. Aquaporins as targets for drug discovery. *Drug Discov. Today* **10,** 485–493 (2005).
27. Verkman, A. S. Role of aquaporin water channels in eye function. *Exp. Eye Res.* **76,** 137–143 (2003).
28. Tsubota, K., Hirai, S., King, L. S., Agre, P. & Ishida, N. Defective cellular trafficking of lacrimal gland aquaporin-5 in Sjogren's syndrome. *Lancet* **357,** 688–689 (2001).
29. Moore, M., Ma, T., Yang, B. & Verkman, A. S. Tear secretion by lacrimal glands in transgenic mice lacking water channels AQP1, AQP3, AQP4 and AQP5. *Exp. Eye Res.* **70,** 557–562 (2000).
30. Ruiz-Ederra, J., Levin, M. H. & Verkman, A. S. In situ fluorescence measurement of tear film $[Na+]$, $[K+]$, $[Cl-]$, and pH in mice shows marked hypertonicity in aquaporin-5 deficiency. *Invest. Ophthalmol. Vis. Sci.* **50,** 2132–2138 (2009).
31. Kosugi-Tanaka, C. *et al.* Protein kinase A-regulated membrane trafficking of a green fluorescent protein-aquaporin 5 chimera in MDCK cells. *Biochim. Biophys. Acta* **1763,** 337–344 (2006).
32. Yang, F., Kawedia, J. D. & Menon, A. G. Cyclic AMP regulates aquaporin 5 expression at both transcriptional and post-transcriptional levels through a protein kinase A pathway. *J. Biol. Chem.* **278,** 32173–32180 (2003).
33. Fushimi, K., Sasaki, S. & Marumo, F. Phosphorylation of serine 256 is required for cAMP-dependent regulatory exocytosis of the aquaporin-2 water channel. *J. Biol. Chem.* **272,** 14800–14804 (1997).
34. Nedvetsky, P. I. *et al.* Regulation of aquaporin-2 trafficking. *Handb. Exp. Pharmacol.* 133–157 (2009).
35. Gilbard, J. P., Rossi, S. R., Heyda, K. G. & Dartt, D. A. Stimulation of tear secretion by topical agents that increase cyclic nucleotide levels. *Invest. Ophthalmol. Vis. Sci.* **31,** 1381–1388 (1990).
36. Gilbard, J. P., Rossi, S. R., Heyda, K. G. & Dartt, D. A. Stimulation of tear secretion and treatment of dry-eye disease with 3-isobutyl-1-methylxanthine. *Arch. Ophthalmol.* **109,** 672–676 (1991).
37. Klenkler, B. & Sheardown, H. Growth factors in the anterior segment: role in tissue maintenance, wound healing and ocular pathology. *Exp. Eye Res.* **79,** 677–688 (2004).
38. Dartt, D. A. Neural regulation of lacrimal gland secretory processes: relevance in dry eye diseases. *Prog. Retin. Eye Res.* **28,** 155–177 (2009).
39. Gaal, V. *et al.* Investigation of the effects of PACAP on the composition of tear and endolymph proteins. *J. Mol. Neurosci.* **36,** 321–329 (2008).
40. Stern, M. E. *et al.* The pathology of dry eye: the interaction between the ocular surface and lacrimal glands. *Cornea* **17,** 584–589 (1998).
41. Takahashi, Y. *et al.* Anatomy of secretory glands in the eyelid and conjunctiva: a photographic review. *Ophthal. Plast. Reconstr. Surg.* **29,** 215–219 (2013).
42. Fosgerau, K. & Hoffmann, T. Peptide therapeutics: current status and future directions. *Drug Discov. Today* **20,** 122–128 (2015).
43. Nakamachi, T. *et al.* IL-6 and PACAP receptor expression and localization after global brain ischemia in mice. *J. Mol. Neurosci.* **48,** 518–525 (2012).
44. Suzuki, R. *et al.* Expression of the receptor for pituitary adenylate cyclase-activating polypeptide (PAC1-R) in reactive astrocytes. *Brain Res. Mol. Brain Res.* **115,** 10–20 (2003).
45. Roach, P. J., Laskin, J. & Laskin, A. Nanospray desorption electrospray ionization: an ambient method for liquid-extraction surface sampling in mass spectrometry. *Analyst* **135,** 2233–2236 (2010).
46. Lanekoff, I. *et al.* Automated platform for high-resolution tissue imaging using nanospray desorption electrospray ionization mass spectrometry. *Anal. Chem.* **84,** 8351–8356 (2012).
47. Lanekoff, I. *et al.* High-speed tandem mass spectrometric in situ imaging by nanospray desorption electrospray ionization mass spectrometry. *Anal. Chem.* **85,** 9596–9603 (2013).
48. Ohtaki, H. *et al.* Pituitary adenylate cyclase-activating polypeptide (PACAP) decreases ischemic neuronal cell death in association with IL-6. *Proc. Natl Acad. Sci. USA* **103,** 7488–7493 (2006).

Acknowledgements

We thank Dr Jerome L. Maderdrut for editorial assistance. In memory of Dr Akira Arimura, for his many helpful suggestions. This work was supported by JSPS KAKENHI Grant Numbers 24592680, 24592681, 23249079, 15K15670, 26293020, 26670122, 16H02684 and 15H01288); the JSPS Program for Advancing Strategic International Networks to Accelerate the Circulation of Talented Researchers, Grant no. S2603 (H.H.). Support was also received from the Hungarian Scientific Research Fund (OTKA, K104984, D.R., P.K., J.F., L.M.), the Lendulet Program, the Arimura Foundation, KTIA_NAP_13-1-2013-0001 (D.R.). PTE AOK KA 34039-2009, 2011, 2012-2013 13-18 (L.M.), VR 621-2013-4231 and SSF ICA-6 (I.L.).

Author contributions

T.N. designed and performed the experiments, evaluated the results, and wrote part of the manuscript. H.O. scored the corneal keratinization and performed the molecular biochemistry. T.S. provided valuable expert advice. N.K. performed the eye drop experiment. L.M., I.L., J.F., P.K. and D.R. performed the mass spectrometry experiment and wrote part of the manuscript. S.Y. performed the immunohistochemical experiment. H.H., N.S. and A.B. supplied the experimental material and edited the manuscript. S.S. designed and supervised the experiments and wrote the manuscript.

Additional information

Supplementary Information accompanies this paper at http://www.nature.com/naturecommunications

Competing financial interests: The authors declare no competing financial interests.

How to cite this article: Nakamachi, T. *et al.* PACAP suppresses dry eye signs by stimulating tear secretion. *Nat. Commun.* 7:12034 doi: 10.1038/ncomms12034 (2016).

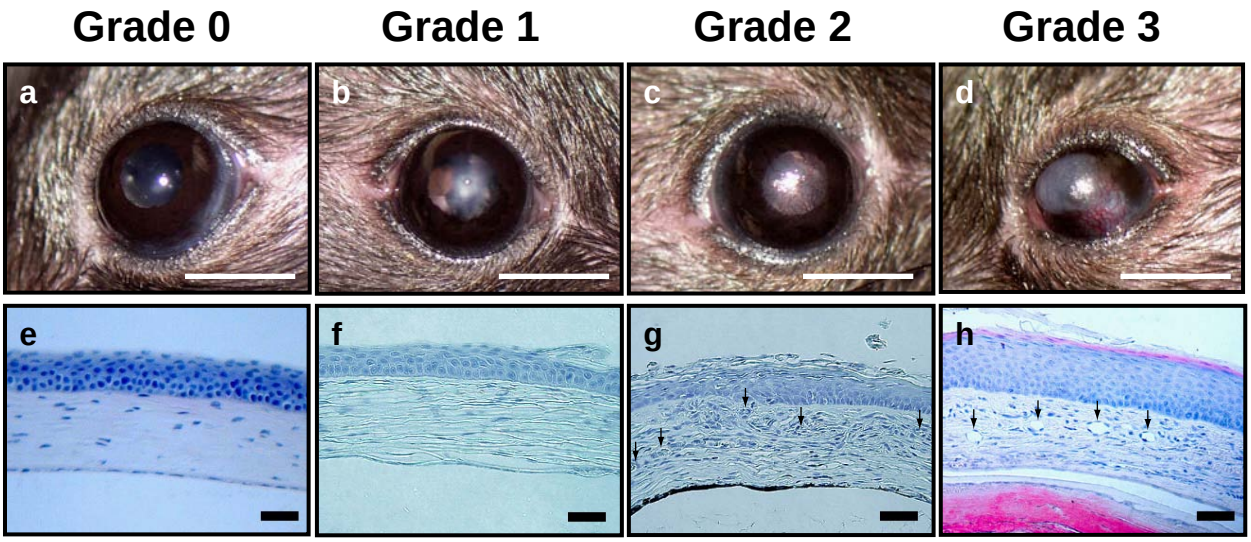

Supplementary Figure 1. Scale of corneal keratinization in mice. Low-power pictures of the corneal surface (**a-d**) and hematoxylin-eosin staining of the corneal surface (**e-f**) are shown. Keratinization of the cornea was classified into four grades (Grades 0-3) by visual observation as follows: (**a,e**) Grade 0 (normal) = no observable abnormality, (**b,f**) Grade 1 = clouded cornea caused by the irregularity of the substantia propia, (**c,g**) Grade 2 = angiogenesis in the substantia propia, and irregularities of the corneal surface, and (**d**,**h**) Grade 3 = hypertrophy of the corneal epithelium and keratinization. Scale bar, 2 mm in **a**-**d**, and 50 μm in **e**-**f**. Arrows indicate newly formed blood vessels.

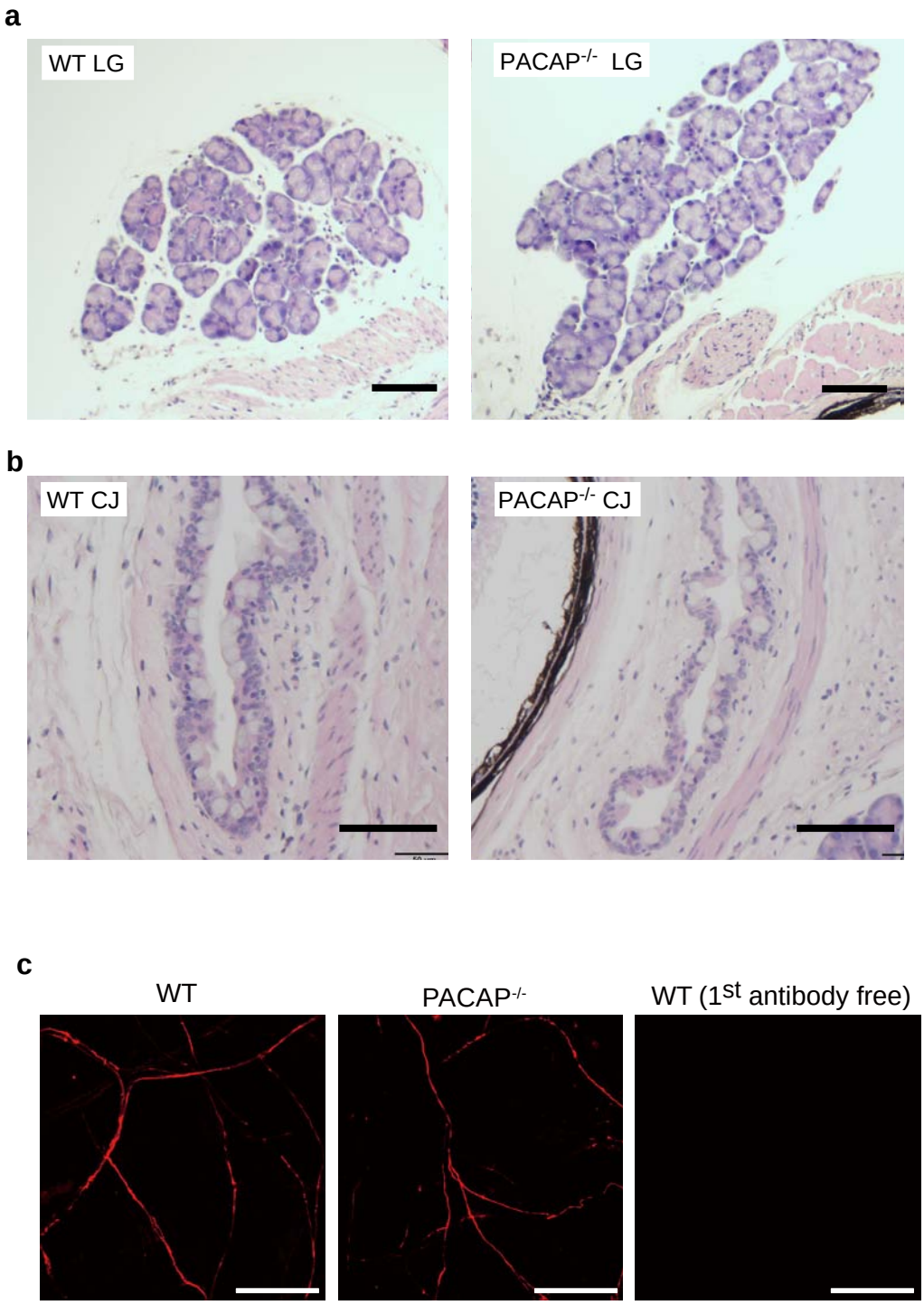

Supplementary Figure 2. Histological observation of lacrimal glands, conjunctival tissues and corneal nerve fibers in female wild-type and PACAP-/- mice. Representative pictures of the lacrimal glands (LG; **a**), conjunctival tissues (CJ; **b**) and Neurofilament 200 immunoreactivity on corneal flat mounts before the onset of keratinization (**c**) are shown. A wild-type cornea to which the primary antibody was not applied was used as a negative control. Scale bar, 50 μm in **a**, **b**, and 200 μm in **c**.

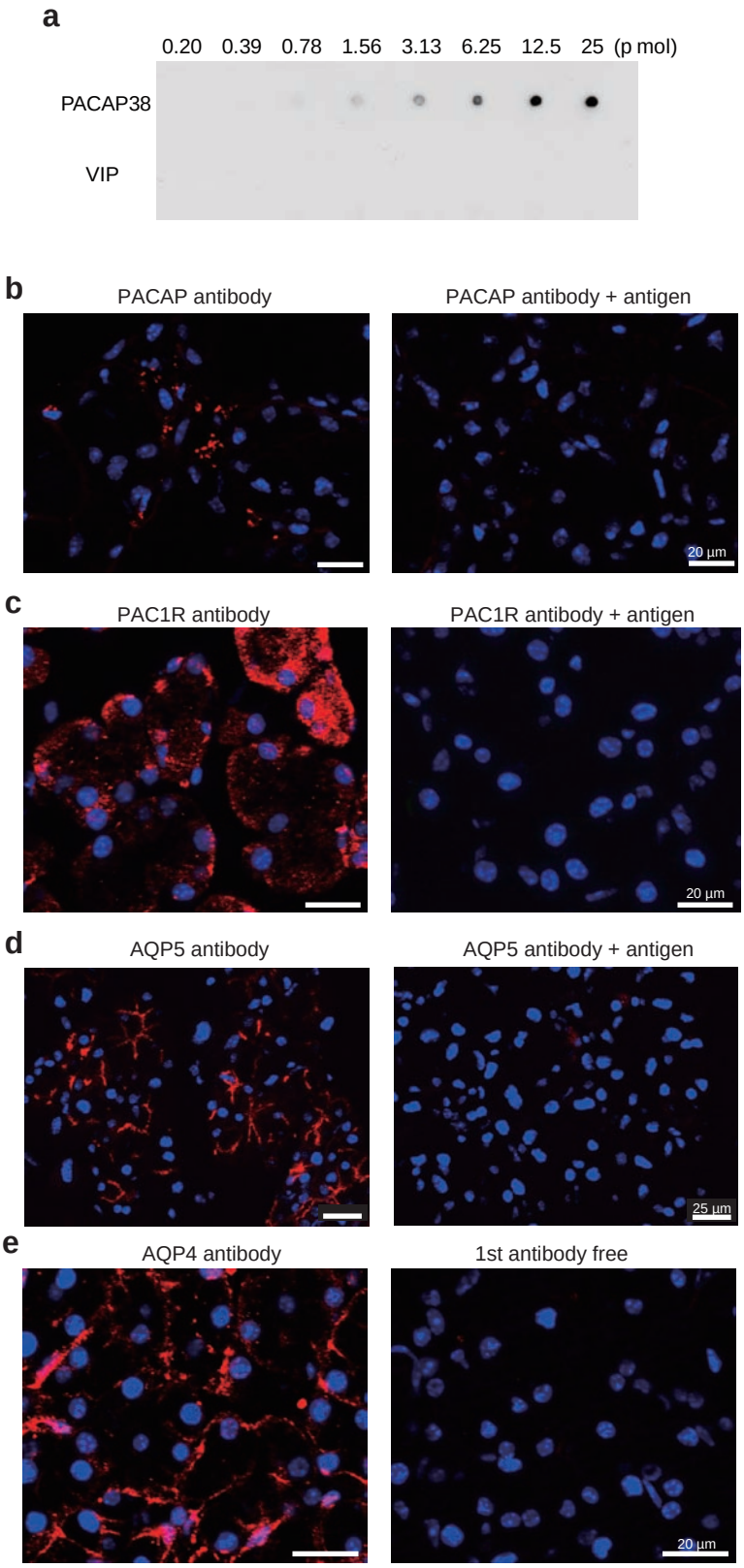

Supplementary Figure 3. Confirmation of the specificity of PACAP, PAC1-R, AQP5 and AQP4 antibodies. (**a**) Dot blotting analysis using PACAP antibody on a membrane treated with different doses of PACAP38 and VIP. (**b**-**d**) Antigen-absorption tests of PACAP, PAC1-R and AQP5 antibody on lacrimal gland section. (**e**) Comparison with AQP4 immunostaining and a primary antibody-free negative control. The same exposure times were used for the panels on the left and the right.

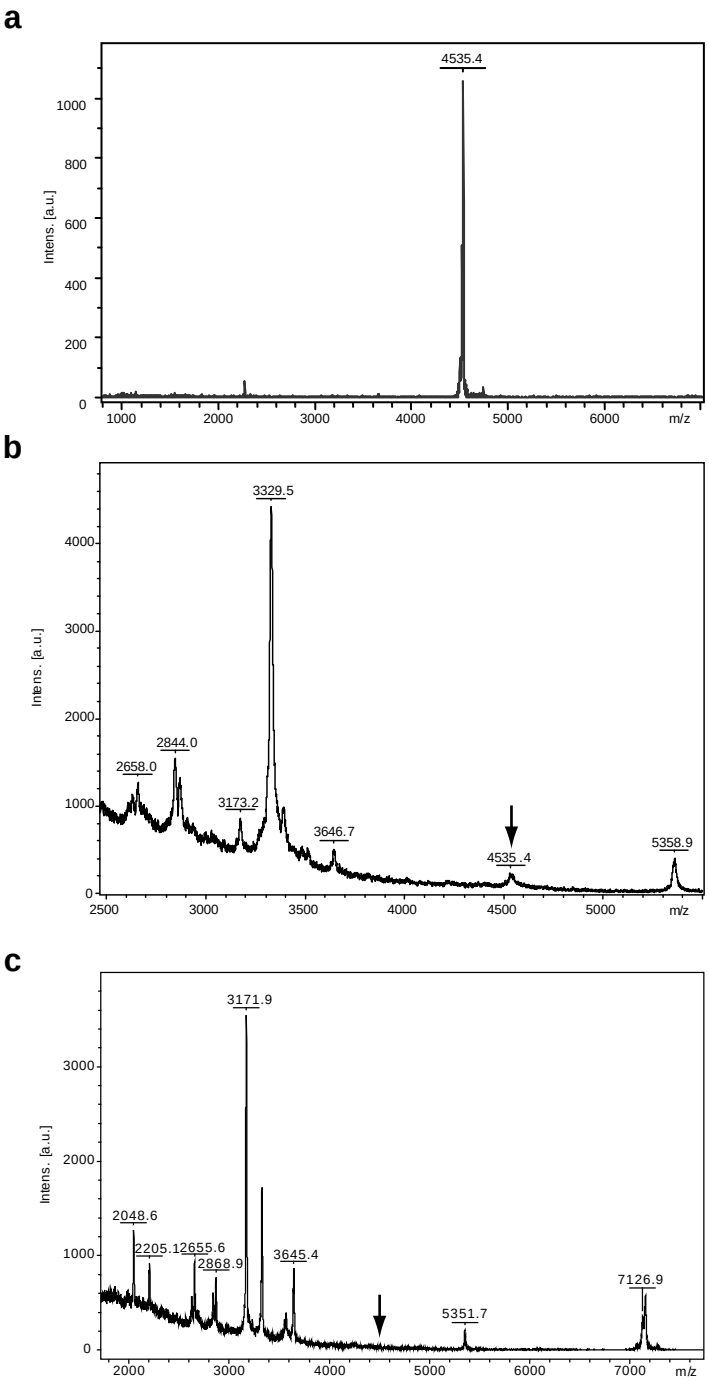

Supplementary Figure 4. MS spectrum analysis of mouse tears. (**a-c**) Typical MALDI TOF MS spectrum of the PACAP38 standard (**a**) and tears from wild-type (**b**) and PACAP-/- (**c**) mice. The position of the PACAP38 peptide peak (m/z 4535.4) is indicated by the black arrows in b and c.

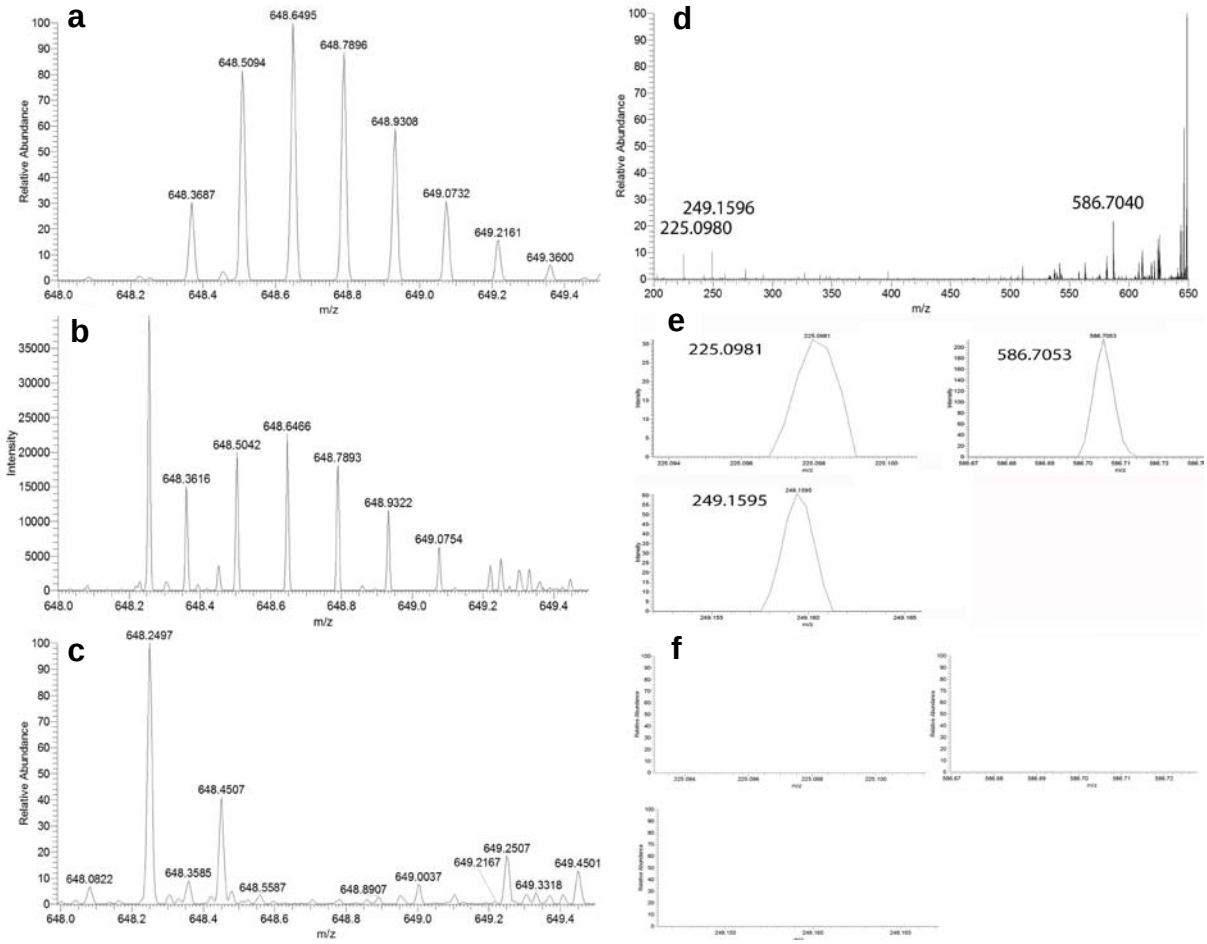

Supplementary Figure 5. Representative nano-DESI SIM spectra of 648.5 ±2 for (**a**) PACAP38 standard (z=7), (**b**) wild-type mouse sample, showing the peaks of PACAP38 and (**c**) PACAP-/- mouse sample without any peaks corresponding to PACAP38. The intensity of 100% relative abundance for the standard is 2.8e6 and 1.1e5 for the PACAP-/- mouse sample. Nano-DESI MS/MS spectra of 648.5 ±1 (precursor ion) for (**d**) PACAP38 standard with the m/z of the three most intense fragments annotated, (**e**) three mass spectra zoomed in to show the respective three fragments from the wild-type mouse sample and (**f**) three mass spectra showing the same m/z range as in **b** without any detected fragments for the PACAP-/- mouse sample.

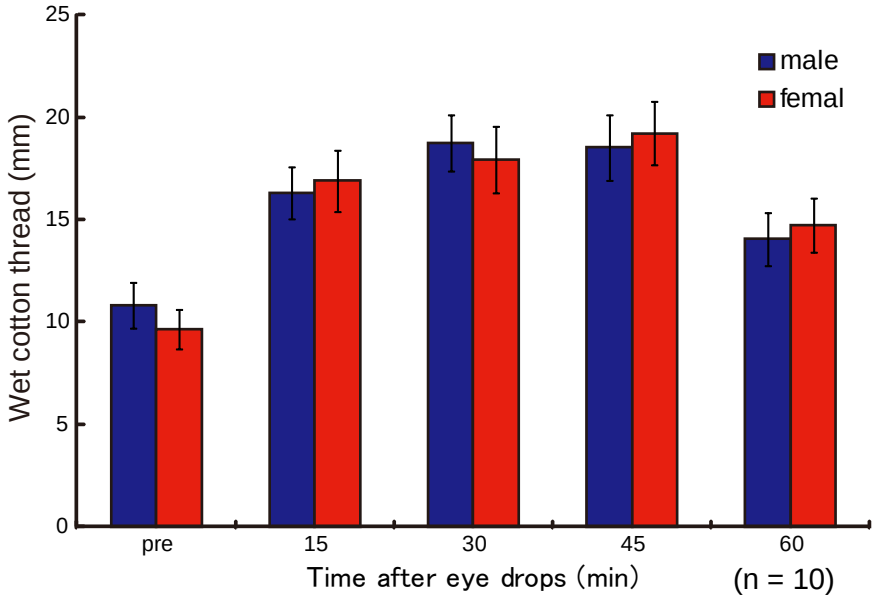

Supplementary Figure 6. PACAP eye drop test in male and female wild-type mice. PACAP (10^{-10} M) was administered in the form of eye drops, and the tear secretion level was measured using the cotton thread method. The basal tear secretion level and the PACAP-induced tear secretion level did not differ significantly between the male and female animals (one-way ANOVA).

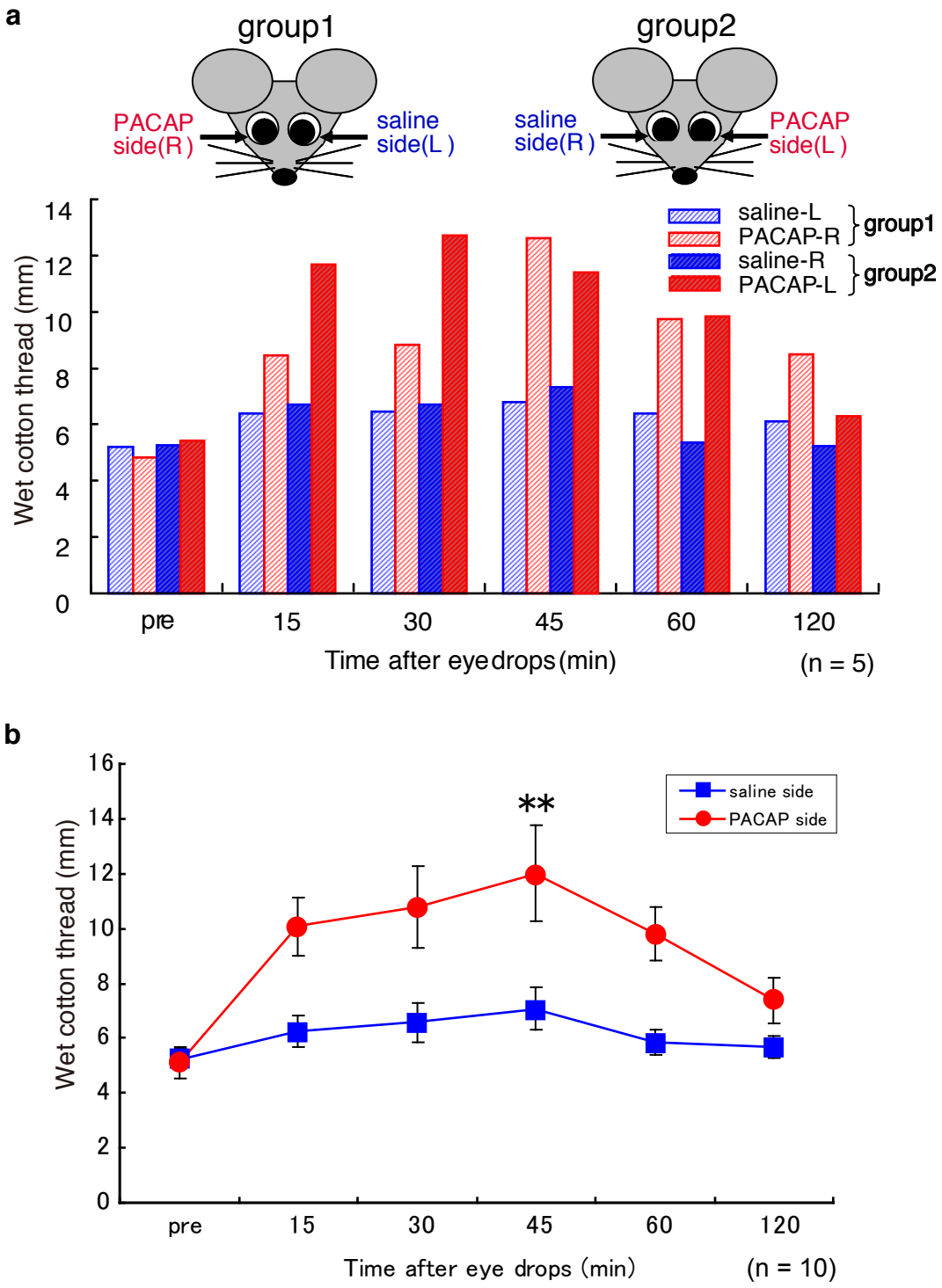

Supplementary Figure 7. Unilateral PACAP eye drop test in male wild-type mice. (**a**) Two groups were prepared. Group 1: PACAP38-treated right side and saline-treated left side; Group 2: saline-treated right side and PACAP38-treated left side (n = 5 per group). (**b**) Summary of both groups (n = 10 per side, one-way ANOVA). PACAP only induced tear secretion on the PACAP38-treated side.

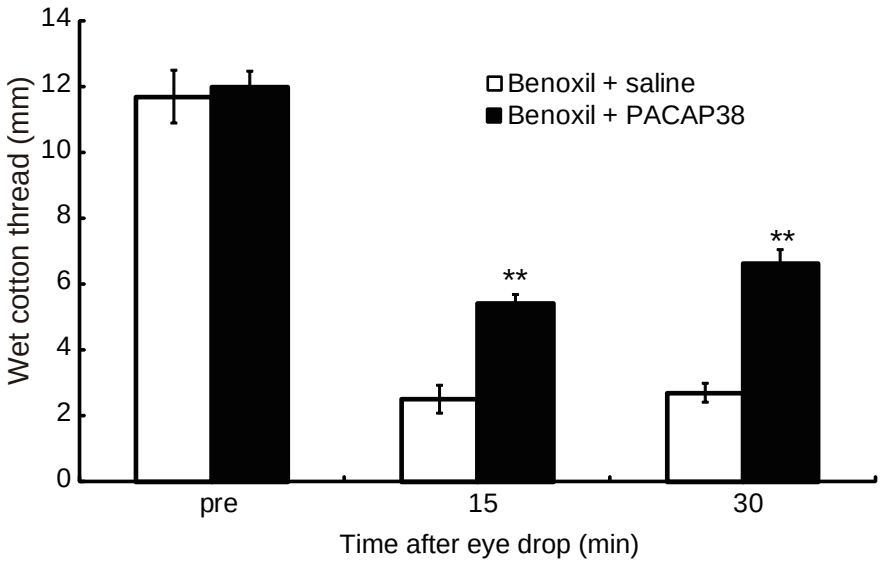

Supplementary Figure 8. Correlation between PACAP-induced tear secretion and corneal reflection. Following pre-treatment with the topical anesthetic, Benoxil, the tear secretion level with or without PACAP38 eye drops was examined in male wild-type mice (n = 10 per group, one-way ANOVA). **:P < 0.01 vs. the saline-treated group.

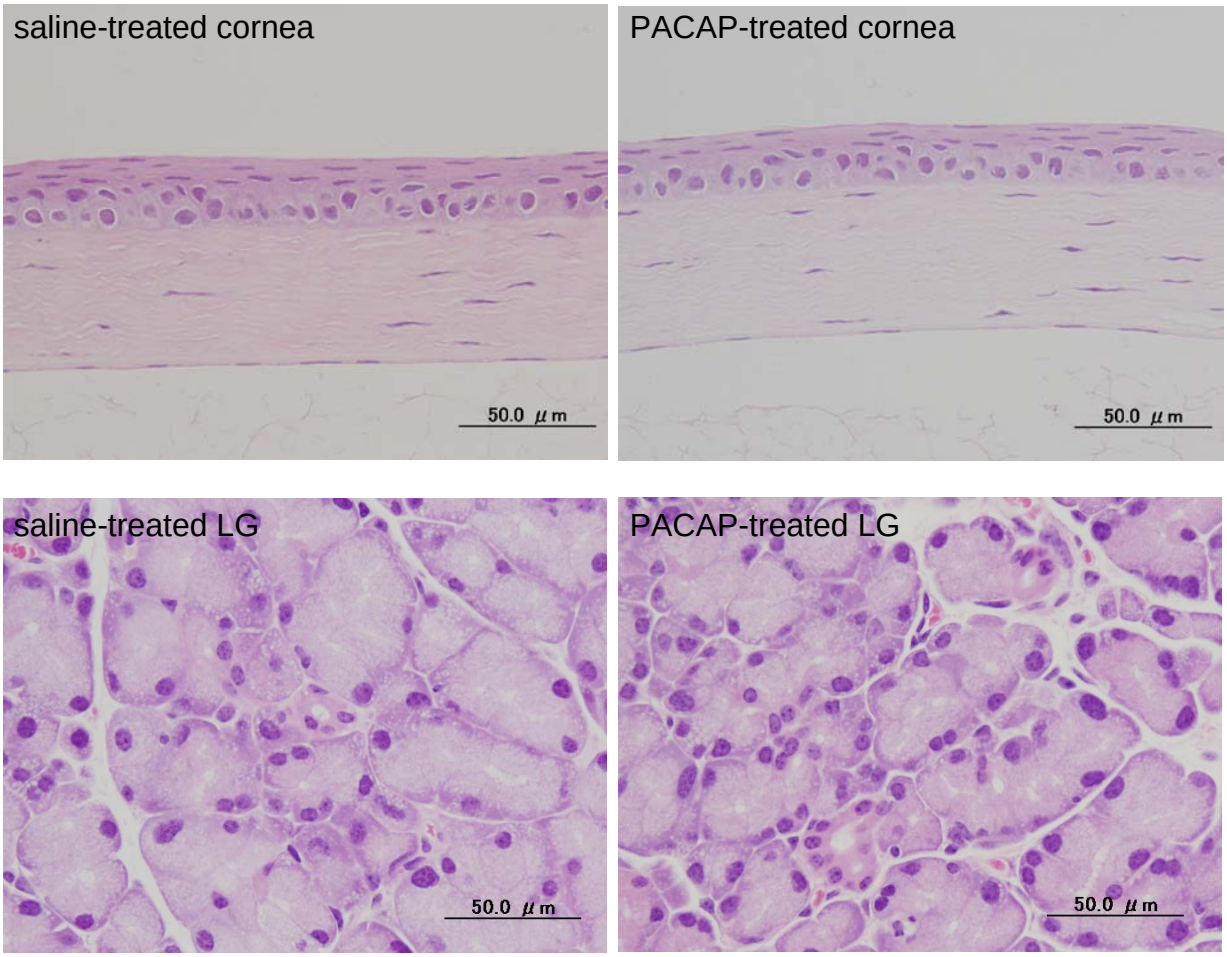

Supplementary Figure 9. Histopathological observation of the cornea and lacrimal gland after administration of PACAP eye drops. The cornea and lacrimal gland from a male wild-type mouse were examined 48 h after application of 10^{-7} M PACAP or saline eye drops. No pathological changes were observed.

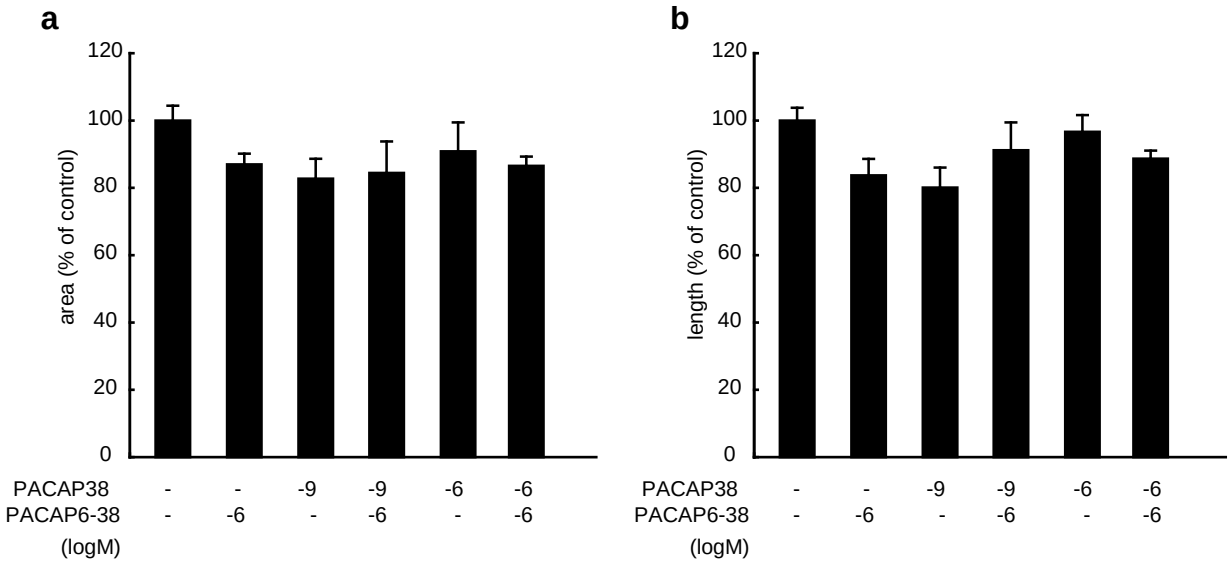

Supplementary Figure 10. Effect of PACAP on angiogenesis in vitro. Effect of PACAP and PACAP6-38 on tube formation by endothelial cells assessed with an angiogenesis kit using a human umbilical vein endothelial cell and fibroblast co-culture system. Administration of PACAP at 10^{-9} or 10^{-6} M with or without 10^{-6} M PACAP6-38 did not affect either the area of CD31-positive tubes (**a**) or the length of the CD31-positive tubes (**b**) in culture (n = 6 per group). There was no significant difference between the treatment groups (one-way ANOVA test)

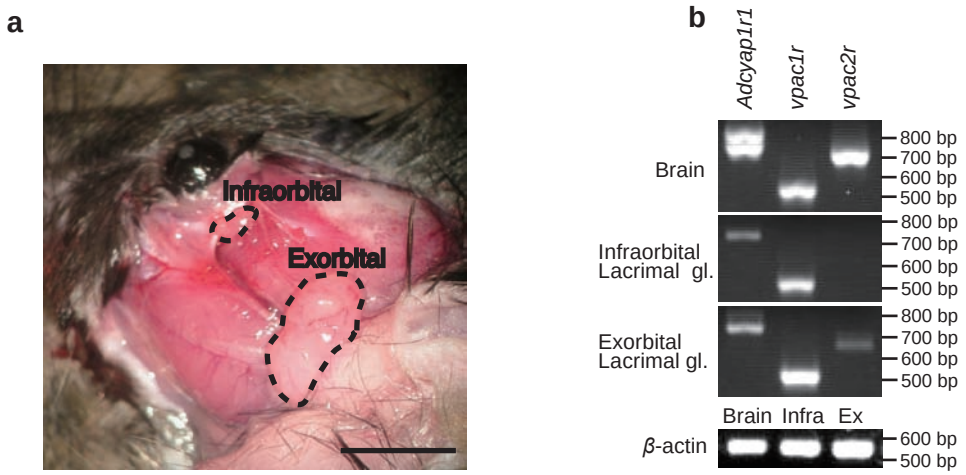

Supplementary Figure 11. Expression of PACAP receptors mRNA in infraorbital and/or exorbital lacrimal glands. (**a**) Macroscopic images of the infraorbital and exorbital lacrimal glands, in male mice. Scale bar, 5 mm. (**b**) PACAP receptor mRNA expression in the infraorbital and exorbital lacrimal glands detected by RT-PCR.

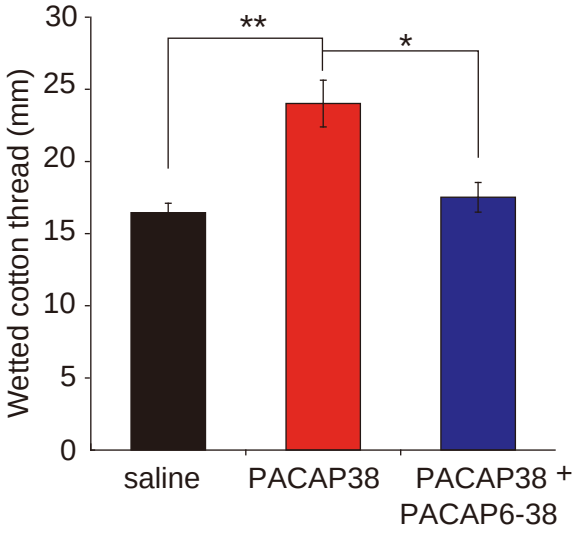

Supplementary Figure 12. Systemic infusion of PACAP38 in male wild-type mice. Effects of systemic injection of PACAP38 or PACAP38 with PACAP6-38 on tear secretion in mice (n = 6 per group, one-way ANOVA). *P < 0.05, **P < 0.01.

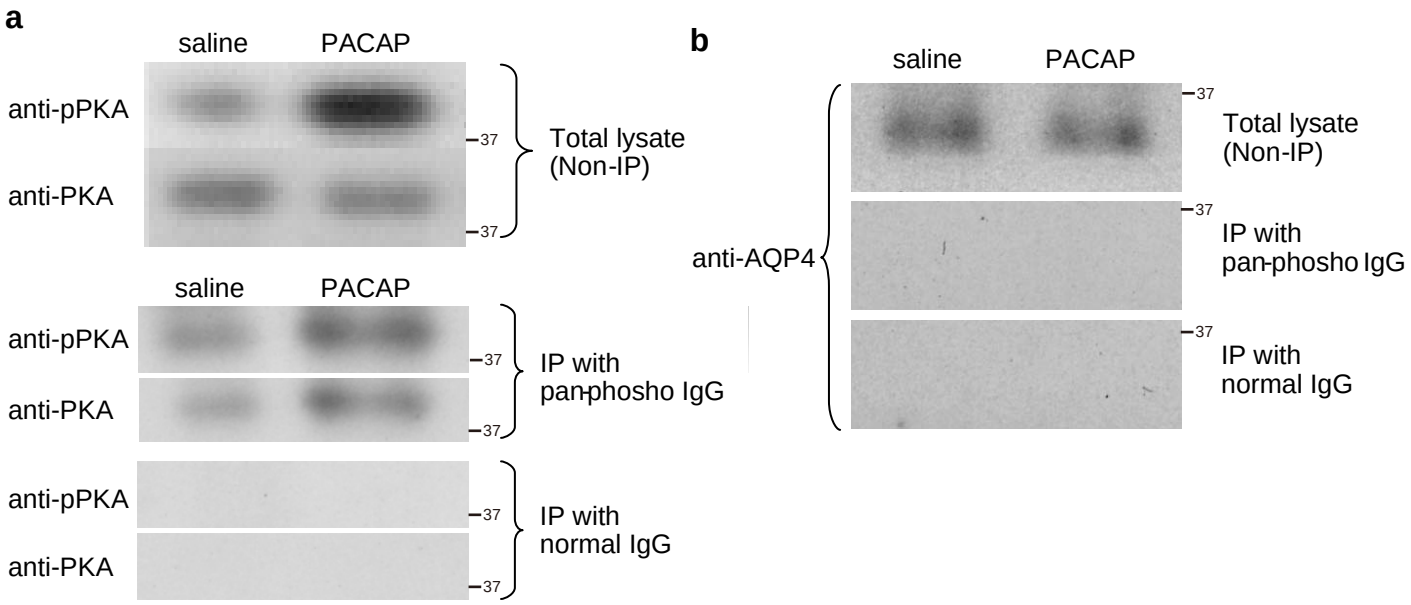

Supplementary Figure 13. Western blot analysis using saline- or PACAP-treated infraorbital lacrimal glands of male wild-type mice and an immunoprecipitation (IP) method. (**a**) Detection of PKA and pPKA with either an anti-PKA antibody with recognition for total PKA, including pPKA, or an anti-pPKA-specific antibody in the total lysate, or after IP with either a pan-phospho IgG or a normal IgG. The pPKA signal was increased in the total lysate from PACAP-treated lacrimal glands, but the total PKA signal did not appear to change. Both pPKA and total PKA signals were increased in the extracts from the PACAP-treated lacrimal glands that were immunoprecipitated with a pan-phospho IgG, but there was no detectable signal in any extract that was immunoprecipitated with a normal IgG. (**b**) Detection of AQP4 with an anti-AQP4 antibody in the total lysate, or after IP with either a pan-phospho IgG or a normal IgG. The AQP4 signals in the total lysate did not differ between saline- and PACAP-treated lacrimal glands. AQP4 signals were not detected after IP with either a pan-phospho IgG or a normal IgG.

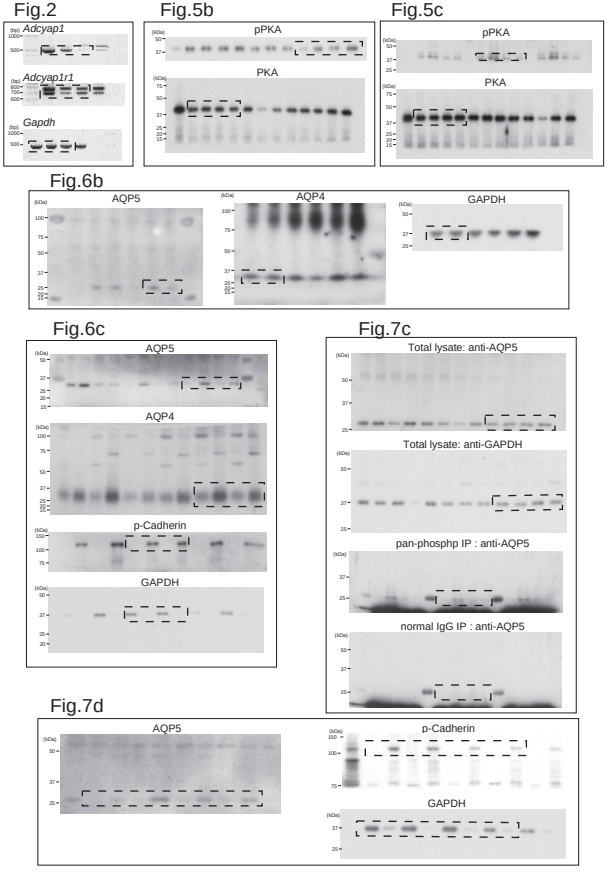

Suppremental Figure14. Uncropped images. Dashed boxes show cropped regions.

Supplementary Table 1. The sequences of mouse AQP5 and control siRNAs.

siRNA NAME	5'- Sequence -3'	Grade	MW
mAQP5#1	CCA UCG AG C UGA CGG CAC AdTdT	HPLC	6667.1
	UGU GCC GUC AGC UCG AUG GdTdT	HPLC	6678.1
mAQP5#2	GGA UGG GAU GGG AGC AGA AdTdT	HPLC	6891.3
	UUC UGC UCC CAU CCC AUC CdTdT	HPLC	6438.9
mAQP5#3	GCU CUU CAG GAG AGA GAU AdTdT	HPLC	6733.2
	UAU CUC UC U CCU GAA GAG CdTdT	HPLC	6567.0
Negative	UAC UAU UCG ACA CGC GAA GdTdT	HPLC	6653.1
control	CUU CGC GUG UCG AAU AGU AdTdT	HPLC	6647.1

Three types of mouse AQP5 siRNA and non-target negative control siRNAs were designed and purchased from BONAC Corporation.

Pituitary Adenylate Cyclase-Activating Polypeptide Enhances Saliva Secretion via Direct Binding to PACAP Receptors of Major Salivary Glands in Mice

YUKO MATOBA,[1,2] NAOKO NONAKA,[1,3] YOSHITOKI TAKAGI,[1] EISAKU IMAMURA,[1,2] MASAYUKI NARUKAWA,[1] TOMOYA NAKAMACHI,[4] SEIJI SHIODA,[5] WILLIAM A. BANKS,[3] AND MASANORI NAKAMURA[1]*

[1]Department of Oral Anatomy and Developmental Biology, Showa University School of Dentistry, Shinagawa-Ku, Tokyo, Japan

[2]Division of Oral Surgery, Yokohama General Hospital, Aoba-Ku, Yokohama, Japan

[3]Geriatrics Research Education and Clinical Center, Veterans Affairs Puget Sound Health Care System, Seattle, Washington, USA

[4]Laboratory of Regulatory Biology, Graduate School of Science and Engineering, University of Toyama, Japan

[5]Global Research Center for Innovative Life Science, Hoshi University, Shinagawa-Ku, Tokyo, Japan

ABSTRACT

Xerostomia, or dry mouth, is a common syndrome that is generally treated with artificial saliva; however, no other effective methods have yet been established. Saliva secretion is mainly under the control of the autonomic nervous system. Pituitary adenylate cyclase-activating polypeptide (PACAP) is recognized as a multifunctional neuropeptide in various organs. In this study, we examined the effect of PACAP on saliva secretion, and detected the distribution of the PACAP type 1 receptor (PAC1R) in major salivary glands, including the parotid, submandibular, and sublingual glands, in 9-week-old male C57BL/6 mice. Intranasal administration of PACAP 38 increased the amount of saliva secreted, which was not inhibited by atropine pretreatment. Immunohistochemical analysis showed that PAC1R was distributed in the three major salivary glands. In the parotid and sublingual glands, PAC1R was detected in striated duct cells, whereas in the submandibular gland, a strong PAC1R immunoreaction was detected in tall columnar epithelial cells in the granular ducts (i.e., pillar cells), as well as in some striated duct cells. PACAP significantly increased the concentration of epidermal growth factor in saliva. These results suggest that PACAP directly regulates saliva secretion by controlling the absorption activity in the ducts, and that pillar cells regulate the function of granular epithelial cells in the granular duct, such as the secretion of growth factors into the saliva. Collectively, these results suggest the possibility of PACAP as a new effective treatment of xerostomia. Anat Rec, 299:1293–1299, 2016. © 2016 Wiley Periodicals, Inc.

Grant sponsor: Grant-in-Aid for Scientific Research from the Ministry of Education, Culture, Sports, Science and Technology of Japan; Grant numbers: 20592148, 21592342, and 15K11022.

*Correspondence to: Masanori Nakamura, Department of Oral Anatomy and Developmental Biology, Showa University School of Dentistry, 1-5-8 Hatanodai, Shinagawa-ku, Tokyo 142-8555, Japan. Fax: +81-3-3785-8190. E-mail: masanaka@dent.showa-u.ac.jp

Received 10 November 2015; Revised 31 March 2016; Accepted 27 April 2016.

DOI 10.1002/ar.23388

Published online 24 June 2016 in Wiley Online Library (wileyonlinelibrary.com).

Key words: salivary gland; PACAP; PAC1R; pillar cell

Saliva has many biological functions such as the promotion of digestion, protection of the oral cavity, mastication, deglutition, taste, and insertion of dentures; hence, it is considered to be an essential component of human health (Pedersen et al., 2002; Llena-Puy, 2006; Mese and Matsuo, 2007; Furuta and Yamashita, 2013). In mammals, salivary glands are divided into the major and minor salivary glands (Amano et al., 2012). The major salivary glands include the parotid, submandibular, and sublingual glands.

Xerostomia, or dry mouth, is a symptom of oral dryness caused by a change in the composition of saliva or reduced saliva flow (van der Putten et al., 2011). This symptom is generally very common and is usually treated with artificial saliva. Secretion of saliva is regulated by several neuropeptides released from autonomic nerve endings (Proctor and Carpenter, 2007). Pituitary adenylate cyclase-activating polypeptide (PACAP) is a neuropeptide that belongs to the secretion/glucagon/vasoactive intestinal peptide (VIP) family (Arimura, 1992), and has shown potent neurotrophic and neuroprotective effects in several *in vivo* and *in vitro* models of brain injury (Arimura et al., 1994; Banks et al., 1996; Uchida et al., 1996; Nakamachi et al., 2011).

Furthermore, recent studies have indicated that PACAP also regulates the function of the exocrine glands. It has been hypothesized that PACAP functions in the sthenic secretion of tears in the lacrimal gland, and thus may be effective for treating dry eyes (Elsås et al., 1996; Gaal et al., 2008). Several studies also suggested that PACAP regulates saliva secretion, and demonstrated its anti-apoptotic effect in the salivary glands (Tobin et al., 1995; Mirfendereski et al., 1997; Kabré et al., 1998; Yanaihara et al., 2000; Kamaishi et al., 2004).

PACAP can interact with three subtypes of receptors: PAC1R and the VIP type I and II receptors. PAC1R is the preferred subtype for PACAP interaction, whereas the others are shared receptors between PACAP and VIP (Harmar et al., 1998). However, few studies have examined the exact location of these receptors in the salivary glands. Intranasal (i.n.) administration of neuropeptides is a safe and simple method. Given that PACAP was shown to enter tissues such as the brain via i.n. administration (Nonaka et al., 2005, 2012), in this study, we examined the effect of i.n. PACAP administration on salivation and investigated the exact localization of PAC1R in the major salivary glands in mice.

MATERIALS AND METHODS

Mice

The experimental protocols were reviewed and approved by the Animal Care Committee of Showa University. Thirty male C57BL/6 mice (aged 8 weeks) were purchased from Sankyo Laboratory Service Corporation (Tokyo, Japan) and maintained under normal conditions at the Laboratory Animal Center of Showa University for at least 7 days before the experiments. Five mice were used for histological and immunohistochemical analysis. The remaining 25 mice used for physiological and biochemical analysis were divided into 3 groups: a control group, a PACAP treatment group, and a PACAP plus atropin treatment group, as described in detail below.

Intranasal Administration of PACAP

The mice were bilaterally given an i.n. administration of 2 μL of saline solution containing 10^{-10} mol/mL PACAP38 (Sigma-Aldrich, St. Louis, MO) as described previously (Nonaka et al., 2005, 2012). The 2-μL solution was delivered to the nasal cavity by pushing a small cannula attached to a 10-μL syringe through the right and left nares (total volume: 4 μL/mouse).

Evaluation of Saliva Secretion

A cotton ball (3 mm in diameter) was prepared and weighed on an analytic electronic scale. The first cotton ball was inserted under the tongue of the mouse. Saliva secretion was then determined as the difference in the weight of the cotton ball before and after saliva collection. The procedure for saliva collection using the cotton ball was conducted at 1 and 2 hr after i.n. administration of PACAP. Control mice were given an i.n. administration of saline.

To inhibit the effect of the parasympathetic nervous system on saliva secretion, some mice were pretreated with an intraperitoneal injection of atropine (5 mg/kg body weight) before i.n. administration of PACAP.

Measurement of Epidermal Growth Factor (EGF) Content in Saliva

EGF levels in the saliva samples were measured by an enzyme-linked immunosorbent assay (ELISA) using the Mouse EGF Quantikine ELISA Kit (R&D Systems, Minneapolis, MN).

Histological and Immunohistochemical Analyses

The three major glands, the parotid, submandibular, and sublingual glands, were dissected after cervical dislocation. Specimens were cut into small pieces and fixed with 4% paraformaldehyde in phosphate-buffered saline (PBS) overnight at 4°C. After fixation, the specimens were immersed in 5, 15, and 30% sucrose, embedded in Tissue–Tek O.C.T Compound (Sakura Finetek USA, Torrance, CA), and quick-frozen in a mixture of acetone and dry ice.

Five-micrometer-thick frozen sections were air-dried for 60 min and rinsed in PBS. Some of the sections were stained with hematoxylin-eosin. For immunohistochemical detection of PAC1R, the other sections were incubated with rabbit anti-mouse PAC1R antibody (Nakamachi

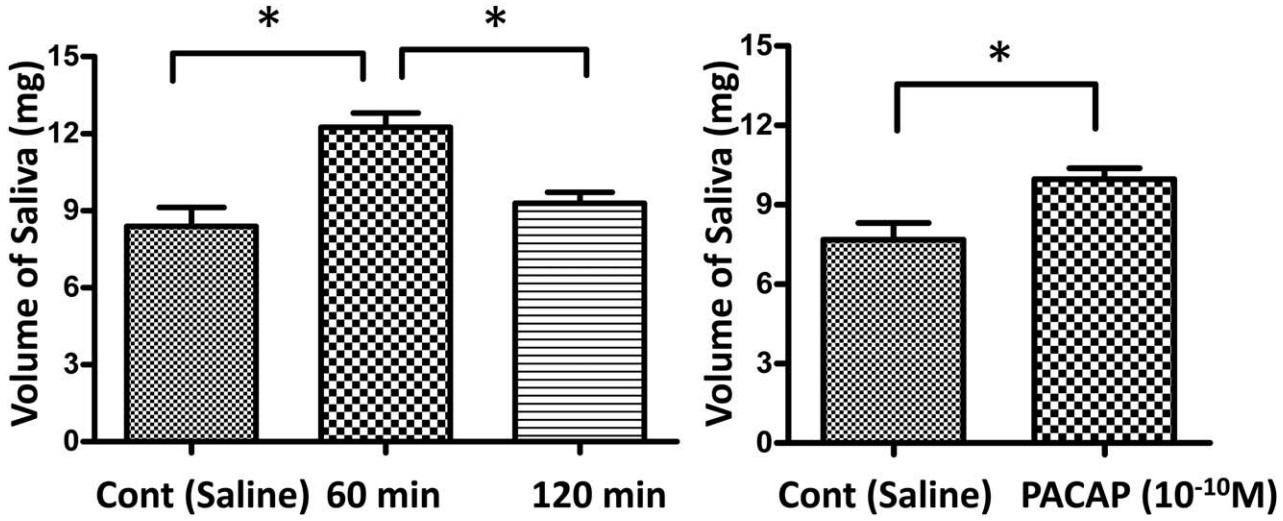

Fig. 1. Effect of PACAP on salivation. (**a**) A significant increase in salivation was induced at 60 min after intranasal administration of 4 μL of a saline solution containing 10^{-10} mol/mL PACAP38. (**b**) The effect of PACAP was not inhibited by atropine pretreatment. *$P < 0.01$.

et al., 2008) overnight at 4°C after being treated with 0.3% H_2O_2 in methanol for 30 min and then with 5% normal goat serum in PBS containing 5% bovine serum albumin and 0.025% Triton X-100. After washing with PBS, the sections were incubated with goat anti-rabbit IgG antibody (Vector Laboratories, Burlingame, CA), followed by an avidin-biotin-horseradish peroxidase complex (Vector Laboratories). After washing, the sections were further incubated with a mixture of the DAB detection kit (KPL, Gaithersburg, MD). Counterstaining was conducted using methyl green. For control experiments, the first antibody was pretreated with an excess of PACAP 38 before application to the sections.

Ultrastructural Analysis

Specimens were fixed with a mixture of 2% paraformaldehyde and 2.5% glutaraldehyde in 0.1 M sodium cacodylate buffer, post-fixed in 2% osmium tetroxide, dehydrated using a graded series of ethanol, passed through propylene oxide, and embedded in EPON 812 (TAAB, Berks, UK). Ultra-thin sections were stained with uranyl acetate and lead citrate.

Statistical Analyses

Statistical significance was evaluated using the Student's unpaired *t*-test, where P values < 0.01 were considered significant.

RESULTS

Effect of PACAP on Saliva Secretion

Intranasal administration of PACAP significantly increased saliva secretion at 1 hr, which then returned to basal levels at 2 hr after the treatment (Fig. 1a). The PACAP-induced enhancement of saliva secretion was not inhibited by the pretreatment with atropine (Fig. 1b).

Immunohistochemical Localization of PAC1R in the Major Salivary Glands in Mice

Parotid gland. The parotid gland is a pure serous gland that consists of acini and intercalated, striated, and collecting ducts. The acini were very small, consisting of 3–4 tall pyramidal cells with a strongly basophilic cytoplasm, and had basally located, large, spherical nuclei. The intercalated ducts were short and narrow and lined by low cuboidal cells with large central nuclei (Fig. 2a,b).

Immunohistochemically, striated cells showed a strong immunoreaction to PAC1R; however, no intense immunoreactions were identified in the intercalated ducts (Fig. 2c).

Sublingual gland. The sublingual gland is a small and compact mucous gland that consists of acini and intercalated, striated, and collecting ducts (Fig. 2d). The mucous cells were cuboidal or columnar basally in the cytoplasm, and the nuclei were flattened and pressed to be basal in the cytoplasm (Fig. 2d,e). The intercalated ducts were short and narrow and lined by a low cuboidal epithelium. The main excretory duct was lined by a stratified columnar epithelium.

Immunohistochemical localization of PAC1R was detected in the striated duct cells. A weak reaction was also detected in the intercalated duct cells (Fig. 2f).

Submandibular gland. The mouse submandibular gland is a pure serous gland, characterized by the presence of granular ducts, which were located between the intercalated and striated ducts (Fig. 2g). The granular ducts display sexual dimorphism, and is well developed in male than in female mice. The acini contained tall pyramidal cells with a pale basophilic cytoplasm and central nuclei (Fig. 2g,h).

Immunoreaction of PAC1R was detected in cells in the granular ducts (Fig. 2i). These immunopositive cells showed a columnar shape, which is referred to as pillar

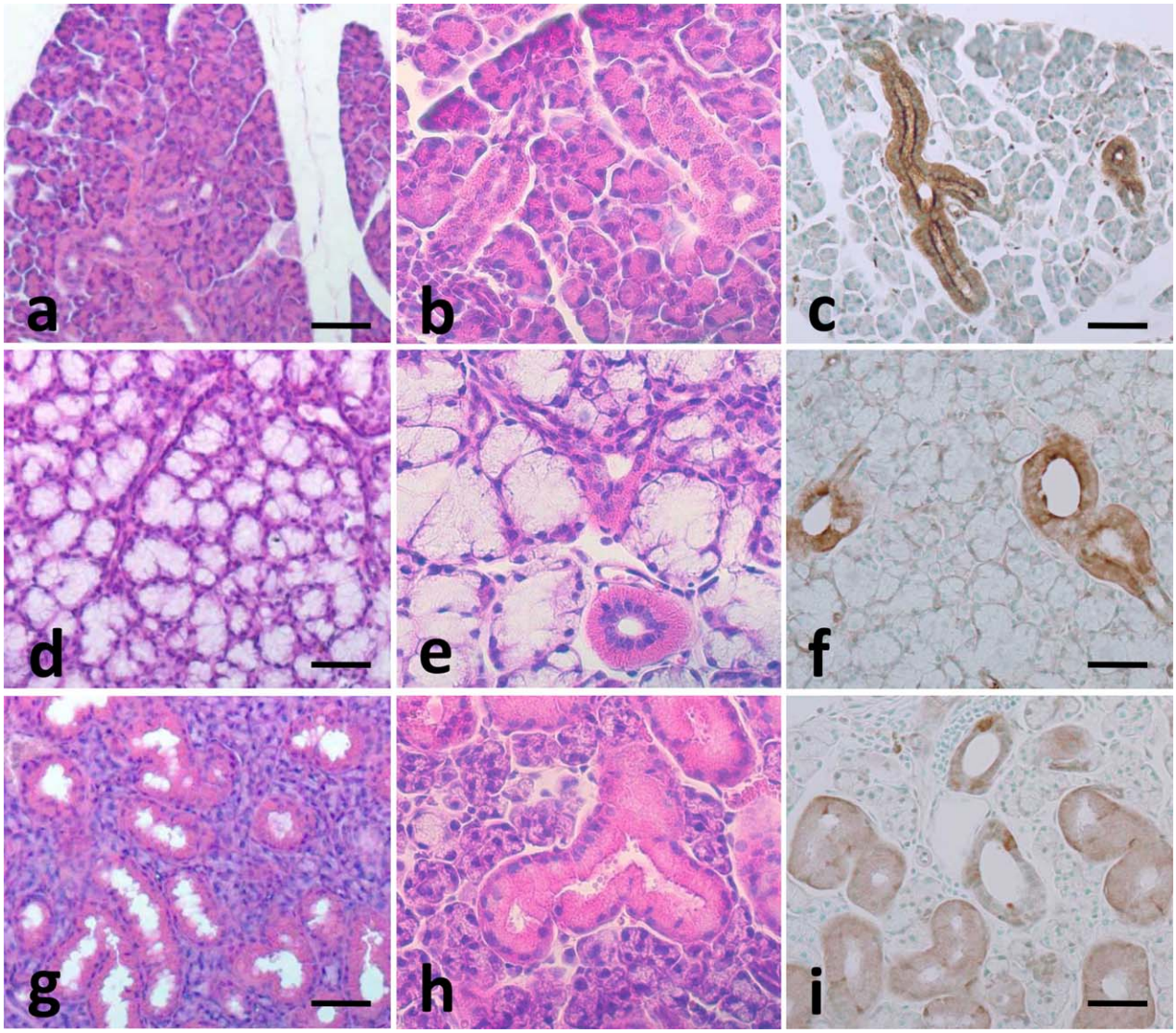

Fig. 2. Histological structure (**a**, **b**, **d**, **e**, **g**, **h**) and immunohistochemical localization of PAC1R (**c**, **f**, **i**). (a, b, c) The parotid gland contained serous acini, and PAC1R was expressed in the striated ducts. (d, e, f) Most of the acini of the sublingual gland were comprised of mucous cells. PAC1R-expressing cells were localized in the striated ducts. (g, h, i) The submandibular gland contained well-developed granular ducts. PAC1R was expressed in the striated duct. Bars = 50 μm.

cells (Fig. 3a). Some of the cells in the striated ducts also showed PAC1R-positive staining (Fig. 2i).

Absorption Control

No immunoreaction of PAC1R was observed in any of the three major salivary glands in the control samples.

Ultrastructure of Pillar Cells in the Granular Ducts

Ultrastructural observations indicated that the pillar cells had an oblong shape and microvilli extending to the apical lumen (Fig. 3b). The cells did not contain any developed secretory granules in the cytoplasm (Fig. 3b).

PACAP-Mediated Changes in the Salivary Content of EGF

PACAP treatment significantly increased the level of EGF in the saliva (Fig. 4), from a control level of 53.67 ± 4.256 to 97.33 ± 16.38 μg/mg following i.n. administration of PACAP.

DISCUSSION

In this study, we intranasally administered PACAP to mice to evaluate the effects on saliva secretion and the potential underlying mechanism with the ultimate aim of developing a new potential target for xerostomia treatment. Intranasal administration is a noninvasive route for drug delivery and is widely used for the local treatment of rhinitis or nasal polyposis. Since drugs can

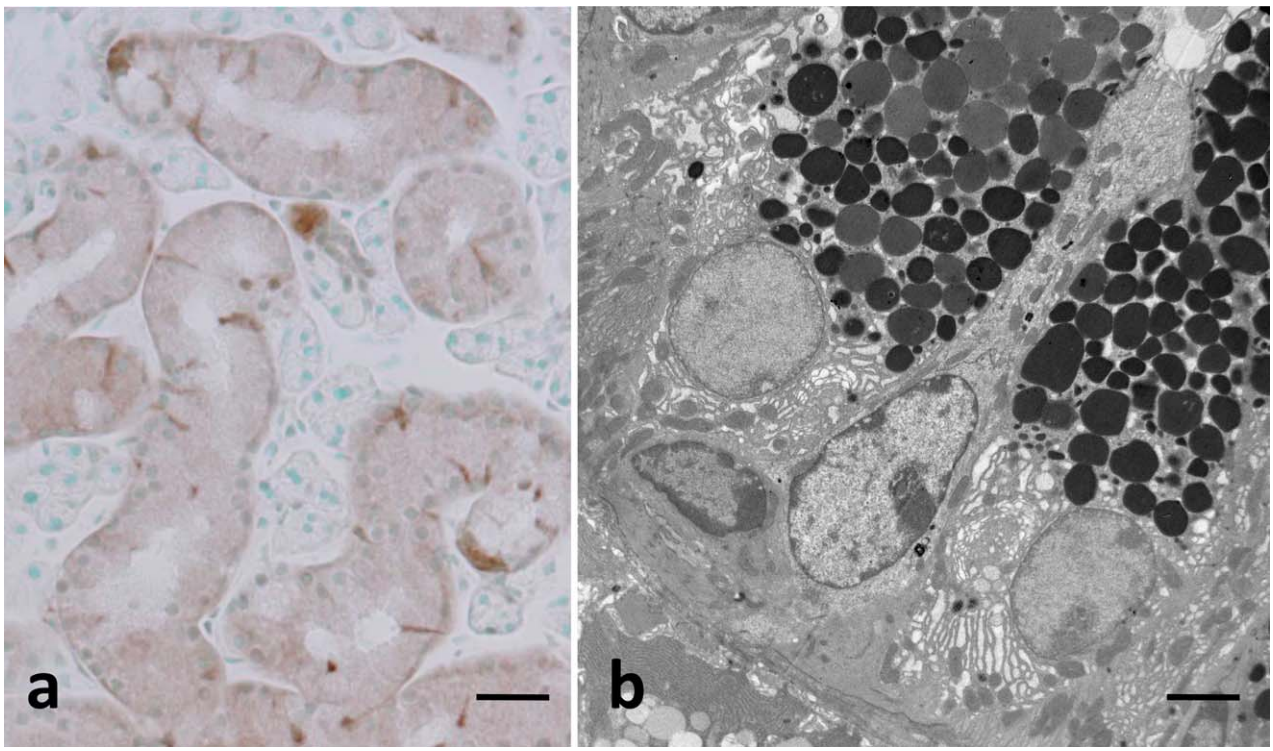

Fig. 3. Immunohistochemical and transmission electron micrographs of pillar cells in granular ducts. (**a**) Immunohistochemical localization of PAC1R. Strong reactions were detected in the pillar cells. Bar = 25 μm. (**b**) Pillar cells contained no secretory granules in the cytoplasm. Bar = 2 μm.

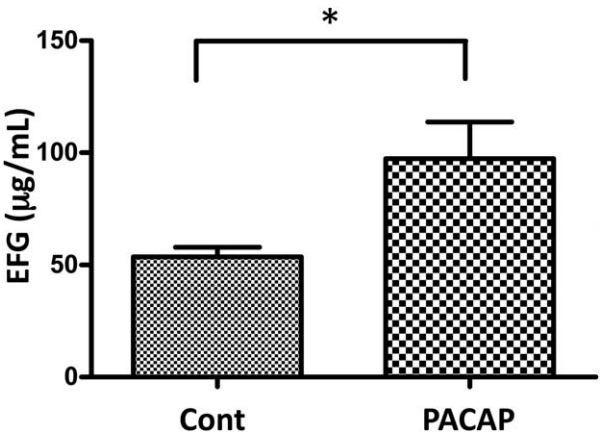

Fig. 4. Effect of PACAP on EGF concentration in the saliva. PACAP treatment increased the EGF concentration at 60 min after intranasal administration of a 4 μL of saline solution containing 10^{-10} mol/mL PACAP38.

be absorbed into the systemic circulation through the nasal mucosa, this route may also be used for treatments of a wide range of acute or chronic conditions requiring considerable systemic exposure (Grassin-Delyle et al., 2012). Indeed, our previous study indicated that PACAP was infused into the brain and peripheral blood following nasal administration (Nonaka et al., 2012).

In this study, PACAP enhanced saliva secretion, supporting previous reports (Tobin et al., 1995; Mirfendereski et al., 1997; Kabré et al., 1998; Yanaihara et al., 2000; Kamaishi et al., 2004). The PACAP-induced enhancement of saliva secretion was not inhibited by pretreatment with atropine, demonstrating that PACAP directly influences the salivary glands. Our preliminary experiment using PACAP labeled with ^{131}I showed the direct accumulation of labeled PACAP in the three major mouse salivary glands following i.n. administration. These results strongly suggested the presence of PAC1R in the salivary glands.

Immunoreactions of PAC1R were mainly detected in the striated duct cells in all salivary glands. It has been reported that neuropeptides stimulate saliva secretion via myoepithelial cell contraction (Ferreira and Hoffman, 2013). In this study, strong immunoreaction of PAC1R was detected in the striated ducts of the parotid and sublingual glands. Therefore, the PACAP-induced increase in the amount of secreted saliva may have been caused not by enhancement of saliva secretion in the acinar cells but rather by inhibition of saliva resorption in the striated ducts.

In the submandibular gland of mice, the granular duct is located between the striated duct and intercalated duct. Furthermore, granular epithelial cells in the granular ducts contain growth factors in their granules (Gresik and Azmitia, 1980; Miyagi et al., 2006). Several studies have suggested that growth factors in the saliva play important roles in homeostasis and wound healing of the mucosa (Marcinkiewicz et al., 1998; Eckley et al.,

2013). In particular, EGF in the saliva has been suggested to induce epithelial regeneration after physical and chemical aggression (Noguchi et al., 1991; Marcinkiewicz et al., 1998; Ohshima et al., 2002).

Strong immunoreactions of PAC1R were observed in the granular ducts, and PAC1R-positive cells were scattered throughout granular ducts; based on their morphology, these cells are commonly known as pillar cells or dark cells (Amano et al., 1993; Mori et al., 1998; Sato and Miyoshi, 1998; Ishii et al., 2005; Amano et al., 2012). A previous ultrastructural study indicated that these cells do not contain well-developed secretory granules but do contain basic fibroblast growth factor in the cytoplasm (Amano et al., 1993); however, their exact function is not known. Mori et al. (1998) determined the expression of S100A1 in the pillar cells and suggested the involvement of these cells in the secretion of secretory granules from granular cells in the granular ducts. In this study, we observed an increased concentration of EGF in the saliva following PACAP treatment. These results suggest that pillar cells stimulated the secretion of EGF from granular cells. However, further studies are needed to examine the precise role of pillar cells in salivation.

Immunopositivity for PAC1R in striated duct of submandibular glands was weaker than that in the parotid and sublingual glands. In this study, we could not measure the amount of saliva from each gland. Submandibular gland is the largest gland in mouse three major salivary glands. Compared to the size of each gland, the increase of saliva secretion seemed to be insufficient. The main function of PACAP in submandibular gland might be the regulation of growth factor secretion not the inhibition of saliva resorption. In this study, some of the cells in striated duct of submandibular gland showed strongly expressed PAC1R. Sato and Miyoshi (1998) showed the dark or pillar cells in striated duct of submandibular gland. Therefore, these immunopositive cells might the precursor of pillar cells. Further ontogenic study is necessary for the development of pillar cells.

The PACAP-induced enhancement of saliva secretion returned to normal levels at 2 hr after the treatment. Neuropeptides such as VIP and calcitonin gene-related peptide also stimulate saliva secretion (Ekström and Ekman, 2005). Recently, cyclodextrin (CD) has also been used as a carrier in a drug delivery system (Challa et al., 2005). Indeed, we reported the effectiveness of CD for the rapid tissue penetration of neuropeptides. Furthermore, the amount of neuropeptides in the tissue differed depending on the specific type of CD used (Nonaka et al., 2012). Therefore, the combination of PACAP, other neuropeptides, and CD might be an effective strategy for the treatment of xerostomia.

In this study, immunoreaction of PAC1R was not restricted on cell membrane. Previous studies also demonstrated the intracellular localization of PAC1R (Anderson et al., 2005; Nakamachi et al., 2008; Fahrenkrug and Hannibal, 2011). It has been demonstrated that PAC1R was rapidly internalized into the cytoplasm (Germano et al., 2001). To clearly show the localization of PAC1R on cell membrane, Merriam et al. (2013) treated the culture cells with Pitspot 2 to inhibit the receptor internalization.

In conclusion, PACAP regulates salivation and the levels of salivary components by directly binding to PAC1R, which is expressed in the striated ducts and pillar cells. Collectively, our results demonstrate the potential effectiveness of using PACAP for treating xerostomia.

LITERATURE CITED

Amano O, Mizobe K, Bando Y, Sakiyama K. 2012. Anatomy and histology of rodent and human major salivary glands. Acta Histochem Cytochem 45:241–250.

Amano O, Yoshitake Y, Nishikawa K, Iseki S. 1993. Basic fibroblast growth factor in rat salivary glands. Cell Tissue Res 273:467–474.

Anderson ST, Kusters DH, Clarke IJ, Pow DV, Curlewis JD. 2005. Expression of pituitary adenylate cyclase activating polypeptide type 1 receptor (PAC1R) in the ewe hypothalamus: distribution and colocalization with tyrosine hydroxylase-immunoreactive neurones. J Neuroendocrinol 17:298–305.

Arimura A. 1992. Pituitary adenylate cyclase activating polypeptide (PACAP): discovery and current status of research. Regul Pept 37:287–303.

Arimura A, Somogyvari-Vigh A, Weill C, Fiore RC, Tatsuno I, Bay V, Brenneman DE. 1994. PACAP functions as a neurotrophic factor. Ann N Y Acad Sci 739:228–243.

Banks WA, Uchida D, Arimura A, Somogyvari-Vigh A, Shioda S. 1996. Transport of pituitary adenylate cyclase-activating polypeptide across the blood–brain barrier and the prevention of ischemia-induced death of hippocampal neurons. Ann NY Acad Sci 805:270–277.

Challa R, Ahuja A, Ali J, Khar RK. 2005. Cyclodextrins in drug delivery: an updated review. AAPS PharmSciTech 6:E329–E357.

Eckley CA, Sardinha LR, Rizzo LV. 2013. Salivary concentration of epidermal growth factor in adults with reflux laryngitis before and after treatment. Ann Otol Rhinol Laryngol 122:440–444.

Elsås T, Uddman R, Sundler F. 1996. Pituitary adenylate cyclase-activating peptide-immunoreactive nerve fibers in the cat eye. Graefes Arch Clin Exp Ophthalmol 234:573–580.

Ekström J, Ekman R. 2005. Sympathectomy-induced increases in calcitonin gene-related peptide (CGRP)-, substance P- and vasoactive intestinal peptide (VIP)-levels in parotid and submandibular glands of the rat. Arch Oral Biol 50:909–917.

Fahrenkrug J, Hannibal J. 2011. Localisation of the neuropeptide PACAP and its receptors in the rat parathyroid and thyroid glands. Gen Comp Endocr 171:105–113.

Ferreira JN, Hoffman MP. 2013. Interactions between developing nerves and salivary glands. Organogenesis 9:199–205.

Furuta M, Yamashita Y. 2013. Oral health and swallowing problems. Curr Phys Med Rehabil Rep 1:216–222.

Gaal V, Mark L, Kiss P, Kustos I, Tamas A, Kocsis B, Lubics A, Nemeth V, Nemeth A, Lujber L, Pytel J, Toth G, Reglodi D. 2008. Investigation of the effects of PACAP on the composition of tear and endolymph proteins. J Mol Neurosci 36:321–329.

Germano PM, Stalter J, Le SV, Wu M, Yamaguchi DJ, Scott D, Pisegna JR. 2001. Characterization of the pharmacology, signal transduction and internalization of the fluorescent PACAP ligand, fluor-PACAP, on NIH/3T3 cells expressing PAC1. Peptides 22: 861–866.

Grassin-Delyle S, Buenestado A, Naline E, Faisy C, Blouquit-Laye S, Couderc LJ, Le Guen M, Fischler M, Devillier P. 2012. Intranasal drug delivery: an efficient and non-invasive route for systemic administration: focus on opioids. Pharmacol Ther 134:366–379.

Gresik EW, Azmitia EC. 1980. Age related changes in NGF, EGF and protease in the granular convoluted tubules of the mouse submandibular gland. A morphological and immunohistochemical study. J Gerontol 35:520–524.

Harmar AJ, Arimura A, Gozes I, Journot L, Laburthe M, Pisegna JR, Rawlings SR, Robberecht P, Said SI, Sreedharan SP, Wank SA, Waschek JA. 1998. International Union of Pharmacology. XVIII. Nomenclature of receptors for vasoactive intestinal peptide and pituitary adenylate cyclase-activating polypeptide. Pharmacol Rev 50:265–270.

Ishii K, Tsubaki T, Fujita K, Ishigami A, Maruyama N, Akita M. 2005. Immunohistochemical localization of senescence marker

protein-30 (SMP30) in the submandibular gland and ultrastructural changes of the granular duct cells in SMP30 knockout mice. Histol Histopathol 20:761–768.

Kabré E, Chaib N, Amsallem H, Moran A, Vandermeers C, Dehaye JP. 1998. Effect of PACAP-27 on adenylate cyclase in ductal and acinar cells of rat submandibular gland. Ann NY Acad Sci 865: 431–437.

Kamaishi H, Endoh T, Suzuki T. 2004. Multiple signal pathways coupling VIP and PACAP receptors to calcium channels in hamster submandibular ganglion neurons. Auton Neurosci 111:15–26.

Llena-Puy C. 2006. The role of saliva in maintaining oral health and as an aid to diagnosis. Med Oral Patol Oral Cir Bucal 11: E449–E455.

Marcinkiewicz M, Grabowska SZ, Czyzewska E. 1998. Role of epidermal growth factor (EGF) in oesophageal mucosal integrity. Curr Med Res Opin 14:145–153.

Merriam LA, Baran CN, Girard BM, Hardwick JC, May V, Parsons RL. 2013. Pituitary Adenylate Cyclase 1 Receptor Internalization and Endosomal Signaling Mediate the Pituitary Adenylate Cyclase Activating Polypeptide-Induced Increase in Guinea Pig Cardiac Neuron Excitability. J Neurosci 33:4614–4622.

Mese H, Matsuo R. 2007. Salivary secretion, taste and hyposalivation. J Oral Rahabil 34:711–723.

Mirfendereski S, Tobin G, Hakanson R, Ekstrom J. 1997. Pituitary adenylate cyclase activating peptide (PACAP) in salivary glands of the rat: origin, and secretory and vascular effects. Acta Physiol Scand 160:15–22.

Miyagi Y, Aiyama S, Kurabuchi S. 2006. Strain-specific and endocrine control of granular convoluted tubule cells and epidermal growth factor expression in the mouse submandibular gland. Anat Rec 291:105–113.

Mori M, Yamada K, Ohomura H, Kudeken Wataru K, Takai Y, Ilg E, Schäfer BW, Heizmann CW. 1998. Immunohistochemical localization of S100A1 and S100A6 in postnatally developing salivary glands of rats. Histochem Cell Biol 110:579–587.

Nakamachi T, Farkas J, Watanabe J, Ohtaki H, Dohi K, Arata S, Shioda S. 2011. Role of PACAP in neural stem/progenitor cell and astrocyte–from neural development to neural repair. Curr Pharm Des 17:973–984.

Nakamachi T, Ohtaki H, Yofu S, Dohi K, Watanabe J, Hayashi D, Matsuno R, Nonaka N, Itabashi K, Shioda S. 2008. Pituitary adenylate cyclase-activating polypeptide (PACAP) type 1 receptor (PAC1R) co-localizes with activity-dependent neuroprotective protein (ADNP) in the mouse brains. Regul Pept 145:88–95.

Noguchi S, Ohba Y, Oka T. 1991. Effect of salivary epidermal growth factor on wound healing of tongue in mice. Am J Physiol 260:E620–E625.

Nonaka N, Farr SA, Nakamachi T, Morley JE, Nakamura M, Shioda S, Banks WA. 2012. Intranasal administration of PACAP: uptake by brain and regional brain targeting with cyclodextrins. Peptides 36:168–175.

Nonaka N, Shioda S, Banks WA. 2005. Effect of lipopolysaccharide on the transport of pituitary adenylate cyclase activating polypeptide across the blood-brain barrier. Exp Neurol 191:137–144.

Ohshima M, Sato M, Ishikawa M, Maeno M, Otsuka K. 2002. Physiologic levels of epidermal growth factor in saliva stimulate cell migration of an oral epithelial cell line, HO-1-N-1. Eur J Oral Sci 110:130–136.

Pedersen AM, Bardow A, Jensen SB, Nauntofte B. 2002. Saliva and gastrointestinal functions of taste, mastication, swallowing and digestion. Oral Dis 8:117–129.

Proctor GB, Carpenter GH. 2007. Regulation of salivary gland function by autonomic nerves. Auton Neurosci 133:3–18.

Sato A, Miyoshi S. 1998. Cells in the duct system of the rat submandibular gland. Eur J Morphol 36:61–66.

Tandler B, Gresik EW, Nagato T, Phillips CJ. 2001. Secretion by striated ducts of mammalian major salivary glands: review from an ultrastructural, functional, and evolutionary perspective. Anat Rec 264:121–145.

Tobin G, Asztély A, Edwards AV, Ekström J, Håkanson R, Sundler F. 1995. Presence and effects of pituitary adenylate cyclase activating peptide in the submandibular gland of the ferret. Neuroscience 66:227–235.

Uchida D, Arimura A, Somogyvari-Vigh A, Shioda S, Banks WA. 1996. Prevention of ischemia-induced death of hippocampal neurons by pituitary adenylate cyclase activating polypeptide. Brain Res 736:280–286.

van der Putten GJ, Brand HS, Schols JMGA, de Baat C. 2011. The diagnostic suitability of a xerostomia questionnaire and the association between xerostomia, hyposalivation and medication use in a group of nursing home residents. Clin Oral Invest 15: 185–192.

Yanaihara N, Kanno T, Asada N, Iwanaga T, Li J, Nagasawa S, Yanaihara C. 2000. VIP- and PACAP-induced salivary chromogranin A secretion in the isolated perfused submandibular gland of rats. Ann N Y Acad Sci 921:218–225.